p38-MK2 signaling axis regulates RNA metabolism after UV-light-induced DNA damage

Dissertation

zur Erlangung des Grades
Doktor der Naturwissenschaften

Am Fachbereich Biologie
der Johannes Gutenberg-Universität Mainz

vorgelegt von
Marina E. Borisova
geboren am 04.05.1989
in Moskau, Russland

Mainz, 2018

Table of content

List of Publications

The majority of the results presented here are published:

Borisova ME, Voigt A, Sahu SK, Tollenaere MAX, Juretschke T, Kreim N, Mailand N, Choudhary C, Bekker-Jensen S, Akutsu M, Wagner SA, Beli P. “p38-MK2 signaling axis regulates RNA metabolism after UV-light-induced DNA damage.” Nat Commun (2018). doi:10.1038/s41467-018-03417-3 [PubMed]

Borisova ME, Wagner SA, Beli P. “Mass spectometry-based proteomics for quantifying DNA damage-induced phosphorylation.” Methods Mol Biol (2017) 1599:215-217. doi:10.1007/978-1-4939-6955-5_16 [PubMed]

Other publications during the PhD:

Heidelberger J, Voigt A, **Borisova ME**, Petrosino G, Ruf S, Wagner SA, Beli P. “Proteomic profiling of VCP substrates links VCP to K6-linked ubiquitylation and c-Myc function.” EMBO Rep (2018). doi:10.15252/embr.201744754 [PubMed]

Sahu SK, Tiwari N, Pataskar A, Zhuang Y, **Borisova ME**, Diken M, Strand S, Beli P, Tiwari VK. “FBXO32 promotes microenvironment underlying epithelial-mesenchymal transition via CtBP1 during tumour metastasis and brain development.” Nat Commun (2017) 8:1523. doi:10.1038/s41467-017-01366-x [PubMed]

Mahendrarajah N, **Borisova ME**, Reichardt S, Godmann M, Sellmer A, Mahboobi S, Heitel A, Schmid K, Kenner L, Heinzel T, Beli P, Krämer OH. “HSP90 is necessary for the ACK1-dependent phosphorylation of STAT1 and STAT3.” Cell Signal (2017) 39:9-17.doi:10.1016/j.cellsig.2017.07.014 [PubMed]

Summary

Ultraviolet (UV) light radiation induces the formation of bulky photoproducts in DNA, resulting in the activation of the DNA damage response. This has a global effect on transcription and splicing. The components and regulatory mechanisms of DNA repair are relatively well established. However, an understanding of the signaling pathway that orchestrates complex changes in transcription and RNA metabolism after UV-light-induced DNA damage is only beginning to emerge. The p38 mitogen-activated protein kinases (MAPK) is a key transducer of cellular stress signaling and is activated by a number of stress-inducing agents, including UV-light. The activation leads to the phosphorylation of other serine/threonine (S/T) kinases, namely MK2, MK3, and MK5 (MK2/3/5). These kinases, in turn, phosphorylate a number of substrates that affect the functionality of diverse cellular processes, such as cell cycle progression, transcription, translation, splicing, and protein trafficking. Phosphorylation by S/T kinases can be recognized by 14-3-3 proteins. The crosstalk between p38 MAPK activation and 14-3-3 recognition has been demonstrated for a few proteins but has not yet been established as a mode of signaling.

Here, we employ quantitative phosphoproteomics and protein kinase inhibition to provide a systems-wide view on protein phosphorylation patterns induced by UV-light and uncover the dependencies of phosphorylation events on canonical DNA damage signaling by the S/T kinases ataxia telangiectasia mutated (ATM) and ataxia telangiectasia and Rad3-related (ATR) and the p38 MAPK pathway. Our data provide evidence that the activation of the p38 MAPK pathway is independent of the ATM/ATR pathways and regulates a different subset of proteins after low dosages of UV-C light. We detect the phosphorylation of p38 MAPK as well as its downstream kinases, MK2/3, shortly after radiation and observe it for up to one-hour. The p38 MAPK acts primarily through the MK2/3 kinase, which recognizes the LXRQX[ST] motif on the substrates. The same motif, when it is phosphorylated, is also recognized by the 14-3-3 family. We identify RNA-binding proteins as primary substrates and 14-3-3 as a direct “reader” of p38-MK2-dependent phosphorylation induced by UV-light. We mechanistically demonstrate that MK2 phosphorylates the RNA-binding subunit of the NELF complex, NELFE, on serine 49 (S49), S51, S115, and S251. NELFE phosphorylation promotes the recruitment of 14-3-3. Further analysis has determined that S115 plays the crucial role in 14-3-3 binding. This interaction between NELFE and 14-3-3 leads to the rapid dissociation of the NELF complex from chromatin. Aligned with this finding, we discover that the transient knockdown of NELFE results in an increased sensitivity of cells to UV-light. Our ChIP-seq analysis demonstrates that the NELF release is accompanied by RNA polymerase II elongation. Altogether, these events seem to promote cell survival during the response to UV-light DNA damage.

Zusammenfassung

UV-Strahlung induziert die Bildung von sperrigen Fotoprodukten in der DNA, was zur Aktivierung der DNA-Schadensfunktion führt. Dies hat einen globalen Einfluss auf die Transkription und das Spleißen. Die Komponenten und Regulationsmechanismen der DNA-Reparatur sind relativ gut etabliert. Ein Verständnis des Signalwegs, der komplexe Veränderungen in der Transkription und im RNA-Stoffwechsel nach UV-Licht-induzierten DNA-Schäden organisiert, beginnt sich jedoch erst zu entwickeln. Die p38 MAPK sind ein Schlüsselwandler für zelluläre Stresssignale und werden durch eine Reihe von Stress-induzierenden Substanzen aktiviert, darunter UV-Licht. Die Aktivierung führt zur Phosphorylierung anderer Serin/Threonin (S/T)-Kinasen, nämlich MK2, MK3 und MK5. Diese Kinasen wiederum phosphorylieren eine Reihe von Substraten, die die Funktionalität verschiedener Zellprozesse beeinflussen, wie z.B. Zellzyklusverlauf, Transkription, Translation, Spleißen und Proteinhandel. Die Phosphorylierung durch S/T-Kinasen kann an 14-3-3 Proteinen erkannt werden. Der Schnittpunkt zwischen p38 MAPK-Aktivierung und 14-3-3 Erkennung wurde für einige Proteine nachgewiesen, ist aber noch nicht als Signalisierungsmodus etabliert.

Hier verwenden wir quantitative Phosphoproteomik und Proteinkinase-Hemmung, um einen systemweiten Überblick über die durch UV-Licht induzierten Proteinphosphorylierungsmuster zu erhalten und die Abhängigkeiten von Phosphorylierungsereignissen von kanonischen DNA-Schadenssignalen durch die S/T-Kinasen ATM und ATR und den p38 MAPK-Pfad zu entdecken. Unsere Daten liefern den Nachweis, dass die Aktivierung des p38 MAPK-Pfades unabhängig von den ATM/ATR-Pfaden ist und eine andere Teilmenge von Proteinen nach niedriger Dosierung von UV-C-Licht reguliert. Wir entdecken die Phosphorylierung von p38 MAPK sowie der nachgelagerten Kinasen MK2/3 kurz nach der Bestrahlung und beobachten sie bis zu einer Stunde lang. Die p38 MAPK wirkt hauptsächlich durch die MK2/3-Kinase, die das LXRQX[ST]-Motiv auf den Substraten erkennt. Das gleiche Motiv, wenn es phosphoryliert ist, wird auch von der Familie 14-3-3 erkannt. Wir identifizieren RNA-bindende Proteine als Primärsubstrate und 14-3-3 als direkten "Reader" der p38-MK2-abhängigen Phosphorylierung, die durch UV-Licht induziert wird. Wir zeigen mechanistisch, dass MK2 die RNA-bindende Untereinheit des NELF-Komplexes, NELFE, auf Serin 49 (S49), S51, S115 und S251 phosphoryliert. NELFE Phosphorylierung fördert die Rekrutierung von 14-3-3. Weitere Analysen haben ergeben, dass S115 die entscheidende Rolle bei der 14-3-3 Bindung spielt. Diese Interaktion zwischen NELFE und 14-3-3 führt zu einer schnellen Dissoziation des NELF-Komplexes vom Chromatin. Ausgehend von diesem Ergebnis stellen wir fest, dass der transiente Knock-down von NELFE zu einer erhöhten Empfindlichkeit der Zellen gegenüber UV-Licht führt. Unsere ChIP-seq-Analyse zeigt, dass die NELF-Freisetzung von der Verlängerung der RNA-Polymerase II begleitet wird. Insgesamt

scheinen diese Ereignisse das Zellüberleben bei der Reaktion auf DNA-Schäden durch UV-Licht zu fördern.

Introduction

1.1 Types of DNA damage and common repair mechanisms

Cells are continuously exposed to DNA damage that arises from both endogenous and exogenous sources; for example, reactive oxygen species (ROS) are produced during cellular metabolism and lead to the oxidation and alkylation of DNA bases, which results in the depurination and modification of nucleotides (Hoeijmakers, 2009). During DNA replication, deoxynucleotide (dNTP) misincorporation results in spontaneous DNA hydrolysis and deamination that can induce interconversion between DNA bases (Ciccia & Elledge, 2010). Moreover, several cellular processes are dependent upon the programmed formation of DNA damage: double-strand DNA breaks (DSBs) are required for chromosome recombination during meiosis, class switch recombination during lymphocyte maturation, and homothallism (i.e., interconversion in yeast).

Exogenous DNA damage induced by chemicals, such as platinum-based drugs, can cause the formation of covalent links between the bases of the same DNA strand (intra-strand crosslinks) or different DNA strands (inter-strand crosslinks), as well as protein-DNA crosslinks. The repair of these DNA lesions may indirectly result in the generation of single-strand DNA (ssDNA) breaks (SSBs) or DSBs (Ciccia & Elledge, 2010; Sonntag, 2006). Exposure to ionizing radiation (IR) also leads to the formation of various DNA lesions, including SSBs and DSBs. Typically, human cells are exposed to these agents during chemotherapy with the purpose of inducing DNA damage and killing cancer cells; however, small doses of some of these agents, including IR and tobacco smoke, are ever-present in our surrounding environment.

Ultraviolet (UV) light is another exogenous source of DNA damage to which organisms are exposed naturally. UV-light from sunlight is commonly divided into three types depending on wavelength (Besaratinia et al., 2011; Diffey, 2002). Type C (280–100 nm) has the shortest wavelength. It is absorbed by stratospheric oxygen, which subsequently transforms into ozone. Type B (315–280 nm) is primarily filtered out by ozone as well and can also be blocked by clouds. Only 95% of Type A (400–315 nm) reaches the planet's surface and takes part in photobiological processes (Diffey, 2002). Despite the majority of UV-B being filtered out and all of UV-C needing to be filtered out, the small percentage of UV-C that reaches the surface of the Earth penetrates cells more efficiently than the more abundant UV-A (Diepgen & Mahler, 2002; Woodhead, Setlow, & Tanaka, 1999). DNA bases strongly absorb UV-light, which results in damage. More specifically, UV-light exposure leads to the formation of dimers between two pyrimidines, and as a result, cyclopyrimidine dimers (CPDs), or 6'–4' photoproducts (6-4PPs), are formed (Franklin & Haseltine, 1986) (Figure 1). Studies of the UV-light-dose-dependent formation of these photoproducts have demonstrated that 6-4PPs are formed less frequently and only after irradiation with UV-B and UV-C light (Besaratinia et al., 2011). In contrast, CPDs accumulate after all types of UV-light

exposure, but similar to 6-4PPs, their formation increases tenfold after exposure to UV-B and UV-C light (Besaratinia et al., 2011). Therefore, it is suggested that CPDs play the most critical role in DNA-damage-dependent changes in organisms due to the high frequency of their formation (Besaratinia et al., 2011). In addition to directly modifying DNA, UV-light also leads to the accumulation of ROS in cells, leading to photooxidation-derived DNA lesions, such as 2,6-diamino-4-hydroxy-5-formamidopyrimidine and 8-oxo-7,8-dihydro-2'-deoxyguanosine. These lesions accumulate if left unrepaired by the cell.

Different types of DNA lesions activate specific types of DNA repair mechanisms. In mammals, the most predominant and well-described pathways are mismatch (MMR), base-excision (BER), nucleotide-excision (NER), and double-strand break repair. In addition, cells activate DNA damage bypass and translesion synthesis (TLS) to continue replication despite lesions occurring during the S-phase of the cell cycle.

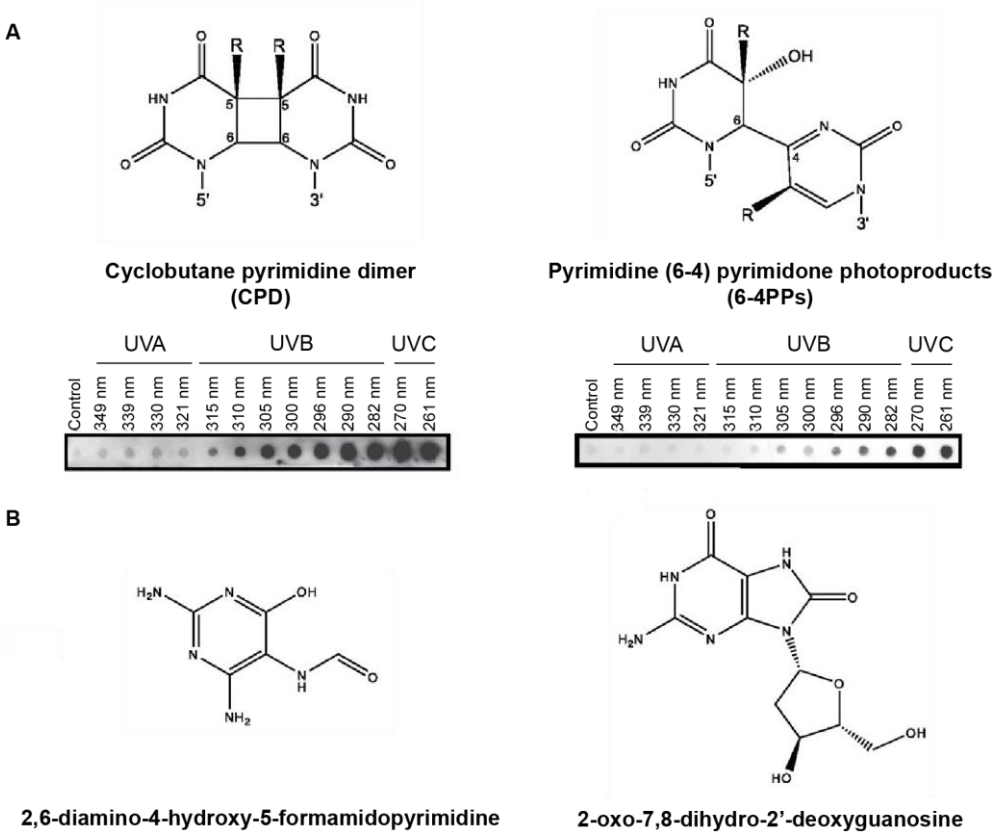

Figure 1. UV-light-induced DNA lesions. A *Chemical structure of CPD and 6-4PPs and determination of their formation in mouse genomic DNA irradiated with various UV-light wavelengths. The probes were analyzed with immunodotblot assay using Anti-Thymine Dimer and Anti-(6-4)PPs monoclonal antibodies (Kamiya Biomedical Co.).* ***B*** *Chemical structure of damaged DNA induced by UV-light indirectly through ROS, 2,6-diamino-4-hydroxy-5-formamidopyrimidine, and 8-oxo-7,8-dihydro-2'-deoxyguanosine. Adapted from Besaratinia et al., 2011.*

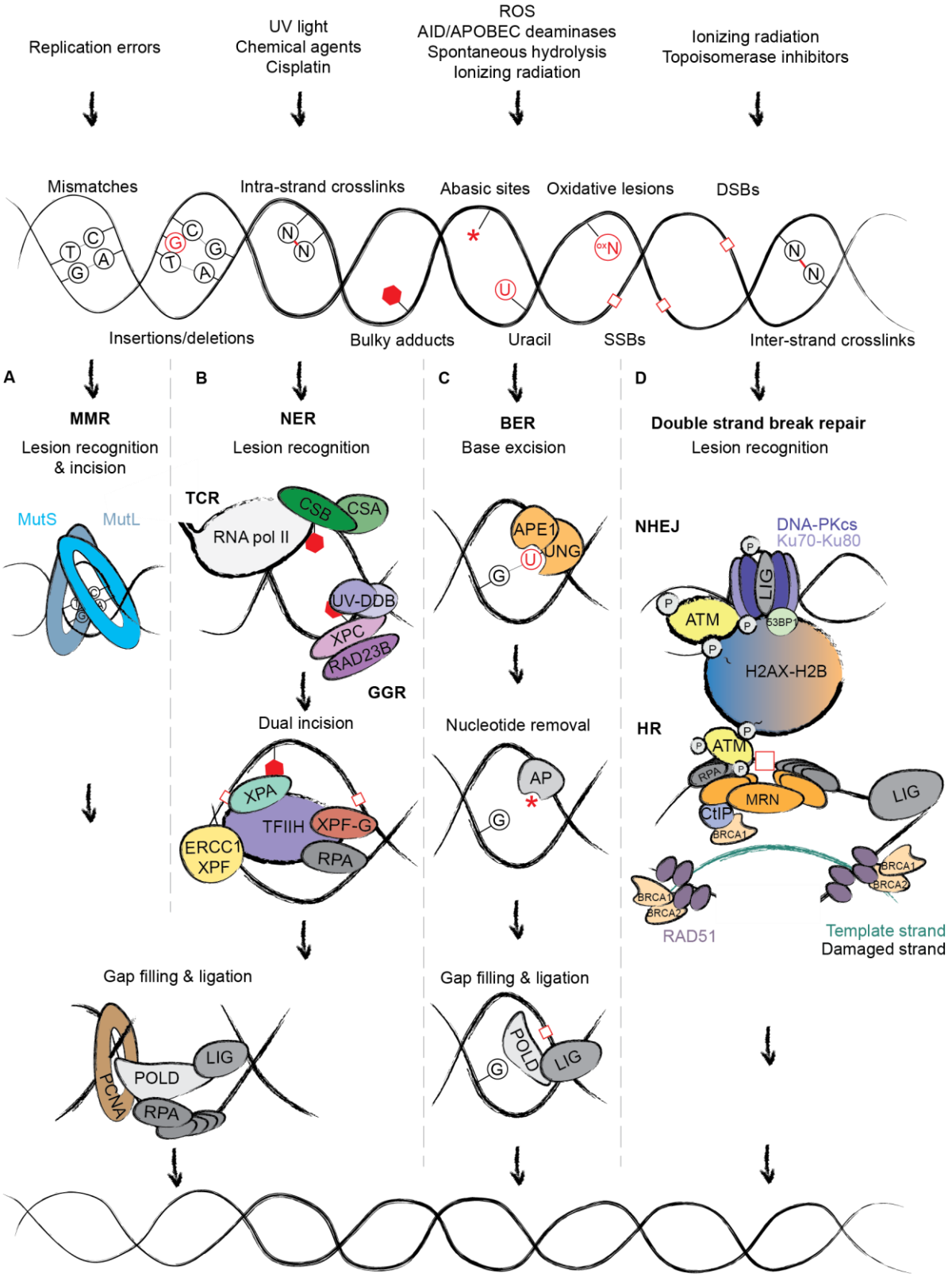

Figure 2. Simplified schemes of DNA lesions and their repair mechanisms in mammals. *Exogenous and endogenous factors (top) can cause various types of DNA damage. DNA lesions are detected and repaired by four major mechanisms:* ***A*** *Mismatch repair (MMR)* ***B*** *Transcription/coupled (TC) and global genome (GG) nucleotide excision repair (NER) pathways* ***C*** *Base excision repair (BER)* ***D*** *Non-homologous end joining (NHEJ) and homologous recombination (HR) pathways. They include three common steps: lesion recognition, end processing, and gap filling with final ligation. The details of the pathways are described below. Adapted from* Ciccia & Elledge, 2010; Fong et al., 2013; Lans et al., 2012; Richard et al., 2011*. Molecule sizes are not scaled.*

1.1.1 Mismatch repair

MMR removes interconversions and errors in DNA introduced during DNA replication (Figure 2A). In addition, MMR machinery can recognize DNA lesions induced by exogenous agents, such as cisplatin (Jiricny, 2006; Li, 2008). In brief, MMR includes the recognition and incision of the lesion, which is followed by the re-synthesis and ligation of the DNA (Larrea, Lujan, & Kunkel, 2010). In eukaryotes, the MMR recognition step comprises the activity of the MutS heterodimer (human homologs are MSH2, MSH3, MSH6), which recognizes base-base mismatches and small nucleotide insertion and deletion mispair. MutS with the MutL heterodimer (human homologs MLH1, MLH3, PMS1, PMS2) facilitate the recruitment and binding of the EXO1 nuclease. PCNA, the replication clamp involved in normal replication, binds to MutS and MutL, helps EXO1 in the incision step (e.g., nucleotide removal) and begins the re-synthesis of the DNA (Gu, Hong, McCulloch, Watanabe, & Li, 1998; Strzalka & Ziemienowicz, 2011). Another DNA replication factor, the RPA70-RPA32-RPA14 complex (RPA), covers naked ssDNA stretches before the DNA polymerase δ (POLD) processes them into DSBs. The final step is the ligation of the remaining nick by DNA ligase I (LIG1).

1.1.2 Base-excision repair

Small base lesions activate BER (Krokan & Bjoras, 2013). Such DNA modifications do not significantly distort DNA structure. For instance, BER detects and repairs 8-oxo-7,8-dihydro-2'-deoxyguanosine and 2,6-diamino-4-hydroxy-5-formamidopyrimidine caused by DNA oxidation as well as uracil and 3-methyladenine caused by deamination or alkylation (Maynard, Schurman, Harboe, de Souza-Pinto, & Bohr, 2008). In the first step, glycosylases recognize the modified nucleotide, cleave the N-glycosyl bond between the sugar and the base, and lead to an abasic site (AP-site) formation (Figure 2C). Over 11 glycosylases exist in mammalian cells, subdivided into mono- or bifunctional glycosylases depending on the reaction mechanism (Krokan & Bjoras, 2013). The monofunctional enzymes function only as glycosylases, such as UNG, and require a partner, such as APE1, for the incision step. Bifunctional enzymes, such as OGG1 and NEIL1, combine both functions; they glycosylate and lyase until the lesion has an AP-site, causing an SSB formation with 3'-phosphate or 3'-α,β-unsaturated aldehyde that requires the 3'-terminal group removal. The AP-site can also form spontaneously after depurination or depyrimidination. Next, the AP-site is cleaved by the AP endonuclease and, at this stage, BER is subdivided into short-patch or long-patch repair. If there is no hindrance, DNA polymerase β (POLB) leads to repair through the short-patch pathway, which replaces only the excised nucleotide. If POLB cannot overcome the 5' terminus, the long-patch BER occurs and rebuilds 2–6 nucleotides around the blocking terminus with the help of PCNA, FEN1, POLB and POLD/E. At last, the LIG1 or LIG1-XRCC1 complex ligates and removes the remaining nick.

1.1.3 Nucleotide-excision repair

NER recognizes DNA photoproducts or bulky lesions (6-4PPs or CPDs) caused by UV-light irradiation or polycyclic aromatic hydrocarbons, such as benzo[a]pyrene or cisplatin (Gong, Kwon, & Smerdon, 2005) (Figure 2B). As in BER, NER proceeds through the excision steps ruled by endonucleases. NER includes two pathways: transcription-coupled and global-genome NER, depending on the transcription state of the region surrounding the lesions.

Transcription-coupled NER (TC-NER) reacts to a stalled RNA polymerase (RNA pol 2), which is recognized by UVSSA, USP7, and CSB/ERCC6. CSB bound to RNA pol 2 forms a complex with CSA/ERCC8, which might pull back RNA pol 2 to release damaged DNA and allow access for other repair factors. These events lead to pre-incision complex formation (Lans et al., 2010; Sugasawa et al., 1998; Volker et al., 2001). An additional mechanism of lesion region clearance includes RNA pol 2 modification with polyubiquitin by the ubiquitin ligases NEDD4 or BRCA1, which leads to the polymerase proteasomal degradation (Wickramasinghe & Venkitaraman, 2016).

The other pathway, global-genome NER (GG-NER), detects lesions in regions with DNA replication or heterochromatic regions with no or low transcriptional activity. This pathway begins with the recognition of lesions by XPC, with the help of RAD23B and CETN2. RAD23 ceases to interact with XPC as soon as it recognizes the damage. In some cases, the UV-DDB complexes, DDB1 and DDB2, help XPC to bind to the lesion by bending out the DNA and facilitating XPC recruitment to the exposed ssDNA.

Next, the pre-incision complex in both GG- and TC-NER pathways recruits the transcription factor TFIIH complex, which unwinds the DNA strand around the recognized lesion using the helicase subunits XPB/ERCC2 and XPD/ERCC3 (Schärer, 2013; Sugasawa et al., 2005). This displaces RNA pol 2 from the lesion, in the case of TC-NER. Meanwhile, XPA and RPA proteins displace XPC-RAD23 and maintain opened DNA. As in MMR, RPA covers the ssDNA. The stabilization complex (XPA-RPA) also helps to orientate endonuclease machinery, including 5’ incision nucleases ERCC1 with XPF/ERCC4 and 3’ incision nuclease XPG/ERCC5 (Lans et al., 2010; Nouspikel, 2009; Volker et al., 2001). A dual incision reaction follows the recruitment of ERCC1-XPF and XPG, which generates a 5’ end with a free phosphate and a 3’ end with free hydroxyl groups, both used in the next steps. The former is involved in the replication process, where POLD and POLE or the error-prone DNA polymerase κ, sliding clamp PCNA, the pentameric clamp loader RFC, and RPA, all are involved in DNA re-synthesis. The latter free group plays a role in the final step — nick ligation by LIG1 and the DNA ligase IIIα-XRCC1 complex. Exonuclease activity could cause long stretches of ssDNA formation if another lesion repair occurs near the replicating sites (Volker et al., 2001).

Mutations in NER proteins lead to hereditary disorders of high skin photosensitivity. A mutation in any of the XP factors (XPA-G) causes Xeroderma Pigmentosum (XP) (Gregersen & Svejstrup, 2018; Tan, Baris, Robson, & Kimonis, 2005; Volker et al., 2001). A mutation in CSA or CSB leads to Cockayne syndrome

(CS), also called Neill-Dingwall syndrome (Tan et al., 2005). Both syndromes are characterized by growth and neurodevelopmental failure, in addition to severe sunlight sensitivity. The loss of function in the regulator of CSA-CSB binding, UVSSA, and some mutations in CSA and CSB lead to UV^{S}S syndrome, which displays dramatic symptoms. Patients with UV^{S}S experience none of the developmental symptoms present in either CS or XP (Gregersen & Svejstrup, 2018).

1.1.4 Double-strand break repair

DSBs represent the most dangerous type of lesions since they can result in the loss of genetic information if unrepaired or inappropriately repaired. Homologous recombination (HR) and non-homologous end joining (NHEJ) repair the DSBs in the cell (Ciccia & Elledge, 2010; Srivastava & Raghavan, 2015). The mechanism of the repair process includes the common steps of recognition, end processing, and ligation; however, the proteins involved in these steps differ in the two pathways (Figure 2D). In addition, HR includes DNA end resection and requires a homologous non-damaged DNA strand for the other strand's reconstitution and complete repair. Conversely, NHEJ proceeds without end resection and ligates the broken ends directly.

NHEJ begins with the recognition of the DSB by the heterodimer Ku70-Ku80, which winds around the broken DNA ends. Ku70-Ku80 guides the recruitment of the downstream NHEJ factors: the DNA-dependent protein kinase catalytic subunit (DNA-PKcs), XRCC4, XRCC4-like factor (XLF), DNA ligase IV (LIG4), Aprataxin-and-PNK-like factor (APLF), and ARTEMIS (Meek, Dang, & Lees-Miller, 2008). The Ku70-Ku80-DNA complex attracts the 5' exonucleases ARTEMIS and APLF to the DSBs. DNA-PKcs, which binds the ends of the lesion, phosphorylates ARTEMIS and activates its endo- and exonuclease activity (Davis & Chen, 2013). ARTEMIS then processes the DNA ends. The XRCC4-XLF complex forms filaments at the processed ends and promotes additional stability at this stage. Moreover, XRCC4-XLF forms a scaffold for downstream factors in case the ends should still be processed for ligation. For example, the recruitment of Aprataxin removes an adenylate group covalently bound to a 5' phosphate. In case of a gap in the sequence, the DNA polymerase μ (POLM) copies the full strand to build up the interrupted fragment. NHEJ finishes with the ligation step by XRCC4-LIG4, with the support of XLF and Ku70-Ku80.

Other proteins, namely MRE11, RAD50 and NBS1, which form the MRN complex, recognize DSBs in the case of HR (R. S. Williams, Williams, & Tainer, 2007). Within the complex, RAD50 tethers the two ends of the broken DNA, MRE11 bears endonuclease and exonuclease functions, and NBS1 contains additional protein-protein interaction domains that lead to DNA repair progression. The recruitment of EXO1 with Bloom helicase (BLM) leads to the formation of ssDNA stretches that are covered with RPA, which is a single-strand binding protein complex (Bolderson et al., 2010; Cruz-García, López-Saavedra, & Huertas, 2014; You & Bailis, 2010). RAD51 recombinase, together with an E3 ubiquitin ligase, BRCA2, displaces RPA on the ssDNA and guides the strand invasion into a homologous dsDNA forming D-loop. At this stage, the invaded strand could be quickly elongated by a DNA polymerase and

ligated with the second untouched ssDNA, organizing the DNA strands into a Holliday junction (HJ) cross (Figure 3). This structure can be moved along the DNA by RTEL1 or cut immediately by MUS81-EME1 nucleases. Alternatively, if the other ssDNA goes through the invasion, the DNA forms a double HJ (dHJ) after the elongation and ligation of the corresponding strands. These steps are controlled by an E3 ubiquitin ligase complex, BRCA1-BARD1, and a transcriptional factor, CtIP. Two methods can resolve the dHJ: Either the BLM-TOPOIII complex dissolves it, or the endonucleases GEN1, MUS81-EME1, or SLX1-SLX4 cleave it to crossover or non-crossover HJ, respectively (Bussen, Raynard, Busygina, Singh, & Sung, 2007; Ciccia, McDonald, & West, 2008; Ip et al., 2008; I. M. Muñoz et al., 2009). Crossover events can lead to the loss of heterozygosity and genomic rearrangements in mitotic cells (Chu & Hickson, 2009).

Alternatively, PARP1/2 can recognize the DSB lesion and guide the DSBs to alternative NHEJ (alt-NHEJ). In alt-NHEJ, the MRN binds to PARP1/2, activating DSB

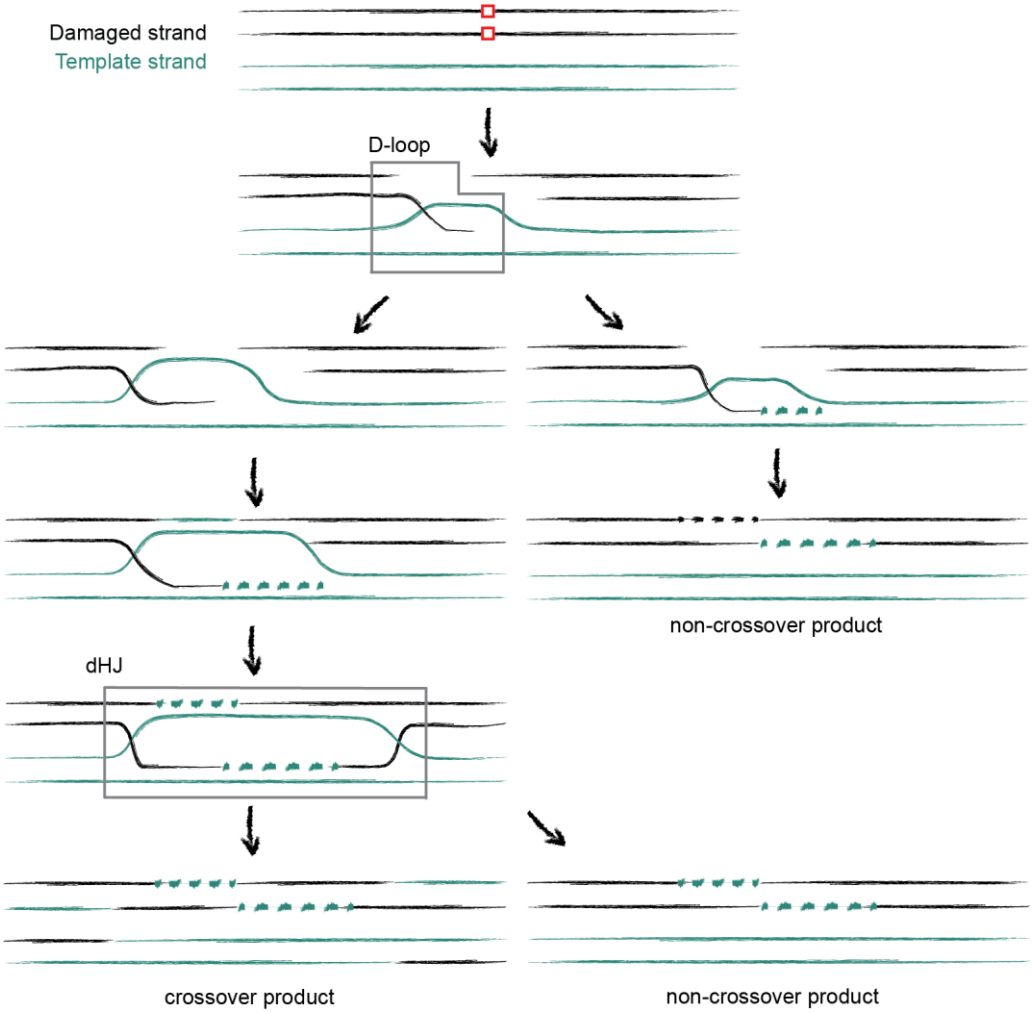

***Figure 3. Simplified mechanism of Holliday junction cross resolution into crossover or non-crossover products during the final steps of HR**. During strand invasion, RAD51 guides DNA to form a D-loop based on strand homology. The invasion step can continue and results in the formation of a double Holliday junction (dHJ, left panel), which results in crossover or non-crossover. The first one requires a symmetric cleavage of both HJ crosses in the opposite orientation by HJ resolvase. The latter one is formed after cleavage in the same direction that leads to dHJ collapse followed by resolution with type I topoisomerase. Alternatively, the D-loop can be directly resolved after the extension with DNA polymerase (left panel). As such, the invaded strand reanneals with the single-strand DNA that is left out of the D-loop and therefore leads to a non-crossover product. Adapted from* Heyer, 2004.

signaling similar to classical NHEJ, and processes ends until short flaps (5–25 nt) are formed. CtIP and BRCA1-BARD1, in complex with the MRN, perform limited DSB resection. Subsequently, POLD rebuilds the damaged region using ssDNA regions with microhomology. Simultaneously, the recruitment of the polymerase inhibits HR events. At last, the strands are ligated by the XRCC1/LIG3 complex (Ciccia & Elledge, 2010; Wang et al., 2006).

NHEJ dominates during the G1 phase, whereas HR requires a sister chromatid and therefore prevails in mammals during late S and G2 phases (Bothmer et al., 2010; Frit, Barboule, Yuan, Gomez, & Calsou, 2014). Alt-NHEJ can be activated in all phases, and it is promoted when cells enter the S-phase accompanied by cyclin-dependent kinases (CDK) activity (Frit et al., 2014).

1.1.5 Replication stress

Replication machinery (replisome) slowing down or stalling, known as replication stress, has many causes, such as the excessive compacting of chromatin, the overexpression of oncogenes, and damaged DNA, including UV-light-induced lesions (Ciccia & Elledge, 2010). Upon replication stress, the MCM helicase that is part of the replication machinery continues to unwind strands after the DNA polymerase has ceased (Figure 4) (Gaillard, García-Muse, & Aguilera, 2015). This causes the formation of single-strand stretches coated with the single-strand binding protein complex RPA. The RPA-ssDNA complex interacts with the ATR interaction protein (ATRIP) and induces an ATR-dependent activation of the replication stress response (Zeman & Cimprich, 2014). Along with ATR-ATRIP, TOPBP1 and ETAA1 play crucial roles in the stalled fork recognition. The response includes the protection of stretches

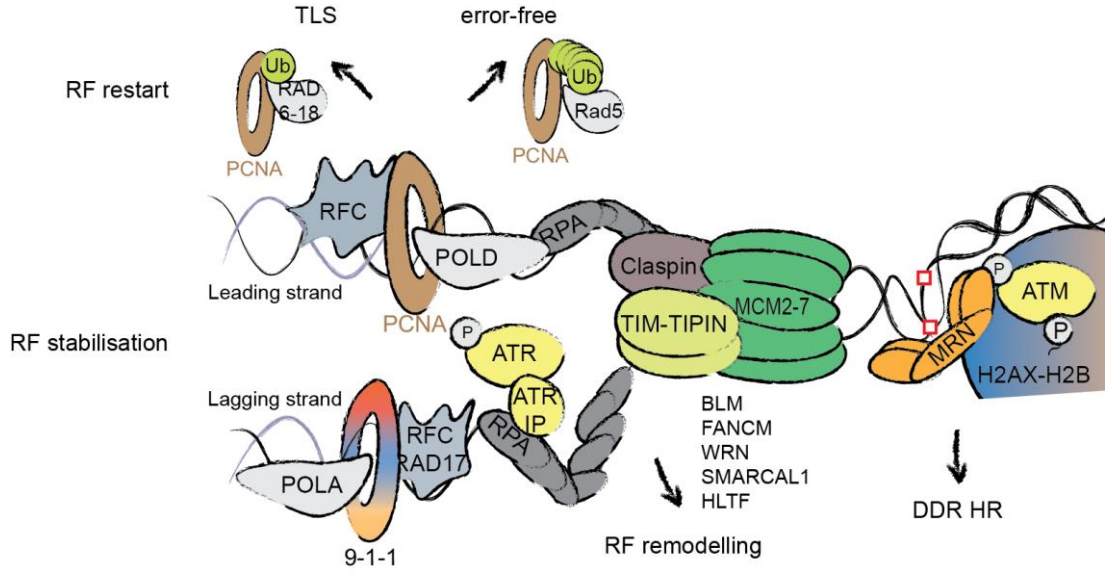

Figure 4. Simplified scheme of the response to replication stress*. Replication involves replicating factor C (RFC), proliferating cell nuclear antigen (PCNA), replicating protein A (RPA), polymerase δ (POLD), and polymerase α (POLA) on the leading and lagging strands, respectively. A slowed down or stalled replication fork (RF) initiates DNA damage response that starts with the clamp loader RAD17 binding to RPA-ssDNA. RAD17-RPA-ssDNA recruits the clamp complex RAD9-HUS1-RAD1 (9-1-1), and together they position TOPBP1. Independently, ATR,, through its binding partner ATR Interaction Protein (ATRIP), binds to the RPA patch. The TOPBP1 and ATR-ATRIP interaction activates ATR. The activated kinase phosphorylates TIM-TIPIN and CLASPIN, which stabilize the RF. ATR phosphorylation guides proteins that restructure RF and let the replication proceed. Adapted from* Gaillard et al., 2015; R. M. Jones & Petermann, 2012; O'Connell & Harper, 2007.

of ssDNA, the suppression of late origin firing, and recombination. The ATR substrates, TIM-TIPIN and CLASPIN, stabilize the stalled replication fork. On the other hand, the PCNA-RFC complex prevents DNA polymerases from dissociating, and the latter serves as a scaffold for DNA synthesis or DNA damage response (DDR) factors (Gaillard et al., 2015). After frozen replisome detection, replication must restart. DNA helicases and translocases such as BLM, FANCM, WRN, SMARCAL1, and HLTF control the restart after binding to RPA-ssDNA (R. M. Jones & Petermann, 2012). These lead to the leading and lagging strands reannealing and restart polymerization by template switching or lesion bypass. If damaged DNA caused the replication stress, the lesion must still be repaired. This mechanism has been thoroughly studied in budding yeast, and two distinct pathways have been identified (Stelter & Ulrich, 2003; H. Ulrich & Jentsch, 2000). Both require the ubiquitin ligase complex RAD6-RAD18 to ubiquitylate PCNA, which leads to the activation of TLS or error-free post-replicative repair. During TLS, the TLS DNA polymerase, lacking the proofreading function, binds to PCNA and replicates over the damaged DNA. In contrast, error-free repair uses the undamaged strand as a template during strand invasion and catalyzes subsequent repair via HR.

1.2 The DNA damage response

Failure in repair mechanisms leads to an accumulation of mutations or chromosome aberrations and subsequently cancer, premature aging, or inborn genetic diseases. DDR combines a number of pathways that lead to DNA damage identification and repair, chromatin remodeling, and control of the cell cycle progression. In particular, DDR regulates replication, transcription, RNA metabolism, and protein production. Therefore, DDR is a critical and tightly regulated process. The activation and further regulation of DDR are mediated by protein posttranslational modifications (PTMs) such as phosphorylation, acetylation, ubiquitylation, SUMOylation, and PARylation.

1.2.1 Phosphorylation: ATM and ATR are central kinases of DDR

The phosphatidylinositol-3-kinases (PI-3Ks) ATM and ATR and the DNA-dependent protein kinase catalytic subunit (DNA-PKcs) play key roles in the signaling cascades of DDR (Ciccia & Elledge, 2010; Lukas, Lukas, & Bartek, 2011; Maréchal & Zou, 2013; Polo & Jackson, 2011). The kinases preferentially recognize and phosphorylate proteins on serine or threonine residues followed by glutamine (S/TQ motif) (Bensimon, Aebersold, & Shiloh, 2011; Kim, Lim, Canman, & Kastan, 1999).

The primary function of DNA-PKcs is to promote NHEJ. After lesion recognition, the Ku70-Ku80 complex activates DNA-PKcs and stabilizes end resection (Ciccia & Elledge, 2010). The autophosphorylation of the DNA-PKcs' ABCDE cluster (around T2609) removes DNA-PKcs from DNA ends, which are then processed by the endonuclease ARTEMIS, nucleases APLF, and kinase/phosphatase PNK prior to DNA ligation. Autophosphorylation of the DNA-PKcs' PQR cluster (around S2056) prevents the ends from excessive processing. If NHEJ fails at this stage, the first

phosphorylation of the ABCDE cluster of DNA-PKcs will promote HR (Srivastava & Raghavan, 2015). The ABCDE cluster can be also phosphorylated by ATM (Ciccia & Elledge, 2010).

ATM exists as noncovalent homodimers in an inactive state, and monomerization leads to the activation of the kinase (Paull, 2015). ATM acts primarily on DSBs and induces a regulatory cascade, particularly in HR. PARP1/2 and/or MRN bind to DSBs and interact with ATM, leading to its activation (J.-H. Lee & Paull, 2005; Uziel et al., 2003). Activated ATM acquires phosphorylation on S1981 via autophosphorylation. Activated ATM phosphorylates over 700 proteins, as identified by quantitative mass spectrometry-based proteomics (Matsuoka et al., 2007). ATM-dependent phosphorylation modulates the activity of the tumor suppressor p53 and many components of the HR pathway, such as CtIP, BRCA1, ARTEMIS. Most crucially for DDR, it phosphorylates the histone variant H2AX on S139 (known as γH2AX). The mediator of DNA damage checkpoint protein 1 (MDC1) binds γH2AX through its phosphorylation-recognizing BRCT domain. The modification of H2AX is catalyzed rapidly after the formation of DSBs and spreads 1–2 mega-bases around the site of DNA damage in an ATM-MDC1-dependent manner (Ciccia & Elledge, 2010; Maréchal & Zou, 2013; Meier et al., 2007; Rogakou, Pilch, Orr, Ivanova, & Bonner, 1998). This serves as a landing ground for factors crucial in DNA repair. In addition, MDC1 interacts with NBS1 and provides additional strength to ATM-MRN binding (Chapman & Jackson, 2008; Melander et al., 2008; L. Wu, Luo, Lou, & Chen, 2008). Another phosphorylation on H2AX, Y142, in addition to S139, inhibits MDC1 binding and therefore stops the spread of the signal. In contrast, single H2AX phosphorylation on Y142 (without S139) recruits the pro-apoptotic kinase JNK1 and, as such, initiates JNK-dependent apoptosis (Cook et al., 2009).

Cell cycle arrest is a crucial step in preventing genomic instability during DDR. ATM activates many kinases, and the checkpoint kinase 2 (CHEK2) is its primary mediator, which regulates the cell division cycle 25C (CDC25C) (Paull, 2015). CHEK2 phosphorylates SMC1, another protein crucial for cell cycle progression and chromosome segregation (Yazdi et al., 2002). Altogether, the direct or indirect ATM-dependent phosphorylation of MDC1, CDC25C, and SMC1 allows the kinase to control the progression through the S and M phases of the cell cycle.

ATR is another universal regulator of DDR. Longer stretches of ssDNA, coated with the RPA complex, activate ATR in many DNA repair pathways, as this is one of the common steps in HR, NER, MMR, and replication restart (Figure 4). In addition, ATR is activated after the formation of long patches in BER, which would also include the RPA coating of ssDNA (Nam & Cortez, 2011). ATR activation requires several preliminary steps. First, the clamp loader RAD17 binds the RPA-ssDNA or RPA-dsDNA complex (L. Zou, Cortez, & Elledge, 2002; Lee Zou et al., 2003). Second, the clamp complex RAD9-HUS1-RAD1 (9-1-1) recognizes RAD17 on DNA and positions TOPBP1 (J. Lee, Kumagai, & Dunphy, 2007; Xu et al., 2008). Independently through its binding partner, ATRIP, ATR binds to the RPA patch (Ball, Myers, & Cortez, 2005; Cortez, Guntuku, Qin, & Elledge, 2001; Unsal-Kaçmaz & Sancar, 2004). These two

modules of TOPBP1 and ATR-ATRIP interact with each other and activate ATR by phosphorylation on T1989. Recently, ETAA1 was demonstrated to activate ATR similarly and in parallel to theTOPBP1-9-1-1 complex (Bass et al., 2016; S. Liu et al., 2006; Mordes, Glick, Zhao, & Cortez, 2008). The recruitment of many other factors to DNA damage sites stimulates the phosphorylation of ATR (S. Liu et al., 2011; Nam & Cortez, 2011). Although ATR phosphorylation is dependent on replication factors, the activation can also occur outside of the S-phase, in the case of UV-light-induced DNA lesions (Iyer & Rhind, 2017; Ward, Minn, & Chen, 2004). Such activation requires on the abovementioned NER response intermediates (Giannattasio et al., 2010; Hanasoge & Ljungman, 2007; Marini et al., 2006). Upon activation, ATR phosphorylates its primary downstream kinase, checkpoint kinase 1 (CHEK1), on S317 (S. Liu et al., 2011). CHEK1 regulates cell cycle progression in the S and G2/M checkpoints through the inhibition of CDC25 proteins and therefore prevents genome instability by blocking premature entry into G2 or mitosis, respectively (Cimprich & Cortez, 2008; Klusmann et al., 2016; Saini, Li, & Dobbelstein, 2015).

Both ATM and ATR can phosphorylate p53, resulting in its activation and therefore covering one more checkpoint in the cell cycle progression (Harris & Levine, 2005). p53 upregulates the transcription of p21, the inhibitor of the CDKs, and arrests cells in the G1 phase (Galanos et al., 2016; Mansilla et al., 2013; Shaw, 1996). Moreover, ATM and ATR have been demonstrated to activate another signaling cascade, guided by p38 MAPK/MK2 after topoisomerase inhibitors and cisplatin (Reinhardt, Aslanian, Lees, & Yaffe, 2007). In the case of p53-deficient cells, instead of p53 activation, p38 MAPK activation through ATM or ATR regulates cell cycle arrest and cell survival (Christian Reinhardt & Yaffe, 2013; Reinhardt et al., 2007).

1.2.2 Other PTMs in the regulation of DDR

The phosphorylation of many proteins, regulated by ATM or ATR, initiates other PTM-dependent cascades in DDR. Ubiquitylation modifies proteins on lysines with a 76-amino-acid-long polypeptide, Ubiquitin (Jackson & Durocher, 2013). Protein ubiquitylation is achieved in a multistep enzymatic process that involves ubiquitin-activating enzymes (E1), ubiquitin-conjugating enzymes (E2), and ubiquitin ligases (E3). Ubiquitin ligases determine the specificity of substrates and the type of ubiquitylation. Ubiquitin can be attached to substrate proteins as a single molecule or as a polyubiquitin chain by binding to one of the internal lysines (K6, K11, K27, K29, K33, K48, K63) or to the N-terminal methionine. The E3 ubiquitin ligase RNF8 binds the phosphate on the MDC1-γH2AX complex and ubiquitylates substrates quickly with K48-linked polyubiquitin chains (Dantuma & van Attikum, 2016; Ramadan, 2012). RNF8, together with the E2 ubiquitin-conjugating protein UBC13, controls DDR via the ubiquitylation of substrates with K63-linked polyubiquitin chains. The RNF8^{UBC13}-MDC1 interaction leads to H1 polyubiquitylation and to the recruitment of the E3 ubiquitin ligase RNF168 (Bohgaki et al., 2013; Mandemaker et al., 2017). The latter monoubiquitylates H2A at K13 and K15 and lengthens ubiquitin with K27-linked polyubiquitin chains, which most probably mediates BRCA1 or 53BP1 binding,

promoting HR or NHEJ, respectively (Bekker-Jensen et al., 2010; Jackson & Durocher, 2013). Ubiquitylation also tightly regulates GG-NER. The primary DNA damage recognition factor, UV-DDB, is a part of the ubiquitin ligase complex DDB1-CUL4A^{DDB2} and ubiquitylates core histones, XPC, and DDB2 itself. Interestingly, whereas DDB2 ubiquitylation leads to proteasomal degradation, the XPC modification causes higher affinity to lesions (Sugasawa et al., 2005).

Another PTM, sumoylation, involves the addition of a small ubiquitin-like protein, SUMO, to substrate proteins. The SUMO E3 ligase PIAS protein family controls the sumoylation of many DDR proteins, such as MDC1, 53BP1, BRCA1, RPA, and RNF168 (Polo & Jackson, 2011). On the one hand, SUMO acts as a “glue” for proteins at DNA lesions (Psakhye & Jentsch, 2012). On the other hand, as in the cases of MDC1 and RPA, it leads to ubiquitylation through SUMO-targeted ubiquitin E3 ligases (STUbLs) and the subsequent proteasomal degradation of its targets. SUMO can also regulate the K48- and K63-linked ubiquitylation balance in the stress response. In particular, the sumoylation of the ubiquitin ligase HERC2 facilitates the interaction between RNF8 and UBC13 (Bekker-Jensen et al., 2010; Dantuma & van Attikum, 2016). During NER, STUbL RNF111 recognizes SUMO on the UV-light lesion sensor XPC and adds a polyubiquitin chain to it (Sugasawa et al., 2005). This leads to the removal of XPC from the DNA lesion and creates space for downstream repair proteins. Another crucial, and possibly the best-studied, DDR-induced ubiquitylation and sumoylation regulate PCNA binding to substrates (Figure 4). At the stalled replication fork, monoubiquitylation, K63-linked polyubiquitylation, or the SUMOylation of PCNA leads either to error-prone TLS or to an error-free post-replicative repair mechanism (García-Rodríguez, Wong, & Ulrich, 2016; Stelter & Ulrich, 2003; H. Ulrich & Jentsch, 2000). PCNA can, depending on its modification state, also recruit NER, BER, and MMR factors and initiate other pathways (Ciccia & Elledge, 2010; H. D. Ulrich, 2012).

Poly-ADP-ribose (PAR) chains, catalyzed by the PARP protein family, facilitate the recognition and recruitment of many factors to photolesions, SSBs, and DSBs (Dantuma & van Attikum, 2016). PARylation modifies chromatin during DDR. ALC1 and CHD4, chromatin remodeling complexes, and the histone variant macro H2A rely on PAR for transient chromatin de-condensation (Polo & Jackson, 2011). For example, rapid PARP1/2 activation at DSBs contributes to MRN recruitment and DNA lesion recognition (Ciccia & Elledge, 2010). PARP1 activation at SSBs brings XRCC1 and LIG3 to the lesion. Due to its relatively short half-life, PARylation is thought to be more transient than the modifications described above. This modification also mediates the release of the histone chaperone complex FACT, involved in chromatin remodeling, during transcription.

DDR also relies on histone methylation and acetylation mediated by chromatin modifiers. Typically, histone 3 lysine 9 (H3K9) methyltransferase SUV39H1 comes rapidly to DSB, binds H3K9me3, and provides a platform for KAP1/HP1 binding and the spread of methylation (Dantuma & van Attikum, 2016). This enhances BRCA1 activity at DNA damage sites. Upon ATM phosphorylation, KAP1 is released, allowing

access for other proteins. Next, acetyltransferase TIP60 binds H3K9me3 and leads to H4K16 and ATM acetylation. The H4K16 acetylation directs methylation on it that will be recognized by 53BP1, and ATM acetylation further enhances its activity toward checkpoint signaling and repair. Acetylation is a tightly regulated process that includes several histone acetyltransferases (TIP60, GCN5, HAT, PCAF) and deacetylases (HDAC1/2/4, SIRT1/6) (Polo & Jackson, 2011). For example, H3K56 deacetylation by HDAC1/2 recruits NHEJ factors to DSBs. On the other hand, the binding of SIRT1 leads to NBS1 (a component of the MRN complex) and CtIP deacetylation, which stimulates RPA and RAD51 binding to DSBs and hence repair through HR.

1.3 Interplay between RNA metabolism and DDR

The exposure of human cells to UV-light induces the formation of bulky UV photoproducts that interfere with DNA replication and transcription (Marteijn, Lans, Vermeulen, & Hoeijmakers, 2014). To maintain genome stability, cells must coordinate DNA repair with cell cycle progression, DNA replication, and RNA metabolism. High throughput approaches, including functional genetic screens and mass spectrometry-based proteomics, have greatly helped to reveal the intricacy of DDR (Beli et al., 2012; Matsuoka et al., 2007; Paulsen et al., 2009). Recent studies employing these approaches have demonstrated that DDR involves hundreds of proteins functioning in different cellular processes, beyond DNA repair and cell cycle regulation. A pervading finding that has emerged from recent studies is the involvement of RNA-binding proteins (RBPs) in DDR, which suggests a tight interplay between the cellular response to DNA damage and the regulation of RNA metabolism.

1.3.1 General mechanism of transcription

Transcription is a highly coordinated process that includes initiation, promoter escape, elongation, and termination (Figure 5). In brief, transcription initiation begins with the recognition of the region upstream of the promoter by general transcription factors and the positioning of RNA polymerase, forming a pre-initiation complex (Thomas & Chiang, 2006). The pre-initiation complex consists of TFIIA, TFIIB, TFIID, TFIIE, TFIIF, TFIIH, and RNA polymerase 2 (RNA pol 2) in the case of eukaryotic mRNA transcription. In the next step, RNA pol 2 unwinds the DNA. After an iterative transcription of a small DNA region with the synthesis of short RNAs, RNA pol 2 escapes the promoter with a transcript longer than ten nucleotides (nt) and enters the elongation phase. The phosphorylation of the carboxy-terminal domain (CTD) of RNA pol 2 regulates the escape and transition into elongation. The CTD contains heptapeptide repeats: Tyr-Ser-Pro-Thr-Ser-Pro-Ser and the number of repeats vary between species. There are 27 repeats in yeast and 52 in humans (Watson et al., 2013). RNA pol 2 in the pre-initiation complex has unphosphorylated CTD, while phosphorylation on S5 of the CTD leads to escape from the promoter.

Introduction

As the elongation phase begins, proteins involved in initiation are exchanged with elongation and RNA processing factors, such as the capping complex that protects RNA from degradation (Watson et al., 2013). These proteins are recruited through the phosphorylated CTD. Shortly after the beginning of elongation, RNA pol 2 complex, with a 40–60 nt-long transcript, is paused, and this halt in transcription is called promoter-proximal pausing (PPP). At this stage, several factors hold RNA pol 2 in the so-called elongation checkpoint, where transcription has ceased but RNA pol 2 is "poised" to continue immediately upon the receipt of appropriate stimuli (Kwak & Lis, 2013; Narita et al., 2007; Yamaguchi, Shibata, & Handa, 2013).

The primary pausing factor is the NELF complex, which inhibits the transcriptional elongation of RNA pol 2 in Drosophila and mammalian cells (Zhou, Li, & Price, 2012). The complex consists of four subunits: NELFA/WHSC2, NELFB/COBRRA1, NELFC/D/TH1, and NELFE/RDBP (Narita et al., 2003). Structural studies have demonstrated that the NELF complex assembles in two steps (Figure 6). First, NELFA, with NELFD/C, and NELFB, with NELFE, form stable subcomplexes. Second, the interaction of NELFB and NELFC/D leads to the full complex assembly. In terms of chromatin binding, NELFB and NELFC can bind single-stranded oligonucleotides *in vitro,* and NELFE has an RNA-binding domain (Vos et al., 2016). The assembled complex interacts with RNA pol 2 through the polymerase association

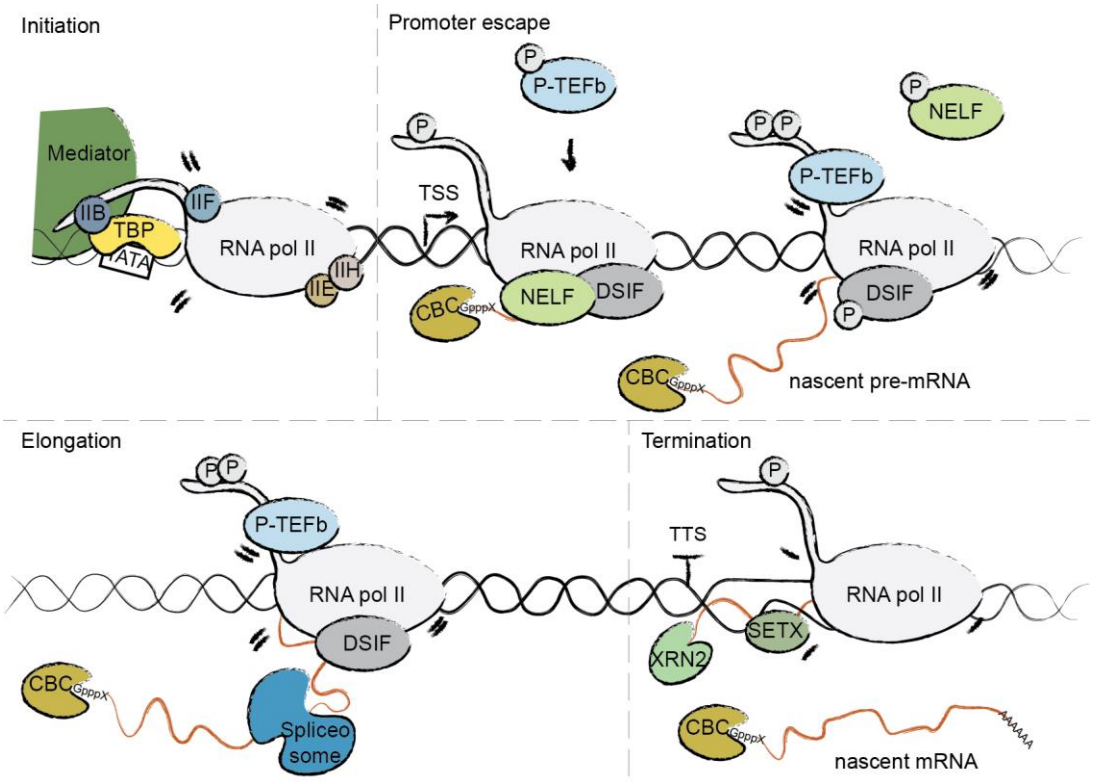

Figure 5. Schematic overview of the transcription steps. *The preinitiation complex that recognizes and assembles on the upstream promoter region initiates transcription. RNA pol 2 binds to it and begins transcription with the help of the mediator complex. Shortly after the promoter (TSS), the RNA pol 2 is paused by the negative elongation factor (NELF) complex and the DRB sensitivity-inducing factor (DSIF), which directly bind to 5' end of the nascent mRNA and regulate the recruitment of the RNA-modifying proteins. The effective elongation is started by the positive transcription elongation factor b (P-TEFb), which phosphorylates NELF, DSIF, and RNA pol 2. During elongation, mRNA is processed directly by the splicing machinery and is released from RNA pol 2 as soon as it runs on PolyA signal sequence (TTS). Adapted from* Loman & Watson, 2013; Orphanides & Reinberg, 2002; Skalska, Beltran-Nebot, Ule, & Jenner, 2017.

domain on NELFA and through the short nascent RNA (Vos et al., 2016; Vos, Farnung, Urlaub, & Cramer, 2018). The knockdown of one of the NELF subunits affects the stability of the others and the binding to RNA pol 2 (Vos et al., 2016).

The pausing is released by the P-TEFb kinase complex, composed of Cdk9 and Cyclin T, when it phosphorylates S2 on the CTD and NELF, together with other factors. PPP has been shown to be a crucial regulatory step for the expression of many genes and seems to be crucial for developmental and stress-induced genes (L. H. Williams et al., 2015). The NELF release from chromatin results in RNA pol 2 proceeding into effective elongation. Simultaneously, components of the splicing machinery bind to RNA pol 2 and, as such, the machinery enters a productive elongation phase and transcribes the entire gene. The average elongation rate is estimated as 1–5 kilobases per minute in mammals (Ardehali & Lis, 2009).

After successful elongation, at the 3' end of the gene, RNA pol 2 encounters the poly-A signal. Once transcribed into RNA, the signal induces the cleavage of the synthesized pre-mRNA and therefore the termination of transcription (Watson et al., 2013). In one model, RNA pol 2 remains bound to DNA and continues transcribing (Watson et al., 2013). The 5' end of the second RNA remains uncapped, which leads to its degradation with a 5'-3' exonuclease and to actual termination. In the other model, RNA pol 2 transcribes after the poly-A site much more slowly, and allosteric modifications in the polymerase lead to its dissociation. As the second RNA is left uncapped, and without the poly-A signal, 5'-3' exonuclease degrades the RNA soon after recognition (Watson et al., 2013).

1.3.2 Regulation of transcription after UV-light-induced DNA damage

Globally, transcription almost immediately ceases, even of undamaged genes, after exposure to UV-light. This is likely to provide space to repair proteins and to prevent collisions between repair and transcription machinery, which would lead to more damage (Boeing et al., 2016; Rockx et al., 2000). GRO-seq analysis after exposure to UV-light has demonstrated that no transcription changes occurred after ten minutes post-radiation (Gregersen & Svejstrup, 2018). Transcription elongation slows down dramatically after ten minutes and maintains the rate up to 25 minutes

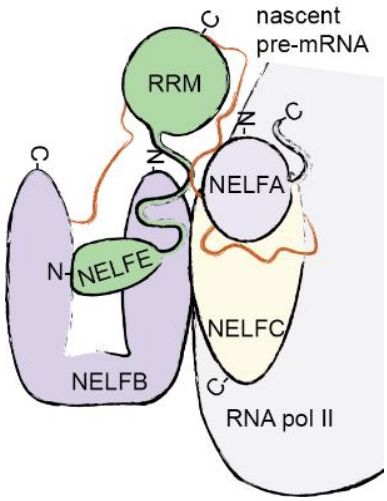

Figure 6. Model of NELF complex organization and binding to RNA and RNA pol 2. *Pairs of NELF subunits, NELFA with C and NELFB with E, form stable complexes and bind to each other through the interaction of NELFB and C. Subunit B holds E between the N- and C-termini. The predicted RNA-recognizing motif (RRM) of NELFE loosely connects to the entire complex. All subunits, except NELFA, bind short nascent pre-mRNA exiting RNA pol 2, NELFA is predicted to interact with the RNA pol 2. The C- and N-termini are depicted for each NELF complex subunit. The NELFA N-terminus is placed behind the protein. Adapted from Vos et al. 2016 and 2018.*

after exposure to UV-light. Simultaneously, RNA pol 2 is released from the PPP, which leads to a global loss of the RNA pol 2 hypophosphorylated form (Gregersen & Svejstrup, 2018). However, transcription does not completely cease; the post-UV-light elongation rate slows to 0.47 kb/min, in comparison to 1.77 kb/min in untreated cells (Williamson et al., 2017). Transcription recovers in two phases. First, transcription initiation recovers while the elongation rate decreases further. At this state, only for short fragments (20–25kb), elongation has been observed (Andrade-Lima, Veloso, Paulsen, Menck, & Ljungman, 2015; Williamson et al., 2017). At the next phase, transcriptional elongation is restored completely after 48 hours post-radiation.

Interestingly, for UV-light-induced DNA damage, as mentioned above, transcription must, on the one hand, be shut down and, on the other hand, be upregulated to express certain DDR factors and proteins that promote cell survival. UV-light-induced DNA damage has been demonstrated to activate transcription factors, in particular, p53. The last one activates the transcription of p21 and, for instance, leads to cell cycle arrest (Mansilla et al., 2013). In p53-deficient cells, UV-light has been shown to cause the activation of the nuclear factor-κB (NF-κB) and activator protein-1 (AP-1) (Cooper & Bowden, 2007). All three transcription factors regulate the expression of genes involved in cell proliferation, cell differentiation, and cell survival.

Locally, DNA damage transiently blocks transcription elongation and the arresting of RNA pol 2 induces TC-NER (Lans et al., 2010). RNA pol 2 should be removed or translocated for successful repair when it is stopped at the lesion. These events are tightly regulated by PTMs. Polyubiquitylation can lead to RNA pol 2 release from DNA and subsequent degradation. This pathway is the major mechanism for RNA pol 2 dislocation. In mammals, it is considered the “last resort” (Gregersen & Svejstrup, 2018). In addition, ubiquitylation can occur during a number of events to pause transcription, even in untreated cells (Wilson, Harreman, & Svejstrup, 2013). Conversely, RNA pol 2 can be translocated either forward or backward. The mammalian CSB, which also participates in DNA damage recognition, might translocate the RNA pol II forward from the lesion, as has been demonstrated in bacteria (Chiou, Hu, Sancar, & Selby, 2018). In mammalian cells, it is more probable that TFIIH releases the dual excision product and “backs up” RNA pol II. Crucially, RNA pol II can proceed with elongation after adduct removal (Chiou et al., 2018; Gregersen & Svejstrup, 2018). The DDR-induced decrease of transcription elongation causes mRNA polyadenylation and transcriptional termination (Gregersen & Svejstrup, 2018), which promotes alternative polyadenylation and preliminary termination, leading to shorter RNA production (Di Giammartino, Nishida, & Manley, 2011).

The components of the repair machinery also play a role in the regulation of transcription. For example, the induction of DNA damage by DDR factors (e.g., XPC, XPG, XPF) is crucial in hormone-inducible gene activation (e.g., RARβ2). At first, DNA topoisomerase IIβ facilitates DSB formation and recruits DDR factors. Subsequently, in addition to gap repair, the proteins stimulate the binding of a set of proteins, such as CTCF, that regulate the 3D chromatin structure and growth arrest and DDR-activated

protein GADD45A that coordinate DNA methylation (Fong, Cattoglio, & Tjian, 2013; Wickramasinghe & Venkitaraman, 2016). Moreover, several proteins are involved both in DNA repair and transcription. The general transcription factors TFIIH and TFIID (including XPG and XPD) function in transcription initiation and are also components of NER (Thomas & Chiang, 2006). In addition, upon DDR induction, a set of RNA processing factors regulates specific genes involved in DNA replication, DNA repair, and cell cycle, such as RAD9, PARP1, BRCA1, ATM, and TP53 by inducing their transcription or stabilizing the transcripts (Blazek et al., 2011). In addition, it has been reported that non-coding RNAs of approximately 21 nt are transcribed after DSB induction, possibly to recruit downstream proteins to the lesions (Chowdhury, Choi, & Brault, 2013; Ohle et al., 2016).

1.3.2 Splicing regulation after UV-light-induced DNA damage

The immediate product of transcription is pre-mRNA, which matures through the cutting out of introns and the joining of exons in a process called splicing, catalyzed by the spliceosome (Shkreta & Chabot, 2015). This complex includes five small nuclear ribonucleoproteins (snRNPs), U1, U2, U4, U5, and U6, and a number of accessory proteins. First, the snRNPs and the accessory proteins define the borders of the splice region: U1 and U2 snRNPs and U2AF recognize the 5' and 3' splice sites and the branching point adenosine, respectively. U6 and U2 snRNPs form the catalytical core with the help of U1 and U4 snRNPs and a set of non-snRNP proteins. These rearrangements produce a free 5' exon and the linkage of the free end of the intron to the 3' exon, forming the so-called lariat intermediate. Second, catalytical core changes lead to the intron lariat excision, and the exons bind to each other, forming mature mRNA. Two types of splicing can be distinguished. Constitutive or unregulated splicing relies only on the spliceosome and splices pre-mRNA uniformly. Alternative splicing requires additional factors, and some exons can be excluded or included in the final transcript. Serine-arginine (SR) factors enhance constitutive and alternative splicing, in addition to regulating transcription (Montecucco & Biamonti, 2013). In contrast, heterogeneous nuclear ribonucleoproteins (hnRNPs) prevent spliceosome binding to splice sites (Montecucco & Biamonti, 2013).

The activation of DDR affects splicing efficiency and decisions. Generally, UV-light damage has been shown to alter transcription elongation and to lead to spliceosome mobilization and the induction of alternative splicing (Lans, Marteijn, & Vermeulen, 2012). In particular, UV-light radiation leads to more frequent inclusions of "weak" exons. It has been demonstrated that UV-light induces the inclusion of the pro-apoptotic mRNA isoforms of Bcl-x and caspase 9 (M. J. Muñoz et al., 2009). The observed alternative splicing requires TC-NER and subsequent ATR activation, which slows elongation at the adduct-containing region. This contrasts with previous studies with apoptosis-inducers, in which the ATM-CHEK2-p53 pathway was demonstrated to phosphorylate SR splicing factors and guide the splicing of the Bcl-x and caspase 9 mRNA toward the pro-apoptotic forms (Montecucco & Biamonti, 2013).

In response to IR, etoposide, MMS, and HU, the ATM phosphorylation-dependent binding of BRCA1 to hnRNP, BCLAF1 promotes the formation of a damage-induced mRNA splicing complex (Vohhodina et al., 2017). This complex regulates the splicing of the transcripts of genome maintenance factors, such as ATRIP and EXO1 (Savage et al., 2014). Likewise, the Ewing sarcoma protein EWS, which binds constitutively to pre-mRNA during alternative splicing, dissociates from CHEK2 pre-mRNA after UV-light exposure (Paronetto, Miñana, & Valcárcel, 2011). Moreover, in response to DNA damage induced by IR or etoposide, ATM/ATR/DNA-PKcs phosphorylate the protein phosphatase PPM1G that promotes pre-mRNA splicing and is localized to DNA damage sites in the activated form (Beli et al., 2012). ATM phosphorylates RNA processing and the stability factor THRAP3 after IR and leads to the exclusion of the protein to DNA damage sites, together with its binding protein BCLAF1 (Beli et al., 2012). Together, they guide selective mRNA splicing and the export of transcripts of DDR factors, such as ATM (Vohhodina et al., 2017).

1.3.3 Regulation of mRNA stability and translation after UV-light-induced DNA damage

At the moment when mRNA is capped, spliced, and polyadenylated, it can be transported from the nucleus to the cytoplasm (Watson et al., 2013). The movement is an active process, which includes quality control and destination labeling.

RNA stability is strongly dependent upon RBPs (Montecucco & Biamonti, 2013). As an example, in untreated cells, GADD45α mRNA is bound with two negative regulating RBPs, protein leading mRNA to degradation AUF1, and a protein inhibiting binding with translation machinery TIAR. UV-light exposure dramatically decreases interaction between GADD45α and RBPs, resulting in GADD45α production (Reinhardt, Cannell, Morandell, & Yaffe, 2011). A quality control is already performed during the splicing phase, with the help of SR and hnRNP proteins, which envelope the matured mRNA and guide mRNA to the export factor NXF1 (Müller-McNicoll et al., 2016).

Finally, mRNA is translated into protein with the help of tRNAs, aminoacyl-tRNA synthetase, and the ribosome that is composed of rRNAs and ribosomal proteins. Despite the majority of DDR factors needing to be first produced for DDR, the translation machinery is predominantly inhibited after UV-light exposure (Powley et al., 2009). The translation that still works under such conditions is initiated through alternative mechanisms, such as a cap-independent mechanism. The UV-light-initiated mRNAs predominantly encode the proteins required for the stress response (Powley et al., 2009). This process is regulated by an initiation factor, eIF2α, that binds to one of the subunits of the ribosome and regulates the assembly of the translation complex on mRNA. UV-light has been demonstrated to result in eIF2α phosphorylation that is DNA-PKcs-dependent (Deng et al., 2002; Powley et al., 2009). In addition, a quantitative proteomics study demonstrated that the ubiquitylation of ribosome subunits leads to the shutting down of translation after doxorubicin-induced DNA damage (Halim et al., 2018).

As mentioned above, mounting evidence suggests an interplay between DNA damage and the distinct steps of RNA metabolism. However, a detailed understanding of how DNA damage caused by UV-light affects RNA processing is still lacking.

1.4 Mitogen-activated protein kinases

MAPKs phosphorylate proteins on Ser/Thr residues and transmit the extracellular stimuli from membrane receptors into cells, inducing a wide range of responses (Cargnello & Roux, 2011). The signaling pathway consists of the evolutionarily conserved cascade of a MAPK, a MAPK kinase (MAP2K), and a MAPK kinase kinase (MAP3K) (Figure 7). Upon stimulation, a small GTP-binding protein of the Ras/Rho family phosphorylates MAP3K. This leads to the phosphorylation of the MAP2K kinase, which then stimulates MAPK. The activity of MAPKs depends on the dual phosphorylation of Thr and Tyr within a conserved Thr-X-Tyr motif, called the activation loop.

1.4.1 p38 MAPK

In mammals, MAPKs consist of seven groups, including an evolutionary conserved p38 MAPK (Cuadrado & Nebreda, 2010). In budding yeast, p38 MAPK is homologous to the product of the *hog1* gene. In mammals, the p38 MAPK family includes four homologs: p38α (MAPK14), p38β (MAPK11), p38γ (MAPK12), and p38δ (MAPK13). They share 60% identity in their amino acid sequences and are activated through the phosphorylation of the activation loop sequence T180-G181-Y182. It appears that the phosphorylation on Y180 plays a more crucial role in kinase activation; whereas phosphorylation on Y182 is crucial for stabilization with substrates and autophosphorylation (Cargnello & Roux, 2011). The p38 MAPK members form subgroups as well: p38α and p38β share 70% similarity, whereas p38γ and p38δ share 75% similarity. (Escós, Risco, Alsina-Beauchamp, & Cuenda, 2016). The latter

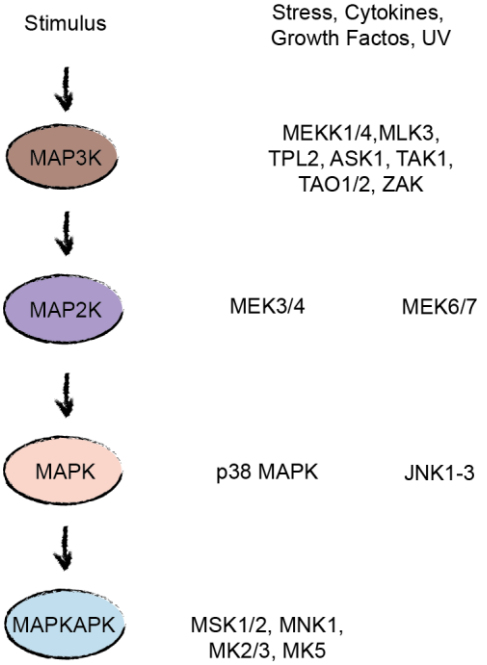

Figure 7. MAPK signaling cascade. *Different stimuli phosphorylate MAP3K, which, after its activation, passes the signal to MAP2K. Finally, MAPK and MAPKAPK are activated sequentially. On the right side are kinases that lead to the activation of p38 MAPK and its very close partner JNK. p38 MAPK, upon activation, phosphorylates MSK1/2, MNK1, MK2/3, and MK2. Adapted from* Cargnello & Roux, 2011.

subgroup also behaves differently toward inhibitors. SB203580 is a pyridinyl imidazole compound that competitively binds to the ATP pocket of MAPKs that specifically inhibits p38α and p38β (Cuadrado & Nebreda, 2010). BIRB796 is an allosteric inhibitor, with less specificity, and it preferably inhibits p38α and p38β. However, in high concentrations, it can inactivate the other two as well. p38α responds the most to stimuli, and it is more abundantly expressed in mammalian cells than the other homologs (Cargnello & Roux, 2011). Although the p38 MAPK family members overlap in substrates, each member possesses some specificity, and some of the substrates are more likely to be phosphorylated by p38α and p38β, rather than the other two. In case one of the four is absent, the others can functionally replace it (Cargnello & Roux, 2011).

Various environmental stresses and inflammatory cytokines activate p38 MAPKs, such as oxidative stress, hypoxia, ischemia, interleukin-1 (IL-1), tumor necrosis factor alpha (TNF-α), and UV-light irradiation (Cargnello & Roux, 2011). The MAPK activation cascade begins with MAP3Ks phosphorylation, which include MEKK1-3(MAP3K1-3), MLK2/3 (MAP3K10/11), ASK1 (MAP3K5), TPL2 (MAP3K8), TAK1 (MAP3K7), TAO1/2, and ZAK1 (Cargnello & Roux, 2011; Cuadrado & Nebreda, 2010). Several MAP3Ks respond to specific stimuli. For example, ASK1 phosphorylates p38α upon oxidative stress in mammalian cells; TAK1 phosphorylation strongly depends on the TRAF family of E3 ubiquitin ligases that act upon TNF-α or IL-1 stimulation (Cargnello & Roux, 2011). In Drosophila cells, after UV-light or peptidoglycan treatment, MEKK1 controls the activation of p38 MAPKs. In addition, the heat shock response requires both MEKK1 and ASK1. These kinases further activate MKK3 and MKK6, which are the primary MAPK kinase activators of p38 MAPKs. MKK6 phosphorylates all p38 MAPK homologs, whereas MKK3 specifically targets p38α, p38β, and p38γ. In addition, p38α can also be phosphorylated by MKK4, which is, in fact, the canonical activator of another MAPK, JNK (Cargnello & Roux, 2011; Cuadrado & Nebreda, 2010). Yet another non-canonical p38 MAPK activation pathway depends on the T-cell receptor (TCR)-proximal kinase ZAP70, together with $p56^{lck}$, which phosphorylates p38α on Y323 and therefore promotes autophosphorylation on the activation loop. Conversely, GADD45α inhibits this activity in T-cells toward Y323 phosphorylation (Cargnello & Roux, 2011).

The activated p38 MAPKs phosphorylate also further targets other downstream kinases, expanding the signaling response. A number of p38 MAPK substrates involved in various cellular processes have been identified in studies using various stimuli to activate the kinase. For example, proteins involved in gene transcription (CREB, p65, p53, SRF, STAT1, and STAT3), mRNA translation (eIF4E and eIF4G), cell cycle control (CDC25B and CDC25C), chromatin (histone H3) and actin remodeling, and cell migration (vimentin, Hsp25/27, CapZIP, and β-crystallin) have been identified as common p38 MAPK substrates (Cargnello & Roux, 2011).

UV-light can activate p38 MAPK directly or via the generation of ROS. Most crucially, p38 MAPK establishes G2/M checkpoint arrest via CDC25B and CDC25C phosphorylation (Reinhardt & Yaffe, 2009). CDC25s are phosphatases that

dephosphorylate CDKs and allow checkpoint transition. The arrest of the cell cycle occurs at G2/M when CDK2-cyclin B is phosphorylated and both CDC25B and CDC25C are sequestered from the nucleus (Bulavin et al., 2001; Cuadrado & Nebreda, 2010). Another cell cycle regulation point induced by UV-light irradiation has been demonstrated through GADD45 p38-dependent phosphorylation, which leads to CDC2-cyclinB complex disruption and therefore the inactivation of the complex and cell cycle arrest (Jinlian, Yingbin, & Chunbo, 2007). Indirectly, p38 MAPK affects the cell cycle through the activation of the tumor suppressor p53, which induces the transcription of a number of genes regulating cell cycle, such as p21 and Gadd45 (Reinhardt & Yaffe, 2009). p21 is required during UV-light-response-establishing G1 checkpoint arrest by inhibiting CDK2-cyclin A. p38 MAPK also influences transcription by histone H3 phosphorylation and therefore opens chromatin. H3 phosphorylation is used to open chromatin around bulky lesions, allowing NER factors to land (DDB2, XPC) (Cargnello & Roux, 2011). p38 MAPK is also responsible for some splicing factors, shuttling between nucleus and cytoplasm. Examples of this include hnRNPA1, together with captured mRNA, accumulating in cytoplasmic stress granules after being phosphorylated by p38-MNK1/2 (Montecucco & Biamonti, 2013). hnRNPA1 is also crucial for the transport of miRNA, which forms the RNA-induced silencing complex (Jean-Philippe, Paz, & Caputi, 2013). The p38-MK2 signaling pathway regulates mRNA translation by the phosphorylation of hnRNPA0, T-cell-restricted intracellular antigen 1-related protein TIAR, and polyA-specific ribonuclease (PARN) (Montecucco & Biamonti, 2013). This also stabilizes 3'-AU-rich mRNAs.

1.4.2 p38 MAPK phosphatases

The MAPK pathways are tightly regulated by phosphatases. MAPK phosphatases (MKPs) or dual-specificity phosphatases (DUSPs) regulate MAPK inactivation (Cuadrado & Nebreda, 2010). They remove phosphates from both residues (T180, Y182) in the activation loop of p38 MAPKs. It has been demonstrated that MKP1/DUSP1, MKP5/DUSP10, MKP7/DUSP16, and DUSP8 can dephosphorylate p38α and p38β MAPKs. Most MKPs share phosphatase activity toward p38 MAPKs as well as to ERK, another large MAPK family (Caunt & Keyse, 2013). Interestingly, signals activating MAPKs upregulate the expression of MKPs, forming a negative feedback loop and limiting p38 MAPK response (Cuadrado & Nebreda, 2010). In addition to MKPs/DUSPs, the protein phosphatase (PP) 2A and PP2C families can regulate p38 MAPKs by the removal of one phosphate from the activation loop. WIP1/PPM1D, the member of the PP2C family, for example, deactivates p38α and hence inhibits the p53 pathway in response to UV-light (Cuadrado & Nebreda, 2010). The UV-light response leads to the p38-dependent activation of MKP1, which dephosphorylates JNK and therefore represses apoptosis (Caunt & Keyse, 2013). The function of the MKPs that target p38 MAPK after UV-light exposure has not been intensively investigated and remains unclear.

1.4.3 MAPK-activated protein kinase family

Further down the cascade, p38 MAPK activation leads to the phosphorylation of the MAPK-activated protein kinase (MAPKAPK) family. Mitogens and stress stimuli activate mitogen- and stress-activated kinases 1 and 2 (MSK1/2) via p38 MAPK and another MAPK, ERK1/2 (Cargnello & Roux, 2011). In addition, UV-light irradiation activates MSK1 via casein kinase 2 (CK2) phosphorylation. Both MSK1 and 2 are similarly abundant in cells and are more expressed in the brain, heart, placenta, and skeletal muscle. They contain two independent kinase domains on the C- and N-termini (CTKD and NTKD), where CTKD is required for the MAPK interaction and activation. In addition, MSK1/2 possesses a nuclear localization signal (NLS) and therefore functions exclusively in the nucleus. MSK1/2 regulates many transcription factors; for example, it phosphorylates ATF1, CREB, and p65 (a subunit of NF-κB). The activation of these transcription factors initiates the expression of several immediate-early genes, such as c-Fos, JunB, and Egr1, in response to extracellular stimuli. Upon exposure to UV-light, MSK1 phosphorylates STAT3 in keratinocytes and fibroblasts (Bito et al., 2010). Moreover, MSK1/2 can phosphorylate the histone H3, limiting the spread of heterochromatin and activating the transcription of genes (Cargnello & Roux, 2011).

Both splice isoforms of MNK1, A and B, have been demonstrated to have basal activity in unstimulated cells; this activity is affected by p38 MAPK and/or ERK1/2 inhibition (Cargnello & Roux, 2011). MNK1 activity depends on the phosphorylation on T209, T214 (which forms the activation loop), and T344. The domain structure of MNK1 includes the NLS and CRM1 protein-mediated nuclear export signal (NES); hence, the protein shuttles between cytoplasm and nucleus. MNK1 regulates protein synthesis and mRNA processing. In particular, it phosphorylates the eukaryotic initiation factor eIF4E and interacts with eIF4G. Furthermore, the phosphorylation of the RBPs hnRNP, A1, and PSF appears to be dependent on active MNKs during T-cell activation.

After exposure to UV-light, heat shock, oxidative stress, hyperosmolarity, and cytokine stimulation, p38 MAPK has been shown to activate MK2/3 (Cargnello & Roux, 2011). Both vertebrate kinase genes, MK2 and MK3, are homologous to those in Drosophila *(MAPk-Ak2*) and *Caenorhabditis elegans (mak-2*). While the structural homologs are absent in yeast, Hog1 (p38 homolog) regulates Rck1/2 in budding yeast and Srk1/Mkp2 in fissifon yeast. MK2 shares 75% sequence identity with MK3, including two NLS and NES at the N-terminus. Interestingly, the export signal of the proteins is activated following phosphorylation on T334, increasing the cytoplasmic localization of the proteins. p38 MAPK phosphorylates MK2/3 on T222 in the activation loop, on T272 within in the kinase domain, and on T334, which regulates autoinhibition. The p38 MAPK phosphorylation of and interaction with MK2 stabilizes both p38 and MK2. Accordingly, MK2 level has been demonstrated to decrease after p38α knockdown (Cargnello & Roux, 2011). Both MK2 and MK3 recognize a similar set of substrates and regulate cytokine production, gene expression, the cell cycle, and cytoskeleton remodeling. Analysis of MK2 and MK3 substrates has revealed a potential motif for recognition: Rx[LN][ST][ILFV]x (Yaffe et al., 1997). Among the

substrates of MK2/3, components of the polycomb complexes have been identified. For instance, HPH2 and BMI1, which are part of the PRC1 complex, have been found to be MK2/3-phosphorylated after stimulation with arsenite or UV-light and to be bound to chromatin mediating tumor gene repression (Cargnello & Roux, 2011). Interestingly, MK2 tends to indicate higher activity in cells (Ronkina et al., 2010). MK3 knockdown affects cell functions non-significantly, and it seems to partially compensate for the lack of MK2, in the case of MK2 deficiency. For instance, the MK2-dependent phosphorylation of SRF and ER81 stimulates their interactions with other factors or DNA and induces the transcription of genes, in particular early, tissue-specific genes or those crucial for development (Cargnello & Roux, 2011). Moreover, MK2 can phosphorylate targets of other kinases with lower affinity, for example, CREB, the MSK1/2 substrate. During the UV-light response, MK2, passing the signal from p38 MAPK, regulates the cell cycle by establishing the G2/M checkpoint through the phosphatases CDC25B and CDC25C phosphorylation (Christian Reinhardt & Yaffe, 2013). Globally, the p38-MK2 axis is required for proper inflammatory response, which motivated the development of MK2 inhibitors (Fiore, Forli, & Manetti, 2016). PF-3644022 is an ATP-competitive molecule that is reported to selectively and reversibly inhibit MK2 (Fiore et al., 2016). However, MK2, MK3, and MK5 demonstrate structural similarity, and the inhibitor can inactivate each to a varying extent (Gaestel, Mengel, Bothe, & Asadullah, 2007).

Finally, MK5 is the MAPKAPK kinase with only 38% homology to MK2/3 (Cargnello & Roux, 2011). Structurally, MK5 contains an NLS and an NES as the other two kinases, but the NES is not regulated in a phosphorylation-dependent manner. Although the overexpression of p38 MAPK activates MK5, no evidence exists of an interaction between p38 MAPK and endogenous MK5. In line with this, traditional p38 MAPK activators, arsenite and sorbitol, do not activate MK5. Accordingly, ERK3/4 is thought to be the primary activator of MK5. Nevertheless, *in vitro* p38 MAPK can phosphorylate MK5 on T182, which is localized in the activation loop and is essential for kinase activity. Generally, little is known about this MAPKAPK. In several recent studies, MK5 was reported to regulate Ras-dependent senescence in fibroblasts and cytoskeletal remodeling (Cargnello & Roux, 2011).

1.4.4 JNK MAPK

Stimulation signals for p38 MAPK also activate the JNK MAP kinase family, which consists of three homologs, JNK1, JNK2, and JNK3 (Cargnello & Roux, 2011). They share 85% identity and are transcribed from three genes, resulting in more than ten distinct spliced forms. Whereas JNK1 and JNK2 are expressed in many tissues, JNK3 prevails in neurons, testes, and cardiac myocytes. JNK activation requires the dual phosphorylation in the Thr-Pro-Tyr triad in its activation loop that is performed by MAPKK, MKK4, and MKK7. Activated JNK can directly induce apoptosis or differentiation and re-localize from the cytoplasm to the nucleus, depending on the bound substrate (Zeke, Misheva, Reményi, & Bogoyevitch, 2016). In the nucleus, JNK can regulate gene expression, which subsequently regulates cell proliferation,

differentiation, survival, and apoptosis. The intensively studied substrate of JNK is c-Jun, which, following phosphorylation, forms the AP-1 complex with c-Fos and regulates early gene transcription (Cargnello & Roux, 2011; Weston & Davis, 2002). In addition, JNK phosphorylates transcription factors such as p53, ATF-2, NF-ATc1, STAT3, c-Myc, and JunB. Recently, JNK was shown to promote the repair of UV-light-induced photoproducts via a yet unknown mechanism that includes the phosphorylation of the microRNA biogenesis protein DGCR8 upon RNA pol 2 stalling(Calses et al., 2017).

1.5 14-3-3 protein family

The regulation of proteins by phosphorylation signaling depends on three classes of proteins: “writers”, “erasers”, and “readers”. The aforementioned kinases play the role of “writers” in cells, whereas phosphatases function as “erasers”. Typically, the recognition of proteins with phosphorylation is regulated by special domains in “reader” proteins. 14-3-3 proteins, proteins with WW, Polo-box, WD40, BRCT, and FHA domains can recognize the serine or threonine phosphorylation catalyzed by kinases activated upon DNA damage (Table 1) (Christian Reinhardt & Yaffe, 2013). For instance, the interaction between a protein containing a phospho-binding domain and its substrate regulates G1, S, and G2 checkpoints, checkpoint maintenance, and the localization of signaling molecules during DDR (Christian Reinhardt & Yaffe, 2013).

The 14-3-3 family was the first to be identified as phosphoserine/phosphothreonine binding (Mohammad & Yaffe, 2009). The proteins are conserved and highly expressed in eukaryotic cells. In humans, the family includes seven homologs: 14-3-3β/YWHAB, 14-3-3ε/YWHAE, 14-3-3γ/YWHAG, 14-3-3η/YWHAH, 14-3-3θ/YWHAQ, 14-3-3σ/YWHAS/SFN, and 14-3-3ξ/YWHAZ. All isotypes have high homology to each other and frequently play redundant roles, although some possess a function that is more homolog specific (Figure 8).

Table 1. Phospho-recognition domains and their binding motifs, kinases recognizing the motif and regulating DDR, and examples of proteins with these domains (Christian Reinhardt & Yaffe, 2013; Mohammad & Yaffe, 2009)..

Domain	Motif	Kinase	Example Protein
14-3-3	RSxp[ST]xP Rxxxp[ST]xP	CHEK1/CHEK2/MK2	14-3-3ε
BRCT	pSxxφ pSxxφ-COOH	ATM/ATR/DNA-PK	BRCA1
FHA	pTxxF pTxx[IL]	–	RNF8
WW	[AP]PP[AP]pY p[ST]P	–	NEDD4
Polo-box	Sp[ST][Px]	CHEK1/CHEK2	PLK1
WD40	DpSGφxpS L[ILP]pTP	–	$SCF^{\beta TrCP}$

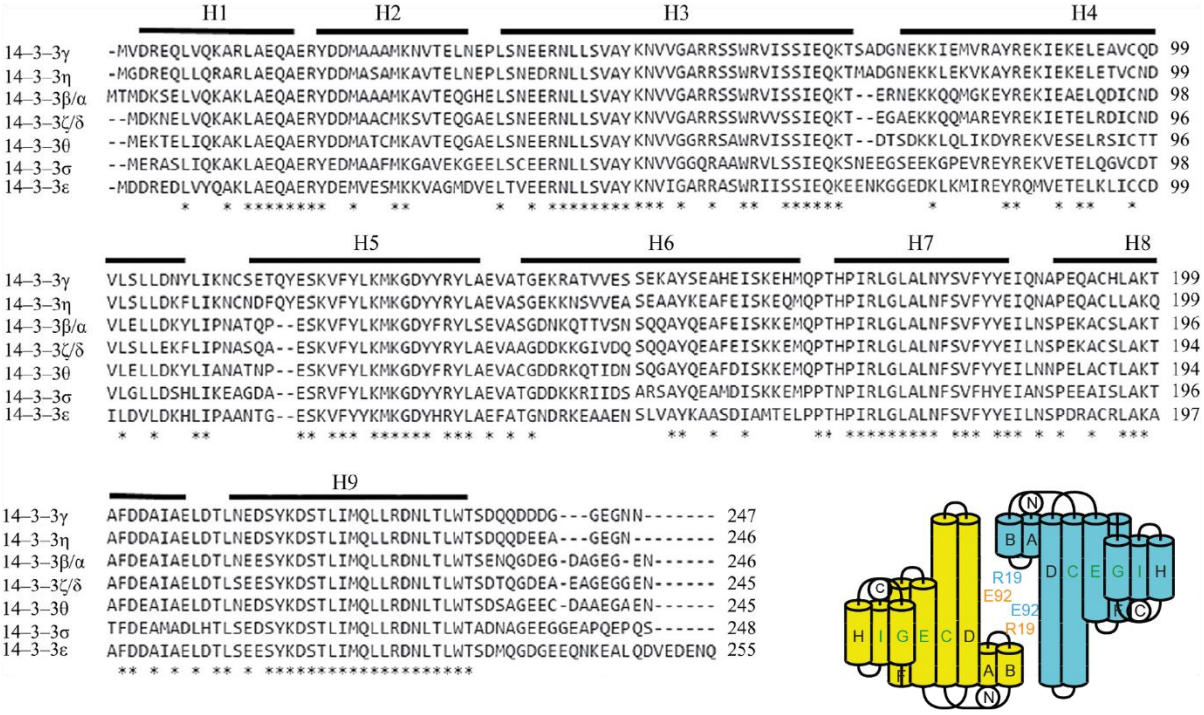

Figure 8. The structure of 14-3-3 homologs. *Multiple sequence alignment of seven 14-3-3 homologs. Asterisks indicate identical residues across the seven sequences. Solid bars indicate the position of nine conserved α-helices* (Babula & Liu, 2015)*. Topology diagrams of the 14-3-3 epsilon as an example (right bottom panel). Topology diagrams were prepared with TopDraw.*

Structurally, 14-3-3 represents the tetratrico peptide repeat superfamily, which generally possesses nine to ten α-helices and forms homo- or, more frequently, heterodimers from the cup-shaped monomers (Figure 9). The assembled complex recognizes two phosphorylated ligands on one or two proteins.

The domain structure of 14-3-3 includes NLS and has been shown to play a crucial role in the transport of bound substrates. Although the predicted motif for 14-3-3 recognition contains RSxp[ST]xP or Rxxxp[ST]xP, where x is any amino acid, a number of targets with non-canonical sequences exist (Madeira et al., 2015; Mohammad & Yaffe, 2009). For example, 14-3-3ξ can bind to p53 after ATM phosphorylation on the second S in KGQSTSRG of p53. This prevents the transcription of some targets of p53, such as apoptosis genes (Waterman, Stavridi, Waterman, & Halazonetis, 1998). Conversely, the 14-3-3 family promotes apoptosis via interacting with the apoptosis signal-regulating kinase (ASK1), the pro-apoptotic protein BAD, and several other proteins (Dougherty & Morrison, 2004). Hence, the primary and well-studied role of 14-3-3 is in the regulation of apoptosis. As the recognition motifs of 14-3-3 and p38 are similar; general stress, and developmental, and DNA damage-inducing stimuli promote substrates for 14-3-3 through the p38 MAPK activation. For example, STAT3 is phosphorylated by p38 MAPK and can subsequently bind to 14-3-3. The interaction augments STAT3 nuclear localization and additionally stabilizes its phosphorylation, which leads to the inhibition of the cytokine expression (Han, Han, Jiao, & Jie, 2015). Therefore, STAT3 phosphorylation blocks both the production and sensing of inflammation and tumor development. In addition, 14-3-3 plays a crucial mitosis-specific role in translation. Its binding separates the translation initiation factor eIF4B from translating polysome, which changes the process from cap-dependent to

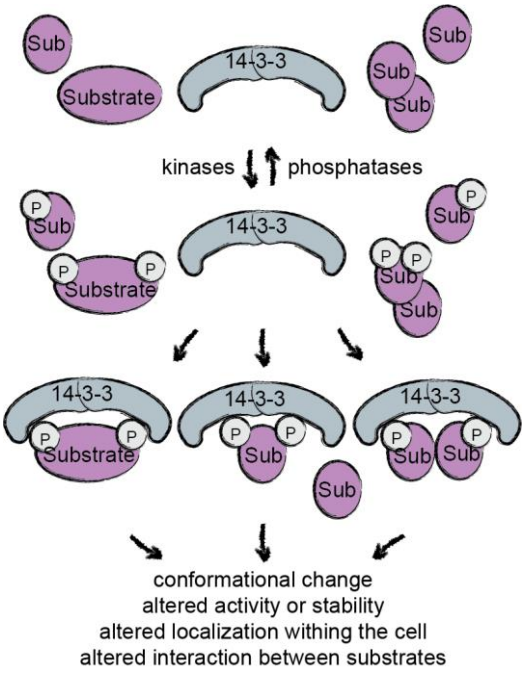

Figure 9. 14-3-3 interaction with substrate(s). *First, substrates as well as 14-3-3 itself must be phosphorylated by a kinase. The activated dimer of 14-3-3 binds to the phosphorylated substrate(s), regulating their function. In addition, this can prevent dephosphorylation by a phosphatase.*

cap-independent (Christian Reinhardt & Yaffe, 2013). As a result, the cap-independent form of CDK11 is translated, which promotes cytokinesis.

The 14-3-3 family plays a critical role in the chromatin-dependent regulation of transcription initiation and the elongation of a set of stimuli-induced genes. It has been demonstrated that Jun1, Fosl1, Cox-1, α-globin, Serpinb2, and heat shock genes, the transcription of which is induced by developmental or stress stimuli, require H3 phosphorylation in their promoter regions for activation. Histone 3 (H3) phosphorylation on S10 and S28 induces 14-3-3 binding, but the exact mechanism is still unclear (Healy, Khan, & Davie, 2011). Some studies have suggested the following possible mechanism: 14-3-3 has been found to interact with chromatin remodelers, SWI-SNF, and the histone acetyltransferase PCAF (Healy et al., 2011). MAPK signaling activation enriches H3, S10, and S28 phosphorylation in the promoter regions and consequently 14-3-3 recruitment, which in turn recruits chromatin remodelers. As a result, the pre-initiation complex accesses the promoter and begins transcription (Healy et al., 2011). The transcription elongation of heat shock genes has been demonstrated to require acetylation on H4K16, which is catalyzed by acetyltransferase MOF interacting with 14-3-3 (Healy et al., 2011). The acetylation serves as a platform for elongation complex recruitment along with P-TEFb and the release of RNA pol 2 from PPP (Healy et al., 2011).

As another example, 14-3-3 recognizes phosphorylated CDC25B and CDC25C due to p38-MK2 and ATR-CHEK1 activity during UV-light DDR at the late S and G2 phases (Christian Reinhardt & Yaffe, 2013). This interaction changes the localization of CDC25B and CDC25C to the cytoplasm. Subsequently, this event keeps CDK1-cyclin B inhibited and stops G2/M progression (Aghazadeh & Papadopoulos, 2016; Cargnello & Roux, 2011). Similarly, 14-3-3 regulates cell cycle progression through CDC25A phosphorylation during G1/S after IR (Manke et al., 2005). In this case, the activation of CHEK1 and CHEK2 are necessary.

Recent studies have described an overlap between the p38-MK2 signaling pathway substrates and 14-3-3 interactors after UV-light irradiation. A complex of proteins called NEXT, nuclear exosome targeting, degrade non-coding RNA. This complex has been demonstrated to interact with 14-3-3ε and 14-3-3ξ upon exposure to UV-light, which regulates the release and accumulation of captured RNA from promoter upstream transcripts and enhances cell survival via a currently unknown

mechanism (Blasius, Wagner, Choudhary, Bartek, & Jackson, 2014). Another UV-light-induced p38-MK2 target, the centriolar protein CP131/AZI1, which usually maintains centrosomal proteostasis, interacts with 14-3-3 and diffuses in the cytoplasm after stress induction (Tollenaere et al., 2015). Despite intensive studies being conducted on the role of 14-3-3 binding to phosphorylated proteins/interactors, no clear understanding yet exists of the p38-MK2-14-3-3 signaling pathway regulating the cellular response to UV-light.

In an interaction partner analyses of 14-3-3, many oncogenic factors have been identified; therefore, the mis-regulation of 14-3-3 proteins is suggested to lead to a higher probability of cancer (Aghazadeh & Papadopoulos, 2016). In line with this, 14-3-3 levels increase in lung, breast, prostate, myeloma, glioma, esophageal, head and neck, oral, pancreatic, ovarian, and skin cancers. 14-3-3γ and 14-3-3ε are used as markers in the hepatocellular carcinoma. In addition, lower levels of 14-3-3γ and 14-3-3θ have been identified in breast cancer; conversely, a higher amount of 14-3-3β has been detected in gastric cancer cells. Thus, 14-3-3 is acknowledged as a potential therapeutic target, and several compounds have been developed to distort the function. Difopein, the most frequently used polypeptide in the literature, blocks 14-3-3 binding sites and leads to the inactivation of 14-3-3 (Babula & Liu, 2015; Tollenaere et al., 2015). The chemical compound BV02 has a similar function (Valensin et al., 2016).

1.6 Aims of the study

UV-light radiation induces the formation of bulky photoproducts in the DNA that globally affects transcription and splicing. However, the signaling pathways and mechanisms that link UV-light-induced DNA damage to changes in RNA metabolism remain poorly understood. This study is designed to deepen the understanding of the cell response to UV-light irradiation.

The primary goal of the project is to decipher the role of the p38-MK2 pathway in UV-light-induced DDR. In particular, we employ quantitative phosphoproteomics and protein kinase inhibition to provide a systematic analysis of the protein phosphorylation patterns induced by UV-light and uncover the dependencies of phosphorylation events on canonical DNA damage signaling by ATM or ATR and the p38 MAP kinase pathway. In addition, we study how p38-dependent phosphorylation regulates transcription after genotoxic stress induced by UV-light through 14-3-3 binding, focusing on the transcriptional elongation regulator protein, NELFE. The provided datasets of UV-light-induced phosphorylation sites and the p38-dependent 14-3-3 interactions will enable further studies focusing on the functions of the p38-MK2 pathway in the regulation of different RNA metabolic processes after exposure to UV-light.

Results

2.1 Identification of p38-dependent phosphorylation sites

2.1.1 UV-light activates p38 MAPK signaling independently of canonical DNA damage signaling

To decipher the signaling downstream of the p38 MAP kinase activated after UV-light exposure, we employed quantitative phosphoproteomics. We first used western blotting to examine the dynamics of p38 MAPK activation after UV-light (40 J/m^2, UVC, one-hour recovery). We have tested various recovery times ranging from five minutes to four hours by monitoring phosphorylated p38 MAPK on T180/Y182. We could observe weak activation of p38 MAPK after five minutes, and the activation peaked between 30- and 60-minutes post-irradiation. After 60 minutes, the phosphorylation gradually decreased, becoming almost undetectable four hours post-irradiation (Figure 10A). By exposing cells to various doses of UV-light, we found that the phosphorylation of p38 MAPK increased in a dose-dependent manner and was detectable after the irradiation of cells with 10 J/m^2 (Figure 10B). In addition to UV-light, treatment of cells with the UV-light-mimetic drug 4-nitroquinoline-1-oxide (4-NQO) and the oxidative stress-inducing agent H_2O_2 resulted in the rapid phosphorylation of p38 MAPK (Figure 10C). In contrast, the double-strand DNA break-inducing agents neocarzinostatin and etoposide and the replication stress-inducing agent hydroxyurea did not lead to marked activation of p38 MAPK early after treatment, although these drugs activated the canonical DDR detected by CHEK1 phosphorylation (Figure 10C). Chemical inhibition of p38 MAPK using SB203580 significantly sensitized U2OS cells to various doses of UV-light, indicating that p38 MAPK promotes cellular survival after UV-light exposure (Figure 10D). In accordance with previous findings (Reinhardt et al., 2007), the specific inhibition of phosphoinositide 3 kinase-like kinases ATM, ATR, or DNA-PKcs did not affect p38 MAPK activation after exposure to UV-light, suggesting that parallel activation of the ATR-CHEK1-dependent canonical DNA damage signaling and p38 MAPK regulates the early response of cells to UV-light (Figure 10E).

2.1.2 p38 MAPK signaling has a broad regulatory role after UV-light

We performed a proteome-wide identification of p38-dependent phosphorylation sites after UV-light exposure to define signaling downstream of p38. To this end, we employed the enrichment of phosphorylated peptides using titanium dioxide (TiO2)-based chromatography, followed by peptide identification using ultrahigh performance liquid chromatography-tandem MS (LC-MS/MS). Stable isotope labeling with amino acids in cell culture (SILAC) was used to quantify the relative abundance of the phosphorylated peptides in distinct experimental conditions. Light-labeled cells were mock-treated and used as the control, medium-labeled cells were irradiated with UV-light (40 J/m2, one-hour recovery), and heavy-labeled cells were pretreated with the specific p38 inhibitor, followed by irradiation with UV-light (Figure

11D). We quantified 13,091 phosphorylation sites, of which 10,448 were identified in two independent replicate experiments (Figure 11B). We observed an excellent quantitative reproducibility between the replicate experiments (Figure 11C,D). To determine significantly regulated phosphorylation sites after UV-light exposure and sites that are affected by p38 MAPK inhibition, we applied a moderated t-test (limma algorithm) (Figure 11E,F). This analysis revealed that 538 (4.1%) and 153 (1.2%) out of 13,091 phosphorylation sites were significantly upregulated and downregulated, respectively, after the irradiation of cells with UV-light (p-value < 0.01, moderated t-test) (Figure 11B). Notably, the UV-light-induced phosphorylation of 138 phosphorylation sites (24.6%) significantly decreased after p38 MAPK inhibition,

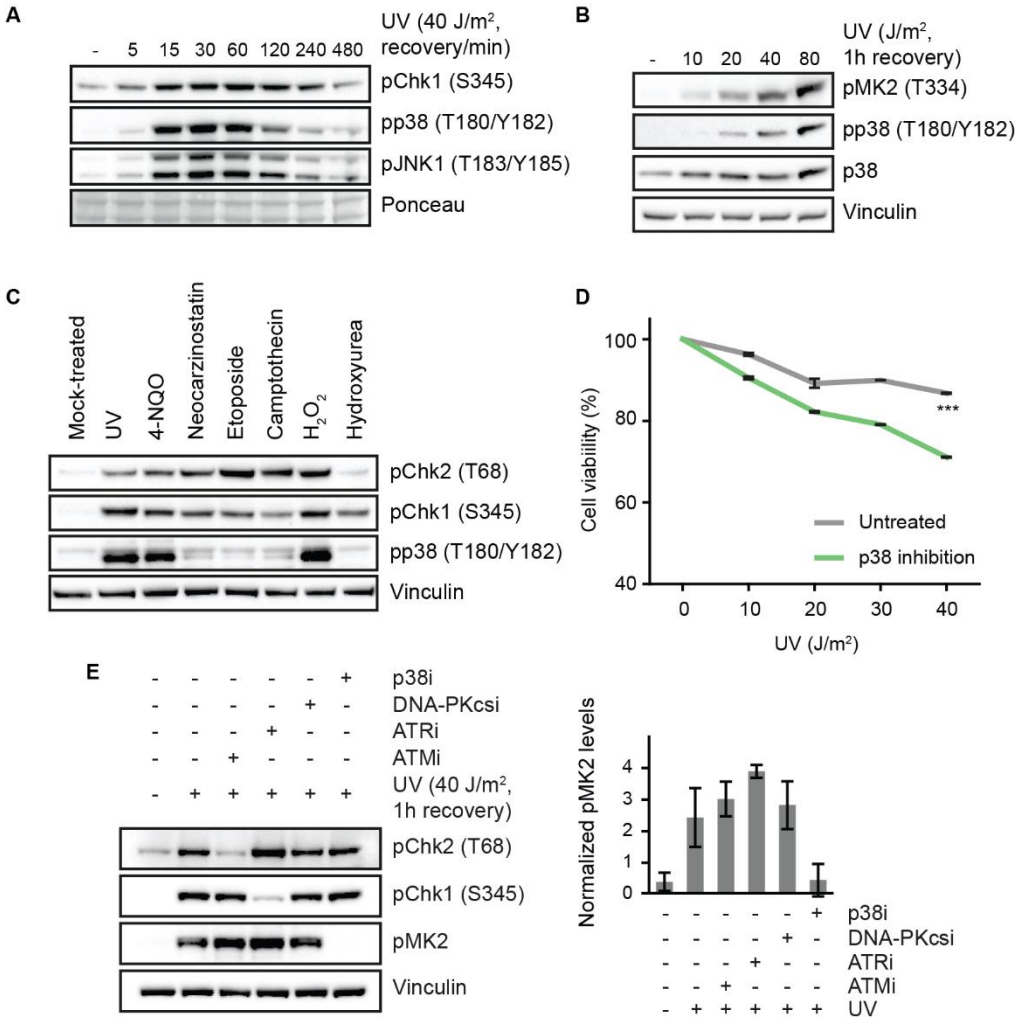

Figure 10. The p38 MAPK signaling pathway is activated separately from ATR, ATM, or DNK-PKcs activation in response to UV-light. A *U2OS cells were treated with UV-light (40 J/m², UV-C) and left to recover for the indicated times.* ***B*** *U2OS cells were treated with increasing doses of UV-light exposure (10 - 80 J/m²) and left to recover for one-hour.* ***C*** *U2OS cells were left untreated or treated with UV-light (40 J/m², one-hour recovery), 4-nitroquinoline 1-oxide (4-NQO), neocarzinostatin, etoposide, camptothecin, H_2O_2, and hydroxyurea.* ***D*** *Cell viability was measured for mock-treated U2OS cells and cells irradiated with various doses of UV-light without and with one-hour pretreatment with the p38 inhibitor. The plot shows the mean and standard deviation of the results obtained in three biological replicate experiments, each performed in three technical replicates. The two-sided Student's t-test was used to assess significance (*** p value < 0.001).* ***E*** *U2OS cells were pretreated for one-hour with ATM inhibitor, ATR inhibitor, DNA-PKcs inhibitor or p38 inhibitor and then irradiated with UV-light (40 J/m², one-hour recovery). The western blot results are quantified and shown on the bar plot, the mean and standard deviation of normalized pMK2 levels quantified from three replicate experiments. For all western blot analyses, total cell lysates were resolved on SDS-PAGE and blotted with the indicated antibodies; activation of p38, JNK1, and CHEK1 was monitored with phospho-specific antibodies.*

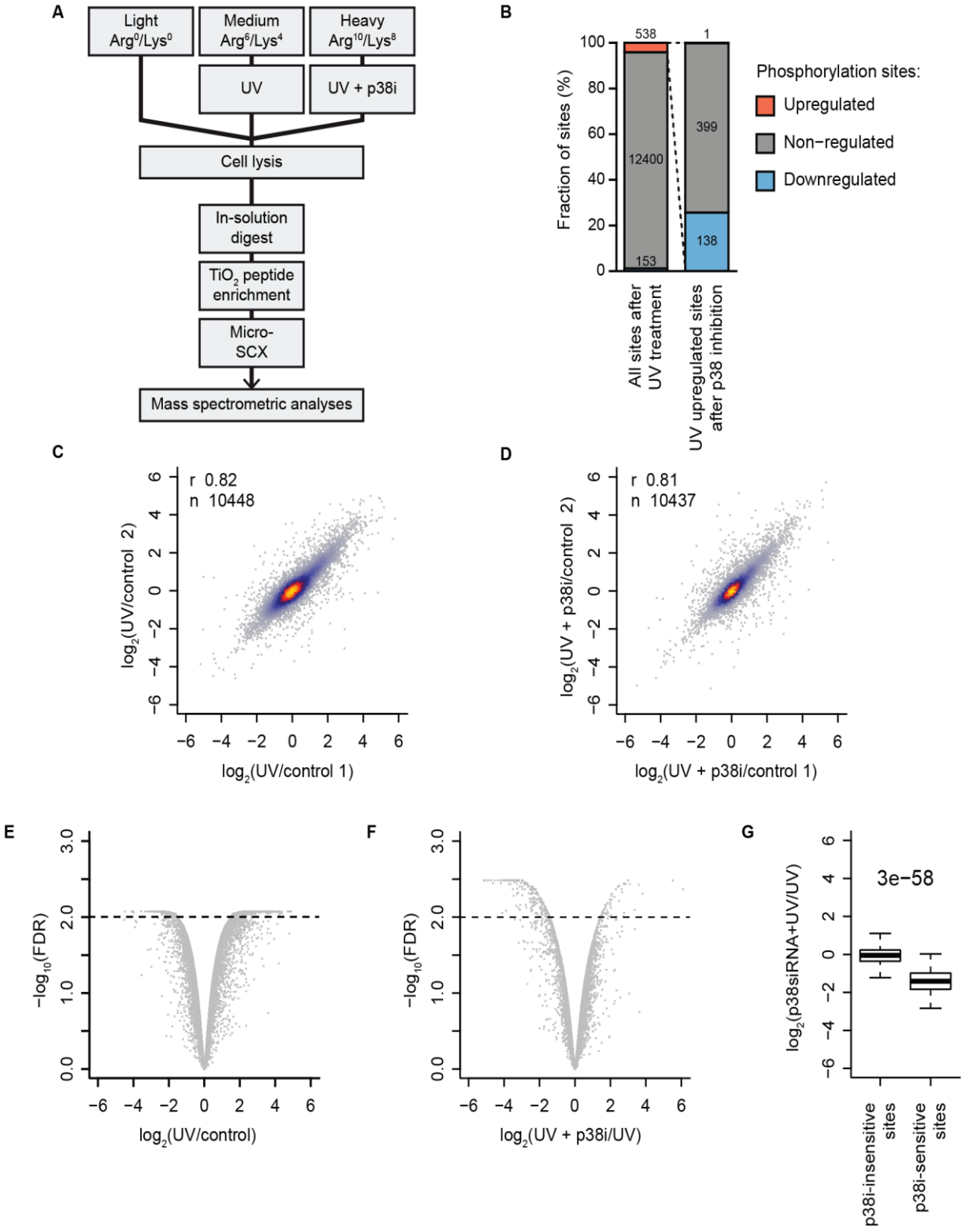

Figure 11. Phosphoproteomics reveals a broad scope of p38 MAPK signaling after UV-light. A *Schematic representation of the strategy used to identify UV-light-induced, p38-dependent phosphorylation sites. SILAC-labelled U2OS cells were mock-treated (Light), irradiated with UV-light (40 J/m², one-hour recovery) (Medium), or pretreated with the p38 inhibitor or transfected with p38 MAPK siRNA, and irradiated with UV-light (40 J/m², one-hour recovery) (Heavy). After in-solution digestion, phosphorylated peptides were enriched using TiO_2 and peptide samples were analyzed by LC-MS/MS.* ***B*** *The bar graph shows the number of significantly up-, non-, and downregulated UV-light-induced phosphorylation sites after p38 MAPK inhibition, identified from two replicate experiments (p-value < 0.01, moderated t-test).* ***C,D*** *Scatter plots show the logarithmized SILAC ratios UV/control and UV+p38i/control of quantified phosphorylation sites in replicate experiments. The color-coding indicates the density. The Spearman's rank correlation was calculated to determine the experimental reproducibility.* *(Continued on the next page)*

Figure 11. E,F *Identification of significantly regulated phosphorylation sites after UV-light or p38 MAPK inhibition from two replicate experiments using the limma algorithm. P value < 0.01 was used as a cut-off to determine phosphorylation sites that significantly increase after UV-light or decrease after p38 MAPK inhibition.* ***G*** *The box plot shows the SILAC ratio of p38i-insensitive sites and p38i-sensitive sites quantified after transient knockdown of p38. Box plot represents the 25th to 75th quartiles with the horizontal line representing the median value.*

indicating that the phosphorylation of these sites is dependent on p38 MAPK activity (Figure 11B). To support our data with the p38 inhibitor, we repeated the experiment with the transient knockdown of p38 MAPK using small interfering RNA (siRNA). The knockdown also decreased the phosphorylation of these sites, demonstrating that phosphorylation indeed occurs in a p38-dependent manner (Figure 11G).

2.1.3 p38 MAPK phosphorylates LXRQXS/T motif after UV-light

An analysis of the amino acid sequence surrounding UV-light-upregulated phosphorylation sites revealed a significant overrepresentation of glutamine (Q) in the +1 position, an S/TQ sequence motif that is known to be recognized by ATM/ATR/DNA-PKcs (Kim et al., 1999; O'Neill et al., 2000) (Figure 12A). To compare the regulatory function of p38 MAPK and ATR after UV-light exposure, we extracted all UV-light-induced phosphorylation sites that conformed to the S/TQ motif. The phosphorylation of 89 S/TQ sites (17%) increased in abundance after UV-light exposure (Figure 12B). The fraction of the S/TQ motif within p38-dependent sites was similar to the fraction of the motif in all quantified phosphorylation sites, indicating that p38-dependent phosphorylation does not target the S/TQ motif (Figure 12B). In contrast, UV-light-upregulated, p38-dependent phosphorylation occurred within a specific sequence motif that is defined by a glutamine (Q) in position –2, arginine (R) in –3, and leucine (L) in –5 (LxRQx[ST]) (Figure 12C). This motif differs from the p38 MAPK motif previously determined using peptide library screening (GPQ[ST]PI) (Manke et al., 2005), suggesting that the majority of p38-dependent phosphorylation

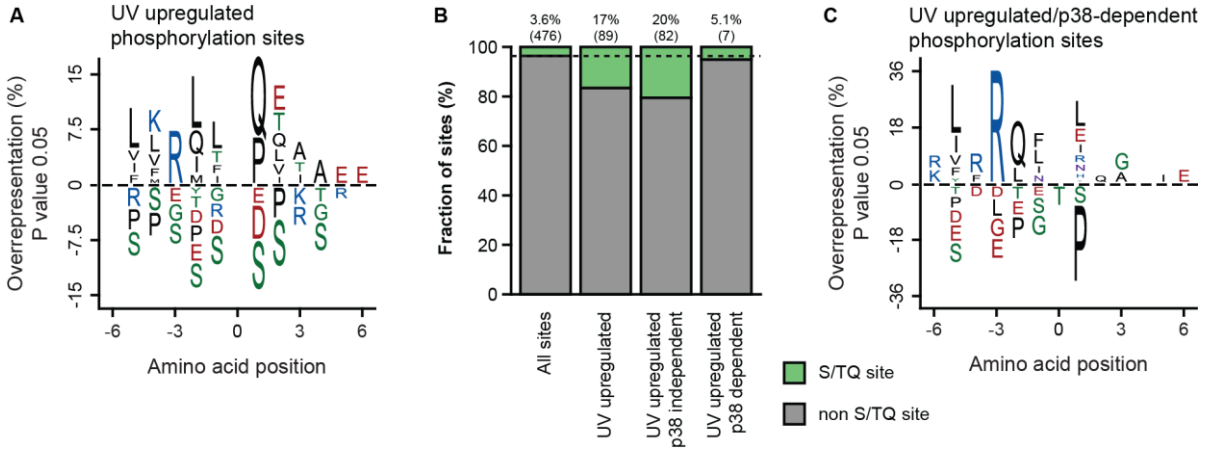

Figure 12. p38 MAPK recognizes a motif for phosphorylation different from the S/TQ motif*.* ***A*** *Sequence motif analysis of p38 UV-light-induced phosphorylation sites. The iceLogo plot shows frequency of six amino acids flanking the phosphorylated residue. The frequencies of amino acids surrounding phosphorylated residues in UV-light-induced phosphorylation sites were compared with frequencies in all quantified phosphorylation sites. A significant overrepresentation of phosphorylation sites conforming to the ATM/ATR/DNA-PKcs motif (S/TQ) is observed among UV-light-induced sites.* ***B*** *The bar graph shows the absolute number and percentage of S/TQ sites among all quantified phosphorylation sites, UV-light-upregulated sites, UV-light-upregulated p38-independent sites, and UV-light-upregulated p38-dependent sites.* ***C*** *Sequence motif analysis of 138 UV-light-induced, p38-dependent phosphorylation sites. The analysis was done as described in A.*

sites induced after UV-light exposure are substrates of kinases acting downstream of p38 MAPK, rather than p38 MAPK itself.

2.1.4 MK2/3 are key transducers of p38-dependent signaling

To determine the contribution of the downstream effector kinases to p38-dependent phosphorylation after UV-light exposure, we employed SILAC-based quantitative MS to compare UV-light-upregulated phosphorylation sites after the chemical inhibition of p38 MAPK or the joint inhibition of MK2, 3, and 5 using PF-3644022, thereby inhibiting one signaling axis that is activated downstream of p38 MAPK (Figure 13A). Phosphorylation site abundance after p38 MAPK and MK2/3/5 inhibition is correlated, demonstrating that much of the p38-dependent phosphorylation is dependent on the MK2/3/5 signaling axis (Figure 13B). Notably, using the limma algorithm, we identified significantly downregulated phosphorylation sites after p38 MAPK or MK2/3/5 inhibition and demonstrated that nearly 60% of UV-light-upregulated, p38-dependent phosphorylation sites also depend on MK2/3/5 activity (Figure 13B,C). To further distinguish the contribution of MK2/3 and MK5 to UV-light-induced phosphorylation, we transiently knocked down MK2/3 or MK5 and monitored the phosphorylation of proteins after UV-light exposure. These analyses demonstrated that MK2/3 double knockdown decreased the phosphorylation of a majority of MK2/3/5 inhibitor-dependent sites, establishing that MK2 and MK3 are the key transducers of p38 MAPK signaling after UV-light exposure (Figure 13C). The previously identified p38-dependent sequence motif represents a combination of sequences that are recognized by p38 MAPK and its downstream kinases that are activated after UV-light (Figure 12C). An analysis of the sequences surrounding the phosphorylation sites that are dependent on both p38 MAPK and MK2/3/5 revealed an enrichment of the same motif (LxRQx[ST]), demonstrating that this motif is recognized by MK2/3 (Figure 13E). This result agrees with a previous study that determined the optimal motif for MK2 in vitro using peptide library screening (Manke et al., 2005).

2.1.5 p38-MK2/3 signaling axis phosphorylates RNA-binding proteins

The identification of UV-light-induced p38-dependent phosphorylation sites delivered an unbiased view of the cellular proteins regulated by p38 MAPK. Gene ontology (GO) enrichment analysis revealed that proteins with p38-dependent phosphorylation sites are involved in the regulation of messenger RNA stability, gene expression, nuclear-transcribed mRNA poly(A) tail shortening, translation, and RNA binding (Figure 14A). In the agreement, p38-dependent phosphorylation sites occurred on proteins in the nucleolus, cytoplasmic stress granules, and focal adhesions, demonstrating that p38 MAPK regulates proteins in the nucleus and cytoplasm (Figure 14A). RNA binding was also the most significantly enriched term among all proteins containing UV-light-upregulated sites, demonstrating that UV-light-induced phosphorylation of RBPs, which is predominantly executed by the p38-MK2/3 signaling axis, is a hallmark of the cellular response to UV-light (Figure 14B). On the other hand, GO enrichment analysis showed that proteins containing UV-light-induced S/TQ

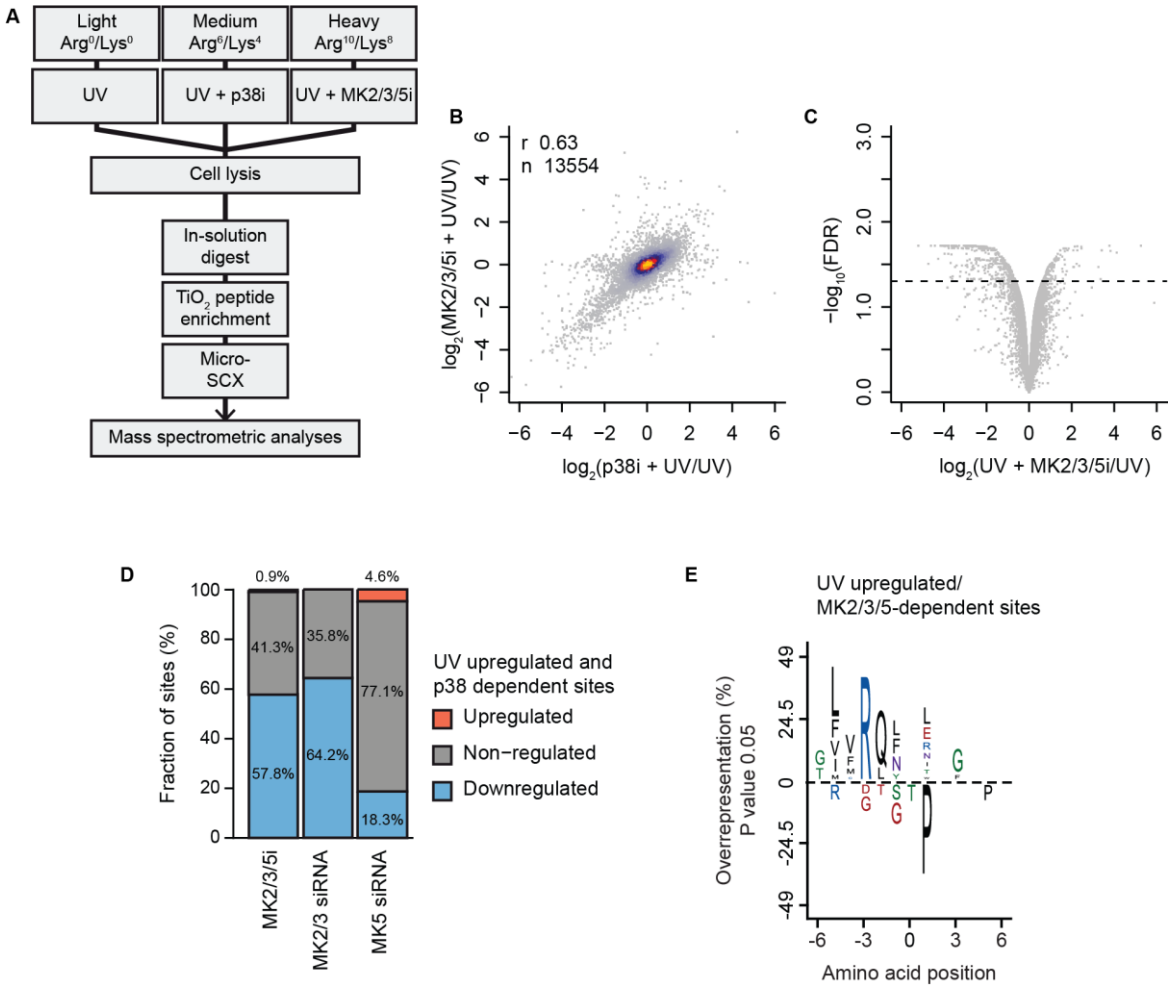

Figure 13. MK2/3 are key transducers of p38 MAPK signaling after UV-light. A *Schematic representation of the strategy used to identify UV-light-induced, MK-dependent phosphorylation sites. SILAC-labeled U2OS cells were mock-treated (Light), pretreated with the p38 inhibitor (Medium) or the MK2/3/5 inhibitor (Heavy), and subsequently irradiated with UV-light (40 J/m^2, one-hour recovery). The phosphoproteome analysis was performed as described in Figure 11.* ***B*** *The scatter plot shows the logarithmized SILAC ratios of quantified phosphorylation sites. The color-coding indicates the density. A majority of UV-light- induced, p38-dependent phosphorylation sites significantly decreased in abundance also after MK2/3/5 inhibition, whereas a smaller fraction of sites decreased in abundance only after p38 inhibition.* ***C*** *Identification of significantly regulated phosphorylation sites after MK2/3/5 inhibition from two replicate experiments was performed using the limma algorithm. P value < 0.05 was used as a cut-off to determine downregulated phosphorylation sites after p38 or MK2/3/5 inhibition.* ***D*** *The bar graph shows the percentage of UV-light-upregulated, p38-dependent sites that are up-, non-, or downregulated after MK2/3/5 inhibition, knockdown of MK2/3 or MK5.* ***E*** *Sequence motif analysis of p38- and MK2/3/5-dependent phosphorylation sites. The analysis was done as described in Figure 12A. The sequence surrounding the phosphorylated residue shows an enrichment of glutamine (Q) in position –2, arginine (R) in –3, and leucine (L) in –5.*

phosphorylation sites are involved in DNA repair and cell cycle and are primarily localized in the nucleus (Figure 14C). They are likely to be direct substrates of ATR. MLH1, PMS2, NBN, FANCI, TOPBP1, RAD1, and CHEK1 display UV-light-upregulated phosphorylation on S/TQ sites. In addition, proteins previously not linked to DNA repair also contain UV-light-induced S/TQ phosphorylation, suggestive of their function in DDR. In contrast, proteins with p38-dependent phosphorylation sites are engaged in functional networks involved in the regulation of RNA metabolism, but not DNA repair (Figure 14D). Among the proteins with p38-dependent phosphorylation sites were subunits of the NELF (NELFE and NELFA) and SMN complexes (GEMIN5 and DDX20), proteins involved in the degradation of ARE-containing mRNA (PARN,

Results

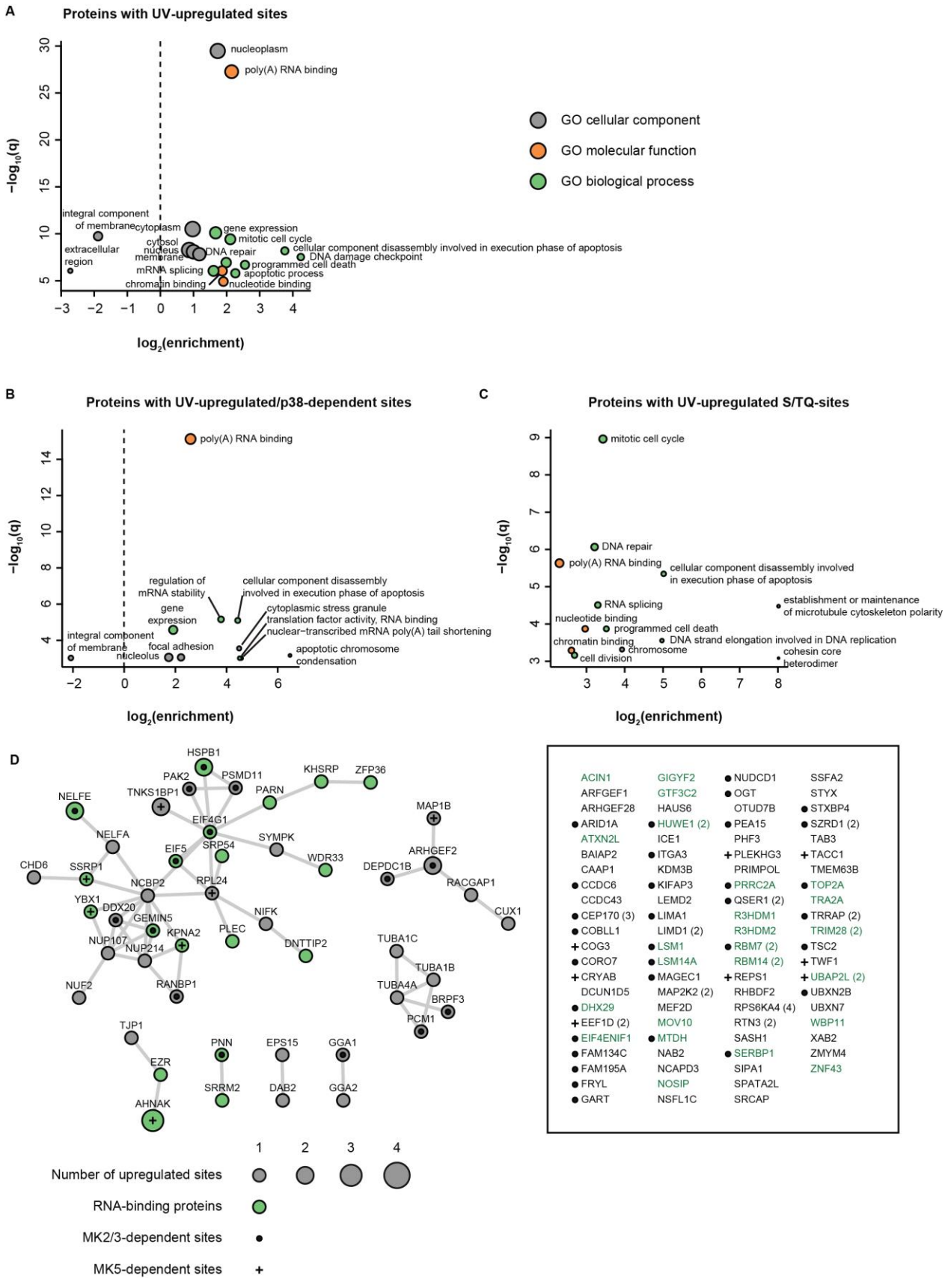
A
Proteins with UV-upregulated sites
nucleoplasm
poly(A) RNA binding
GO cellular component
GO molecular function
GO biological process
integral component of membrane
cytoplasm
gene expression
mitotic cell cycle
cytosol
nucleus
DNA repair
cellular component disassembly involved in execution phase of apoptosis
extracellular region
membrane
DNA damage checkpoint
programmed cell death
mRNA splicing
apoptotic process
chromatin binding
nucleotide binding
−log10(q)
log2(enrichment)
B
Proteins with UV-upregulated/p38-dependent sites
poly(A) RNA binding
regulation of mRNA stability
cellular component disassembly involved in execution phase of apoptosis
gene expression
cytoplasmic stress granule
translation factor activity, RNA binding
nuclear−transcribed mRNA poly(A) tail shortening
integral component of membrane
focal adhesion
nucleolus
apoptotic chromosome condensation
C
Proteins with UV-upregulated S/TQ-sites
mitotic cell cycle
DNA repair
poly(A) RNA binding
cellular component disassembly involved in execution phase of apoptosis
RNA splicing
establishment or maintenance of microtubule cytoskeleton polarity
nucleotide binding
programmed cell death
chromatin binding
DNA strand elongation involved in DNA replication
chromosome
cell division
cohesin core heterodimer
D
HSPB1
PAK2
PSMD11
KHSRP
ZFP36
TNKS1BP1
PARN
NELFE
MAP1B
EIF4G1
NELFA
SYMPK
EIF5
SRP54
ARHGEF2
WDR33
CHD6
SSRP1
DEPDC1B
NCBP2
RPL24
RACGAP1
YBX1
CUX1
DDX20
NIFK
GEMIN5
PLEC
KPNA2
TUBA1C
NUP107
DNTTIP2
NUP214
TUBA1B
NUF2
RANBP1
TUBA4A
BRPF3
PCM1
TJP1
PNN
EPS15
GGA1
EZR
SRRM2
DAB2
GGA2
AHNAK
1 2 3 4
Number of upregulated sites
RNA-binding proteins
MK2/3-dependent sites
MK5-dependent sites
ACIN1
ARFGEF1
ARHGEF28
● ARID1A
ATXN2L
BAIAP2
CAAP1
● CCDC6
CCDC43
● CEP170 (3)
● COBLL1
+ COG3
● CORO7
+ CRYAB
DCUN1D5
● DHX29
+ EEF1D (2)
● EIF4ENIF1
● FAM134C
● FAM195A
● FRYL
● GART
GIGYF2
GTF3C2
HAUS6
● HUWE1 (2)
ICE1
● ITGA3
KDM3B
● KIFAP3
LEMD2
● LIMA1
LIMD1 (2)
● LSM1
● LSM14A
● MAGEC1
MAP2K2 (2)
MEF2D
MOV10
● MTDH
NAB2
NCAPD3
NOSIP
NSFL1C
● NUDCD1
● OGT
OTUD7B
● PEA15
PHF3
+ PLEKHG3
PRIMPOL
● PRRC2A
● QSER1 (2)
R3HDM1
R3HDM2
● RBM7 (2)
RBM14 (2)
+ REPS1
RHBDF2
RPS6KA4 (4)
RTN3 (2)
SASH1
● SERBP1
SIPA1
SPATA2L
SRCAP
SSFA2
STYX
● STXBP4
● SZRD1 (2)
TAB3
+ TACC1
TMEM63B
● TOP2A
TRA2A
● TRRAP (2)
TRIM28 (2)
● TSC2
+ TWF1
+ UBAP2L (2)
● UBXN2B
UBXN7
WBP11
XAB2
ZMYM4
ZNF43

KHSRP, and ZFP36), mRNA polyadenylation (WDR33 and SYMPK), and translation (EIF5, EIF4G1, SRP54, and DHX29) (Figure 14D).

2.1.6 p38 MAPK promotes dissociation of RNA-binding proteins from chromatin

To study the functional consequence of p38-dependent phosphorylation and its possible impact on nuclear processes after UV-light exposure, we analyzed whether the composition of the chromatin proteome is altered upon the inhibition of p38 MAPK. To this end, we isolated chromatin-associated proteins from cells and used SILAC-based quantitative MS to monitor the p38-dependent changes in the chromatin proteome after UV-light exposure (Figure 15A,B). We identified 48 proteins that were recruited to and 44 that dissociated from chromatin after the exposure of cells to UV-light (p-value <0.01, moderated t-test). In addition to DNA repair factors, which comprised a large group of proteins that were enriched on chromatin, we also found a significant enrichment of 24 proteins annotated with the GO term “RNA binding” on chromatin. In particular, this group included 14 proteins functioning in ribosome biogenesis and annotated with the GO term “maturation of SSU-rRNA from tricistronic rRNA transcript (SSU-rRNA, 5.8 S rRNA, LSU-rRNA)” (Figure 15C). Well-known DNA repair factors were recruited to chromatin after the exposure of cells to UV-light, including RPA1/2, PCNA, XPA, MSH2/6, PMS1, MLH1, and FANCD2 (Figure 15D). Some DNA repair factors, including CHEK1, DDB1/2, and CCAR2, were excluded from chromatin in response to UV-light; however, the recruitment or removal of DNA repair factors was not affected by p38 MAPK inhibition (Figure 15D). UV-light exposure resulted in the rapid dissociation of some RBPs from chromatin, including all components of the NELF and NEXT complexes (Figure 15E). The latter, which consists of the RBM7 and ZCCH8 subunits, was previously reported to be removed from chromatin upon UV-light exposure, in a p38-dependent manner (Blasius et al., 2014; Tiedje et al., 2015). Further, we focused on signaling proteins that recognize the peptides phosphorylated by the p38-MK2/3 pathway.

Figure 14. p38 MAPK phosphorylates RNA-binding proteins after UV-light. A *GO terms significantly enriched among proteins with UV-light-induced phosphorylation sites. The dot plot shows significantly overrepresented GO terms associated with proteins containing UV-light-induced phosphorylation sites, compared to proteins containing non-regulated sites. The significance of the enrichment of a specific term was determined using Fisher’s exact test. P-values were corrected for multiple hypotheses testing using the Benjamini and Hochberg FDR.* ***B*** *The dot plot shows significantly enriched GO terms associated with proteins containing p38-dependent phosphorylation sites, compared with proteins with non-regulated phosphorylation sites. The analysis was done as described in A.* ***C*** *The dot plot shows significantly overrepresented GO terms associated with proteins containing S/TQ phosphorylation sites, compared with proteins with non-regulated phosphorylation sites. The analysis was done as described in A.* ***D*** *Analysis of functional interactions among proteins with UV-light-upregulated, p38-dependent phosphorylation sites. The functional interactions were obtained from the STRING database and visualized using Cytoscape. Proteins with UV-light-upregulated, p38-dependent sites that do not form a functional network are indicated on the right, and proteins annotated with “RNA-binding” GO-molecular function term are indicated in green. Proteins with MK2/3-dependent phosphorylation sites are indicated with circles, and proteins with MK5-dependent sites with crosses.*

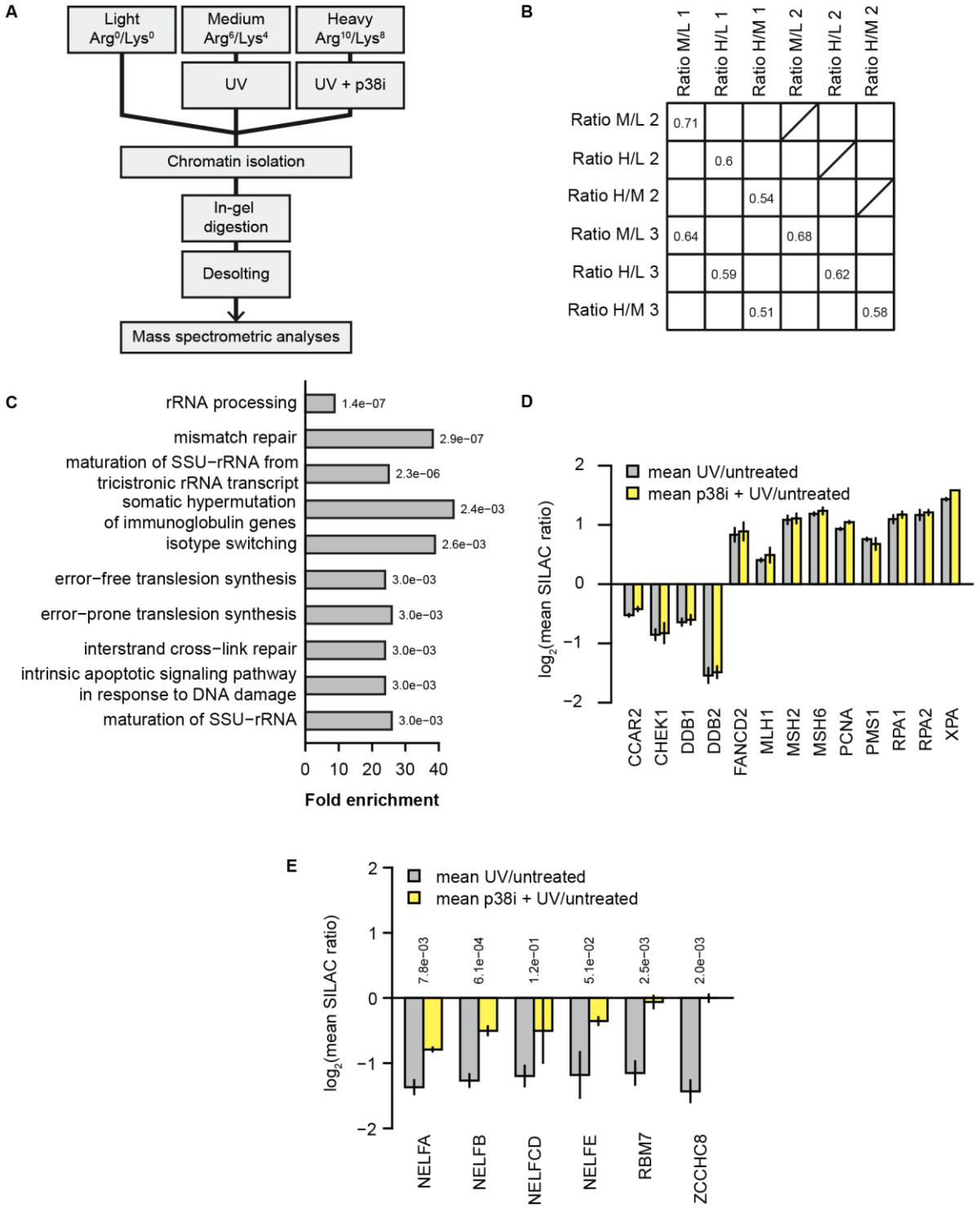

Figure 15. p38-dependent phosphorylation of RNA binding complexes promotes their dissociation from chromatin. ***A*** *Schematic representation of the strategy used to identify UV-light-induced, p38-dependent change in the chromatin proteome. SILAC-labelled U2OS cells were mock-treated, irradiated with UV-light (40 J/m², one-hour recovery) or pretreated with the p38 inhibitor and irradiated with UV-light. Chromatin-associated proteins were extracted from cells, digested in-gel into peptides and peptide samples were analyzed by LC-MS/MS.* ***B*** *The Spearman's rank correlation was calculated to determine the experimental reproducibility.* ***C*** *The bar plot shows the GO-BP (biological process) terms associated with proteins specifically enriched on or removed from chromatin after UV-light (40 J/m², one-hour recovery). The significance of the enrichment of a specific term was determined using Fisher's exact test. P-values were corrected for multiple hypotheses testing using the Benjamin and Hochberg FDR.* ***D*** *The bar plot shows selected proteins associated with DNA repair and cell cycle that are significantly recruited or removed from chromatin after UV-light. The error bars show the mean and SD of SILAC ratios quantified from three replicate experiments. Two-sided Student's t-test was used to assess the significance.* ***E*** *The NELF complex subunits are removed from chromatin in a UV-light and p38-dependent manner. The bar plot shows selected proteins whose removal from chromatin after UV-light is dependent on p38. The error bars show the mean and SD of SILAC ratios quantified from three replicate experiments. Two-sided Student's t-test was used to assess the significance.*

2.2 14-3-3 "reads" p38-MK phosphorylation induced by UV-light

The motif phosphorylated by MK2/3 resembles the motif that can be recognized by the proteins of the 14-3-3 family. It was previously demonstrated that the MK2-dependent phosphorylation of specific substrates could lead to the recruitment of 14-3-3 proteins in response to UV-light exposure. Therefore, we investigated whether 14-3-3 binding to proteins phosphorylated by p38-MK2 acts as a general regulatory mechanism in cells exposed to UV-light. We employed SILAC-based quantitative MS to compare the interaction profile of Flag-Strep-14-3-3ε in cells irradiated with UV-light and in cells pretreated with the p38 inhibitor and subsequently irradiated with UV-light (Figure 16A). Notably, this analysis revealed that nearly 30% of identified 14-3-3ε interactors bind to 14-3-3ε after UV-light exposure in a p38-dependent manner (Figure 16B). The GO analysis of interaction partners demonstrated the enrichment of ATP binding proteins and DNA binding proteins. In addition, a number of RBPs were detected, including TNS1, RBM7, NELFE, EIF4G1, CPSF1, SMC1A, and ZNF106 (Figure 16C, Table 2).

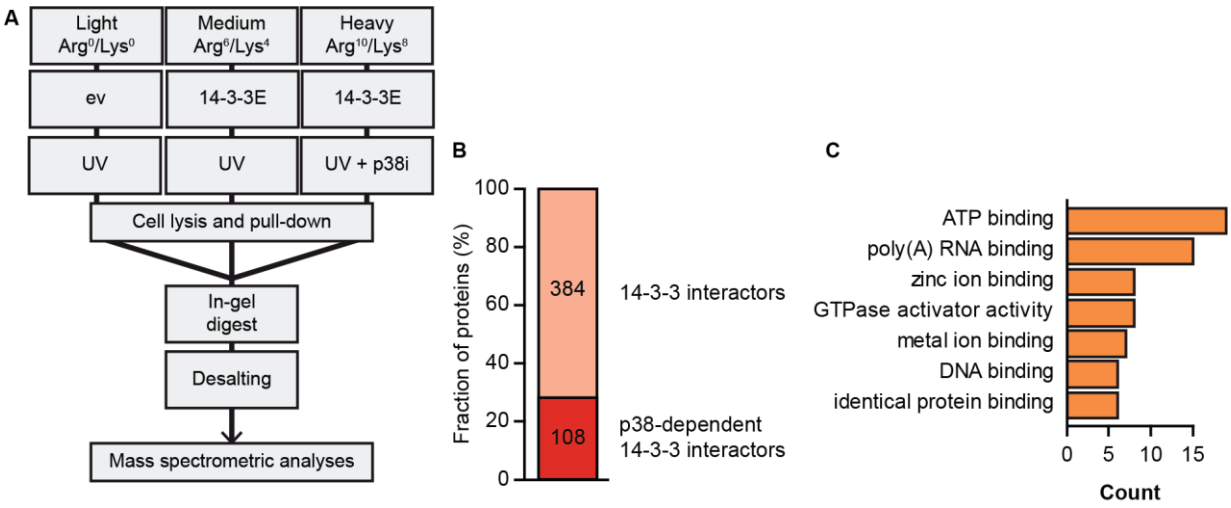

Figure 16. The 14-3-3 family recognizes the p38-phosphorylated substrates. A *Schematic representation of the strategy used to identify 14-3-3ε interactors upon UV-light irradiation without and with one-hour pretreatment with the p38 inhibitor. SILAC-labelled U2OS cells expressing empty vector (ev) were mock-treated (Light). Cells expressing Flag-Strep-14-3-3 ε were medium and heavy labeled and the heavy-labeled cells were pretreated with the p38 inhibitor. All conditions were irradiated with UV-light (40 J/m^2, one-hour recovery). The proteins binding to 14-3-3 were enriched with StreptActin beads; after SDS-PAGE separation, samples were digested and analyzed by LC-MS/MS.* ***B*** *The bar graph shows 14-3-3 interaction partners and p38-dependent interactions that are indicated in light and dark red, respectively. 384 proteins were significantly enriched in 14-3-3 pull downs after UV-light (p-value < 0.05, moderated t-test). 108 out of 384 proteins (28%) bound to 14-3-3 in a p38-dependent manner.* ***C*** *The bar plot shows the number of proteins with the indicated GO-molecular function terms that were enriched among p38-dependent 14-3-3 interaction partners.*

Table 2. p38 The MAPK signaling pathway and 14-3-3 family share their targets. *Selected RNA-binding proteins identified as p38-dependent interaction partners of 14-3-3. The UniProt ID, protein name, gene name, position(s), and sequence window of UV-light-induced phosphorylation sites identified in the phosphoproteomics screen are indicated. The phosphorylated amino acids are highlighted in bold.*

UniProt ID	Gene names	UV up	p38-dependent	Position(s)	Sequence window(s)
A1L390	PLEKHG3	+	+	S759	SISRFNpSLPRPDP
Q15154	PCM1	+	+	S93	RYMSQMpSVPEQAE
Q9HBL0	TNS1	+		S764;S960	PLTQSRpSGYIPSG; EEMEGTpSPSSPPP
P28290	SSFA2	+	+	S668	ILKSLApSIEAKCS
Q9Y4A5	TRRAP	+	+	S2051;S2077	SIKRGLpSVDSAQE; VFGRSQpSLPGADS
Q07157	TJP1	+	+	S1111	PFDNQHpSQDLDSR
Q9Y580	RBM7	+	+	S136;S204	IIQRSFpSSPENFQ; RKVRMNpSYPYLAD
P18615	NELFE	+	+	S51;S115	GVKRSLpSEQPVMD; PFQRSIpSADDDLQ
P49815	TSC2	+	+	S1364	PIERVVpSSEGGRP
Q04637	EIF4G1	+	+	S1209	GLRKAApSLTEDRDR
Q10570	CPSF1	+		S766	EEARRSpSQPPADR
Q14683	SMC1A	+		S360;S966	MEEESQpSQGRDLT; EDSVSGpSQRISSI
Q6NZY4	ZCCHC8	+		T479	PPLPRGpTPPPVFT
Q8WUF5	PPP1R13L	+		S183	FLGRAGpSPRGSPL
Q96FS4	SIPA1	+	+	S837	FLHSQNpSLSPRSS
Q96L91	EP400	+		S181;S2086	VLVRQIpSLSPSSG; EEFVVLpSQEPSVT
Q9H2Y7	ZNF106	+		S937	ATQRRHpSAQLSSD
Q9NYL2	ZAK	+		S3;S7;S587; S610;S649	____MSpSLGASFV; MSSLGApSFVQIKF; QIASNTpSLQRSQS; HFDGQDpSYAAAVR; LTKNFSpSLHLNSR
Q5VZ89	DENND4C	+		S989	SEDKLFpSPVIARN

2.3 UV-light-induced NELFE phosphorylation mediates 14-3-3 binding

We identified the RNA-binding subunits of the NELF complexes NELFA and NELFE as substrates of p38-MK2/3-dependent phosphorylation after UV-light exposure. In addition, NELFE was the factor that strongly interacted with 14-3-3 after UV-light exposure, dependent on p38 MAPK activation. Therefore, we focused on NELFE for a better understanding of how p38-MK2/3, together with 14-3-3, orchestrates the cellular response to UV-light.

2.3.1. NELFE transiently interacts with 14-3-3 after UV-light exposure in an MK2-dependent manner

In accordance with our previous results, an affinity purification of transiently expressed GFP-NELF subunits (NELFA, NELFB, NELFC/D, and NELFE) and a subsequent western blot analysis allowed us to validate that 14-3-3 interacts strongly with NELFE and much more weakly with others (Figure 17A). In addition, we applied an orthogonal approach, and, after affinity purification of GFP-NELFE, the samples were subjected to LC-MS/MS analysis. This experiment again confirmed that UV-light exposure dramatically increases the binding of NELFE to distinct 14-3-3 proteins

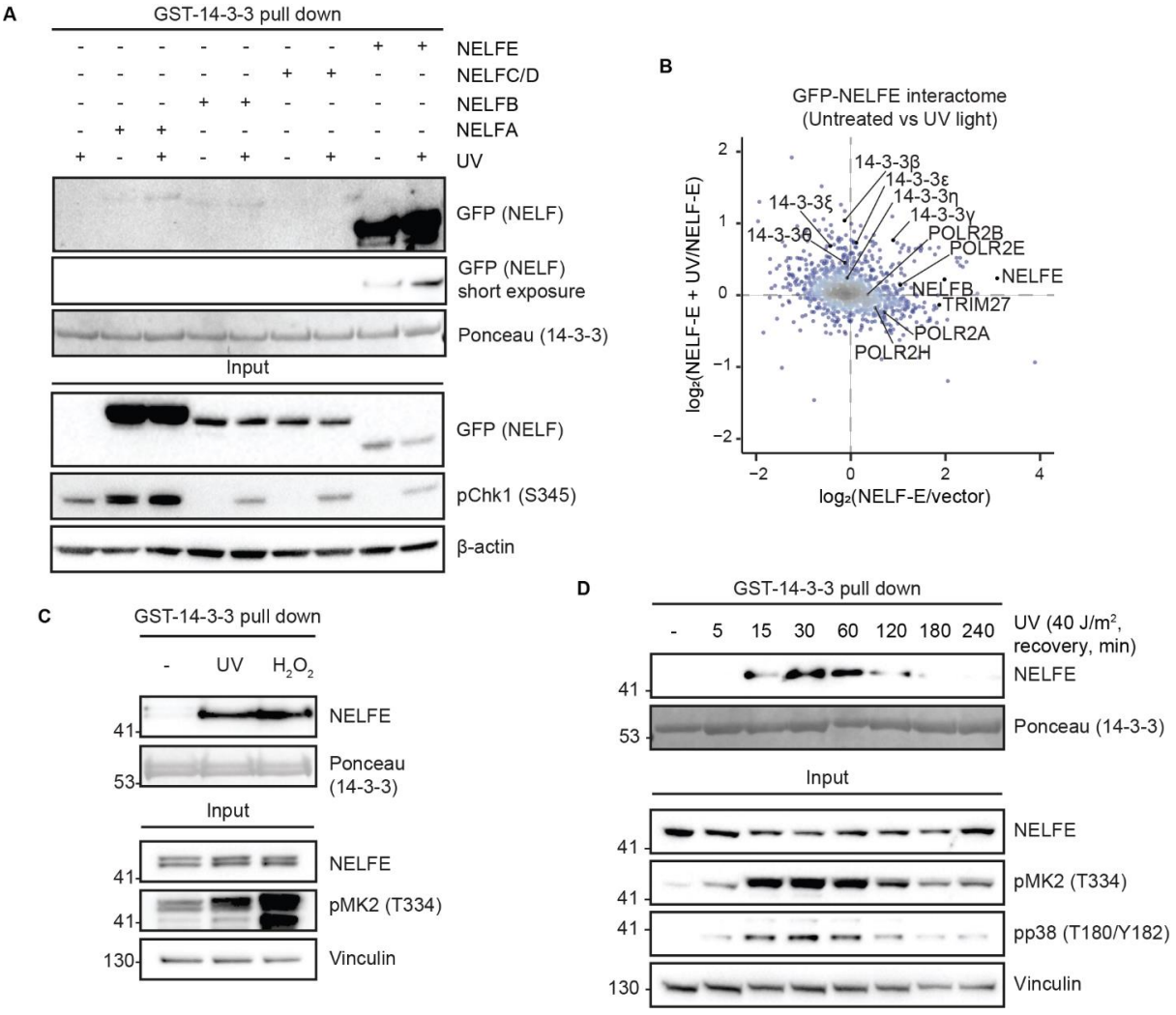

Figure 17. NELFE and 14-3-3 transiently interact after UV-light as well as treatment with H_2O_2. A *Only NELFE, from the four NELF subunits, interacts strongly with 14-3-3 after UV-light. Total cell lysates, which were collected from cells transiently expressing one of the NELF subunits tagged with GFP, were incubated with GFP Trap agarose beads and analyzed by western blot.* ***B*** *Identification of UV-light-induced NELFE interaction partners. SILAC-labelled U2OS cells expressing GFP-NELFE were mock-treated or irradiated with UV-light (40 J/m², 1h recovery). Cells were lysed, and protein extracts were incubated with GFP Trap agarose beads. Enriched proteins were resolved on SDS-PAGE and digested in-gel into peptides. Peptides were extracted from gel and analyzed by LC-MS/MS. The scatter plot shows the logarithmized SILAC ratios of proteins quantified in the pull down. The color-coding indicates density.* ***C*** *NELFE interacts with 14-3-3 after UV-light and oxidative stress induced by treatment with H_2O_2 for one-hour. Total cell extracts from differentially-treated U2OS cells were incubated with recombinant GST-14-3-3. Enriched proteins were resolved by SDS-PAGE and subjected to western blotting.* ***D*** *Dynamics of NELFE interaction with 14-3-3 after UV-light. U2OS cells were exposed to UV-light and left to recover for the indicated time points. After cell lysis, protein extracts were incubated with recombinant GST-14-3-3 and the eluates were resolved by SDS-PAGE and subjected to western blotting.*

(Figure 17B). Moreover, the interaction between NELFE and 14-3-3 also occurs after oxidative stress-inducing agent H_2O_2, which aligns with an earlier observation that UV-light, 4-NQO, and H_2O_2 activate p38 MAPK (**Figure 10**C and Figure 17C). NELFE interaction with 14-3-3 already occurred 15 minutes after UV-light exposure and peaked at 30–60 minutes post-irradiation, indicating that NELFE binding to 14-3-3 is dynamic and has a role early after the exposure of cells to UV-light (Figure 17D).

To examine whether UV-light-induced interaction between NELFE and 14-3-3 is dependent on NELFE phosphorylation, we performed pull downs from cells treated with the p38 MAPK or MK2/3/5 inhibitor before irradiation with UV-light. Notably, the binding between NELFE and 14-3-3 was completely abolished after p38 MAPK or MK2/3/5 inhibition (Figure 18A). The knockdown of p38 MAPK or MK2 also inhibited the binding between NELFE and 14-3-3, demonstrating that MK2, and not MK3 or MK5, is responsible for the phosphorylation of NELFE in U2OS cells (Figure 18B). The interaction between NELFE and 14-3-3 after UV-light exposure and its dependency on p38 MAPK were also validated in HaCaT, HEK293T, and RPE-1 cells, demonstrating that this interaction is not restricted to U2OS cells (Figure 18C). The UV-light-induced, p38-dependent phosphorylation of NELFE could also be readily detected by western blotting using phospho-specific antibodies recognizing the 14-3-3-binding motif (Figure 18D).

2.3.2 NELFE phosphorylation on S115 regulates its binding to 14-3-3

We found that NELFE was phosphorylated on eight serine residues after UV-light exposure (Table 3). Notably, the UV-light-induced phosphorylation of NELFE on serine 49 (S49), S51, S115, and S251 was dependent on p38 MAPK and MK2 (Figure 19A). In accordance with our data that NELFE binds to 14-3-3 after UV-light exposure, the phosphorylation sites S51, S115, and S251 reside within 14-3-3-binding motifs (Table 3). To determine the importance of the identified phosphorylation sites for the UV-light-induced binding of NELFE to 14-3-3, we mutated S49/51, S115, and S251 to alanine and performed pull downs using GST-14-3-3 and lysates expressing NELFE serine-to-alanine mutants. Wild-type green fluorescent protein (GFP)-NELFE was efficiently pulled down using GST-14-3-3, whereas the S115A mutant of NELFE did not interact with GST-14-3-3 (Figure 19B). An analysis of the sequence surrounding these phosphorylation sites predicted that NELFE S49/51A and S251A bind more weakly to GST-14-3-3, indicating that these phosphorylation sites also contribute to the interaction (Figure 19B). The S115 phosphorylation of NELFE increased twofold, and a phosphorylation site occupancy analysis revealed that this phosphorylation affects nearly the complete cellular pool of NELFE after UV-light exposure, indicative of the physiological importance of this modification (Figure 19C). The absolute occupancies of phosphoserine 49, 51, and 251 were lower than phosphoserine 115 but were substantially increased after UV-light exposure, in line with the results that these phosphorylation sites also contribute to the binding between NELFE and 14-3-3 (Figure 19C). Recombinant MK2 could also phosphorylate NELFE on S51, S115, and S251 in vitro (Figure 19D). To study the effect of single phosphorylation sites, we

mutated S115 to aspartate (D) or glutamate (E). Aspartic and glutamic acids are known to mimic a phosphorylated amino acid (Lin, Heylbroeck, Pitha, & Hiscott, 1998). Although we expected the NELFE mutants to already bind to GST-14-3-3 in unstimulated cells, no increase occurred in the interaction (Figure 19E). As other NELFE modifications, such as phosphorylation on S51, could contribute to the interaction, we performed the pull downs after UV-light exposure. Unfortunately, UV-light-induced conditions also failed to improve the interaction (Figure 19F). Thus, we could not use the phospho-mimicking mutations for further studies.

Table 3. The phosphorylation sites identified on NELFE by phosphoproteomics. *The position, SILAC ratios, 14-3-3 binding prediction and sequence window are indicated. UV-light-induced, p38-dependent phosphorylation sites are highlighted in bold.*

Position	UV	p38i+UV	14-3-3 motif	Sequence window
S49	**3.28**	**0.73**		**QGGVKRpSLSEQPV**
S51	**3.03**	**0.64**	**+**	**GVKRSLpSEQPVMD**
S115	**1.47**	**0.32**	**+**	**PFQRSIpSADDDLQ**
S131	1.37	0.45		RRPQRKpSLYESFV
S139	2.33	2.49		YESFVSpSSDRLRE
S251	**1.21**	**-1.30**	**+**	**PFRRSDpSFPERRA**
T272	0.98	0.80		VYGEDMpTPTLLRG
S281	1.06	1.54		LLRGAFpSPFGNII
S353	-1.15	-0.40		SLAVQNpSPKGCHR

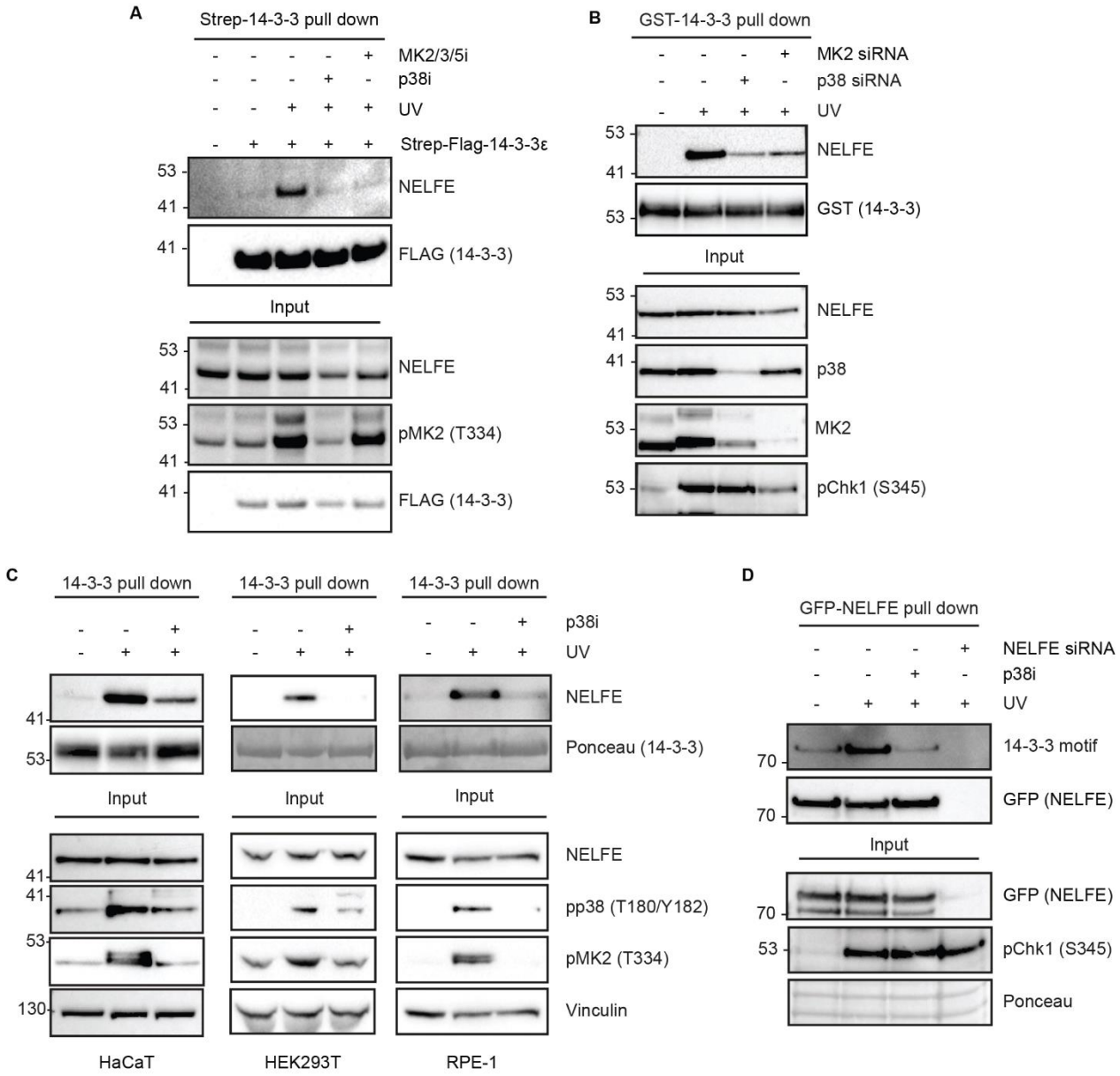

Figure 18. UV-light-induced phosphorylation of NELFE by MK2 leads to 14-3-3 binding. A *NELFE interaction with 14-3-3 after UV-light is p38- and MK2/3/5-dependent. U2OS cells expressing Flag-Strep-14-3-3 or an empty vector were mock-treated, irradiated with UV-light or pretreated with the p38 or MK2/3/5 inhibitor, and then irradiated with UV-light.* ***B*** *NELFE interaction with GST-14-3-3 is abolished in p38 and MK2 knockdown cells. U2OS cells were transfected with non-targeting, p38- or MK2-targeting siRNA and then irradiated with UV-light.* ***C*** *NELFE interaction with GST-14-3-3 in HaCaT, HEK293T and RPE-1 cells.* ***D*** *NELFE is phosphorylated after UV-light on a 14-3-3-binding motif. GFP-NELFE was pulled down using GFP Trap agarose. Phosphorylation of NELFE was detected using antibodies recognizing the 14-3-3 motif. NELFE knock down was used as control. Cells were lysed and protein extracts were incubated with StrepTactin, GFP Trap, or recombinant GST-14-3-3 agarose. Enriched proteins were resolved by SDS-PAGE and selected proteins were detected with the indicated antibodies.*

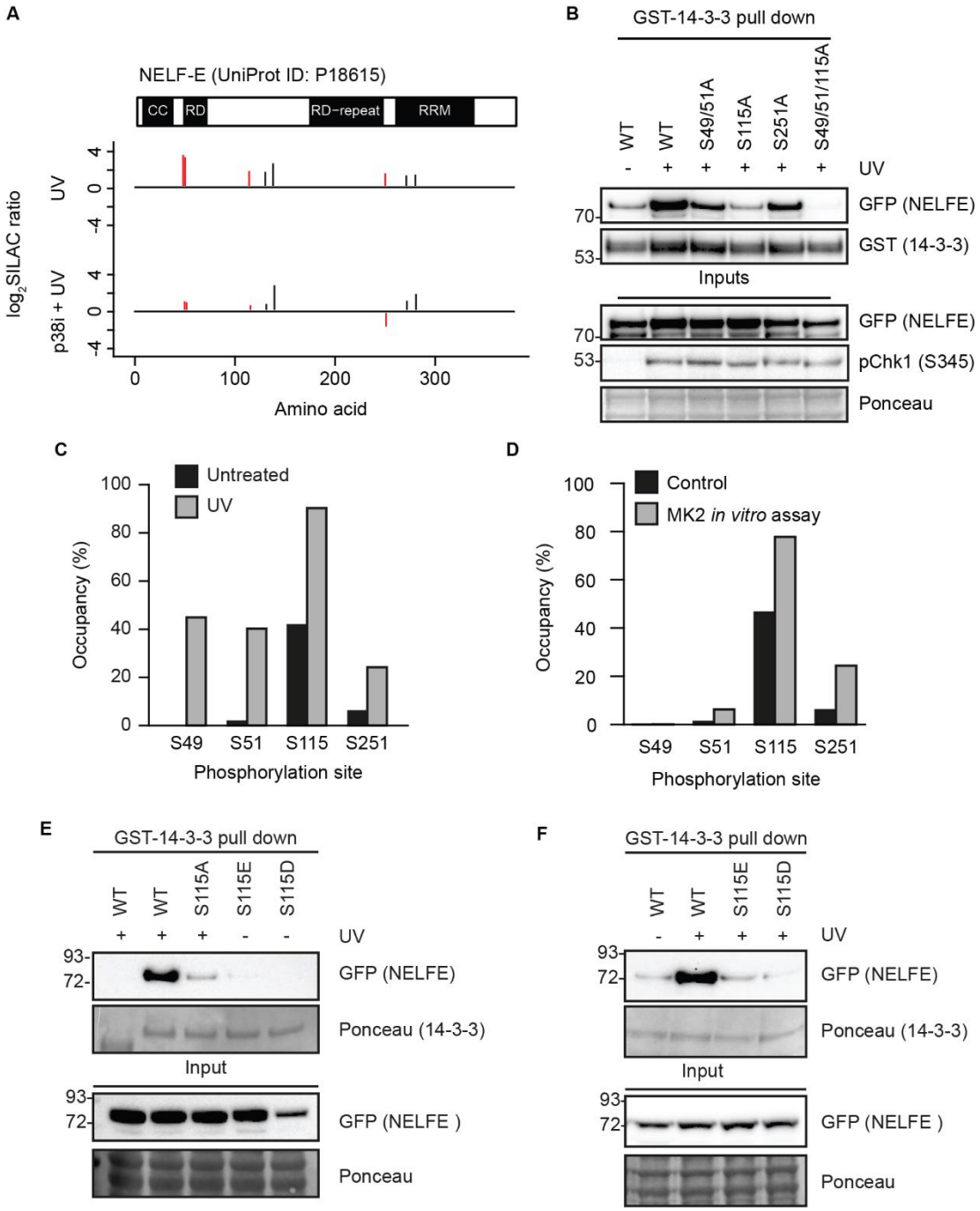

Figure 19. MK2 phosphorylates several sites on NELFE and mediates interaction with 14-3-3 after UV-light. ***A*** *Schematic representation of NELFE domain organization and phosphorylation sites that were identified by phosphoproteomics. The SILAC ratios quantified for phosphorylation sites on NELFE after UV-light and p38 inhibition are indicated. UV-light-induced, p38-dependent phosphorylation sites are labelled in red.* ***B*** *Serine 115 phosphorylation is required for the interaction of NELFE and 14-3-3. U2OS cells expressing GFP-tagged wild-type NELFE or NELFE serine-to-alanine mutants were irradiated with UV-light. Protein extracts were incubated with GST-14-3-3, and enriched proteins were resolved on SDS-PAGE.* ***C*** *Absolute occupancy of S49, S51, S115, and S251 phosphorylation on NELFE in undamaged cells and after UV-light was determined by MS.* ***D*** *Purified MK2 can phosphorylate immunoprecipitated NELFE on S51, S115 and S251 in vitro.* ***E, F*** *S115E or S115D does not mimic NELFE S115 phosphorylation. U2OS cells expressing GFP-tagged wild-type NELFE or NELFE serine-to-aspartate/glutamate mutants were left untreated or irradiated with UV-light. Protein extracts were incubated with GST-14-3-3 and enriched proteins were resolved on SDS-PAGE.*

2.3.3 Phosphorylated NELFE on S115 binds directly to 14-3-3

As the majority of NELFE is phosphorylated on S115 after UV-light exposure, we focused on this phosphorylation site (Figure 20A,C). Interestingly, S115 in NELFE is highly conserved in evolution, suggesting that the phosphorylation of this residue is also of regulatory importance in other organisms (Figure 20B). To confirm that S115 phosphorylation is required for the binding of NELFE to 14-3-3, we compared the interaction partners of the GFP-tagged wild-type NELFE and S115A mutant after UV-light exposure. Indeed, this experiment demonstrated that endogenous 14-3-3 does not bind to the NELFE S115A mutant (Figure 20D).

To investigate whether the binding between NELFE and 14-3-3 after UV-light exposure is direct, we synthesized a biotinylated phospho-peptide centered around S115 and performed pull downs with recombinant 14-3-3. We could observe the binding of 14-3-3 to the phosphorylated peptide, whereas no binding was detected if the peptide was dephosphorylated before the pull-down (Figure 20E). To further investigate the binding mode of NELFE and 14-3-3, we determined the crystal structure by molecular replacement, using the previously reported 14-3-3ε structure as a search model (PDB: 2BR9). The crystal structure of 14-3-3ε in complex with the phosphorylated NELFE peptide revealed that the overall structure of the nine helices (αA to αI) of 14-3-3 and the peptide orientation were similar to previously reported complexes of 14-3-3ε and other phospho-peptides (Yang et al., 2006). It was demonstrated that 14-3-3 proteins form hetero- and/or homodimers and that 14-3-3ε preferentially forms heterodimers (D. H. Jones, Ley, & Aitken, 1995). Although the asymmetric unit of the crystal contained one 14-3-3ε and one phosphorylated peptide, 14-3-3ε forms homodimers with axial symmetry in the crystal (Figure 20F). As reported for other 14-3-3-phospho-peptide complexes, the N-terminal four helices, αA, αB, αC, and αD, are essential, and two salt bridges between Arg19 on one molecule and Glu92 on the other are the driving force for the 14-3-3 dimer formation (Gardino, Smerdon, & Yaffe, 2006). In addition, Tyr85, sitting under the conserved lysine position on αD, forms an accessorial hydrogen bond with Glu22, supporting homodimer formation in the crystal. 14-3-3ε has a peptide-binding groove, composed of αC, αE, αG, and αI, that catches the phosphorylated peptide. In particular, the conserved triad of Arg57, Arg130, and Tyr131 forms a positively charged patch, directly interacting with the phosphate group of the phosphorylated peptide (Figure 20F). In addition, a few hydrogen bonds and salt bridges between the primary chain of the phosphorylated peptide and 14-3-3ε contribute to the complex formation and adjust its relative orientation (Figure 20F, Table 1).

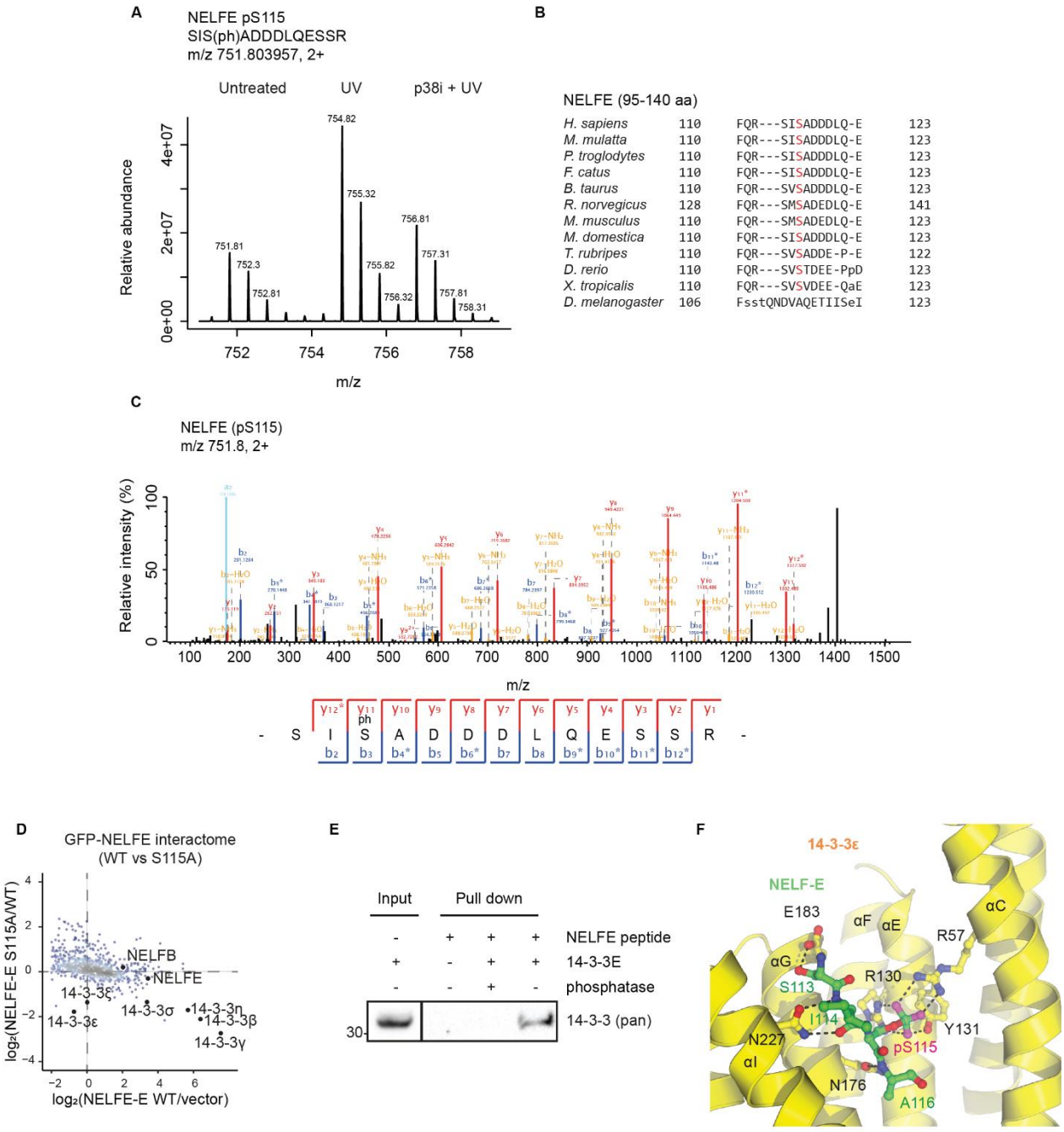

Figure 20. NELFE phosphorylation on S115 is required for the direct interaction with 14-3-3. A *Mass spectrometric parent ion scan of the peptide SISADDDLQESSR corresponding to S115 in NELFE. The SILAC triplet shows the relative abundance and mass to charge (m/z) of the phosphorylated peptide in mock-treated cells and cells irradiated with UV-light without or with pretreatment with the p38 inhibitor.* ***B*** *Multiple sequence alignment of the NELFE peptide sequence corresponding to serine 115 across evolution.* ***C*** *Mass spectrometric fragment ion scan of the peptide corresponding to phosphorylated serine 115 in NELFE.* ***D*** *NELFE S115A mutant does not bind to 14-3-3. SILAC-labelled cells overexpressing GFP-tagged wild-type NELFE or NELFE S115A mutant were irradiated with UV-light. UV-light-irradiated U2OS cells overexpressing GFP alone were used as control. Cells were lysed and protein extracts were incubated with GFP Trap agarose beads. The scatter plot shows the logarithmized SILAC ratios of quantified proteins. The color-coding indicates the density.* ***E*** *Recombinant 14-3-3 binds to phosphorylated NELFE peptide. Biotinylated phosphorylated NELFE peptide corresponding to S115 (QPFQRSI**S**ADDDLQE) was bound to NeutrAvidin agarose. Phosphorylated and dephosphorylated peptides were incubated with purified 14-3-3.* ***F*** *Structure of 14-3-3ε in complex with NELFE phosphorylated peptide. Structure of the 14-3-3ε in cartoon representation (yellow) and NELFE phosphorylated peptide in ball and stick model (green).*

2.4 NELF phosphorylation regulates transcriptional elongation

Finally, we studied the function of NELFE and its phosphorylation by the p38-MK2 pathway upon UV-light exposure. In untreated cells, the NELF complex inhibits the transcriptional elongation of RNA pol 2 in Drosophila and mammals. Therefore, we questioned whether NELFE plays a role in cell survival, DNA damage repair, and transcription regulation during the cellular response to UV-light.

2.4.1 NELFE is required for cell survival after UV-light exposure

We previously observed that the inhibition of p38 MAPK results in cellular sensitivity to UV-light (**Figure 10**D). To better understand the NELFE function, we tested the effect on cell survival after UV irradiation with the knockdown of NELFE. NELFE depletion decreases cell survival after UV-light irradiation (Figure 21A). This highlights the importance of NELFE and the p38-signaling pathway for cell survival after UV-light exposure. In addition, it was recently demonstrated that XPC knockdown decreases the activation of p38 MAPK after UV-light exposure (Schreck et al., 2016). In line with this, we performed a GST-14-3-3 pull-down in cells transfected with XPC and CSB siRNAs and found that the knockdown of either resulted in the decreased binding of 14-3-3 to NELFE (Figure 21B). We also demonstrated the reduced activation of p38 MAPK in these cells. This suggests that 14-3-3 and NELFE interaction is partially dependent on DNA damage recognition by the NER machinery.

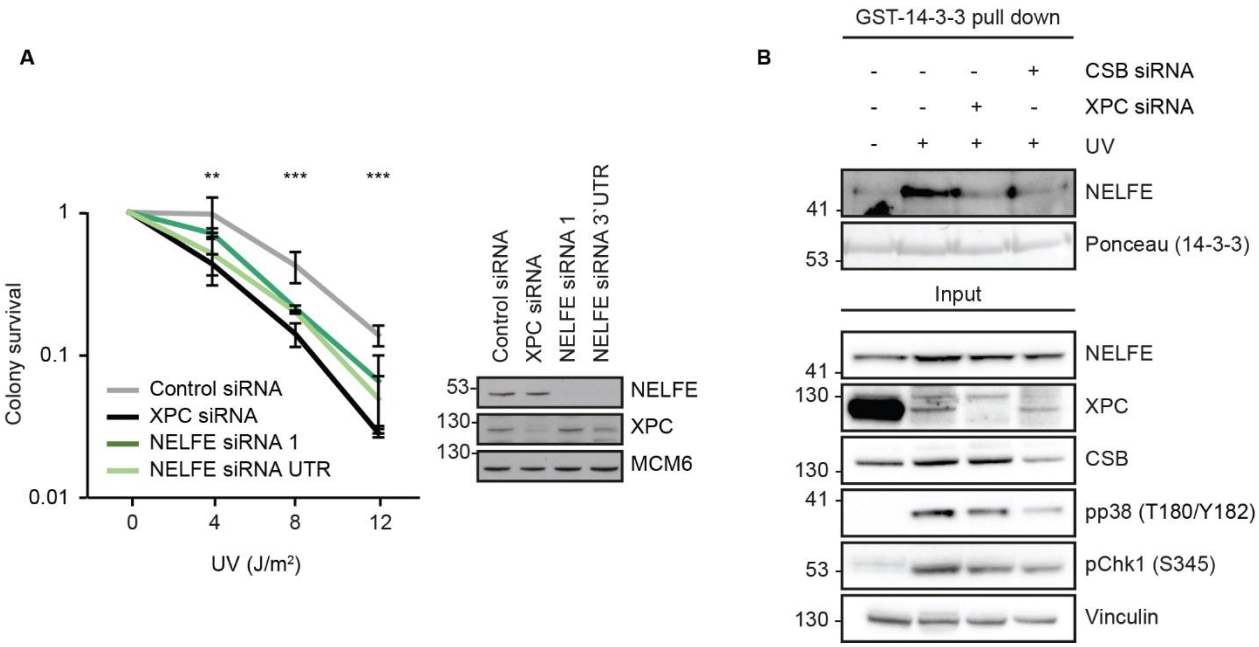

Figure 21. NELFE promotes cell survival and interacts with 14-3-3 after DNA damage recognition by XPC or CSB. A *Knockdown of NELFE reduced the ability of U2OS cells to form colonies after UV-light. The error bars show the mean and SD of results obtained in three replicate experiments performed in three technical replicates. Two-sided Student's t-test was used to assess the significance (***p-value < 0.001, **p-value < 0.01).* ***B*** *NELFE interaction with 14-3-3 is partially dependent on the NER machinery. U2OS cells were transfected with a non-targeting siRNA or siRNA targeting XPC or CSB and then irradiated with UV-light. After cell lysis, protein extracts were incubated with recombinant GST-14-3-3.*

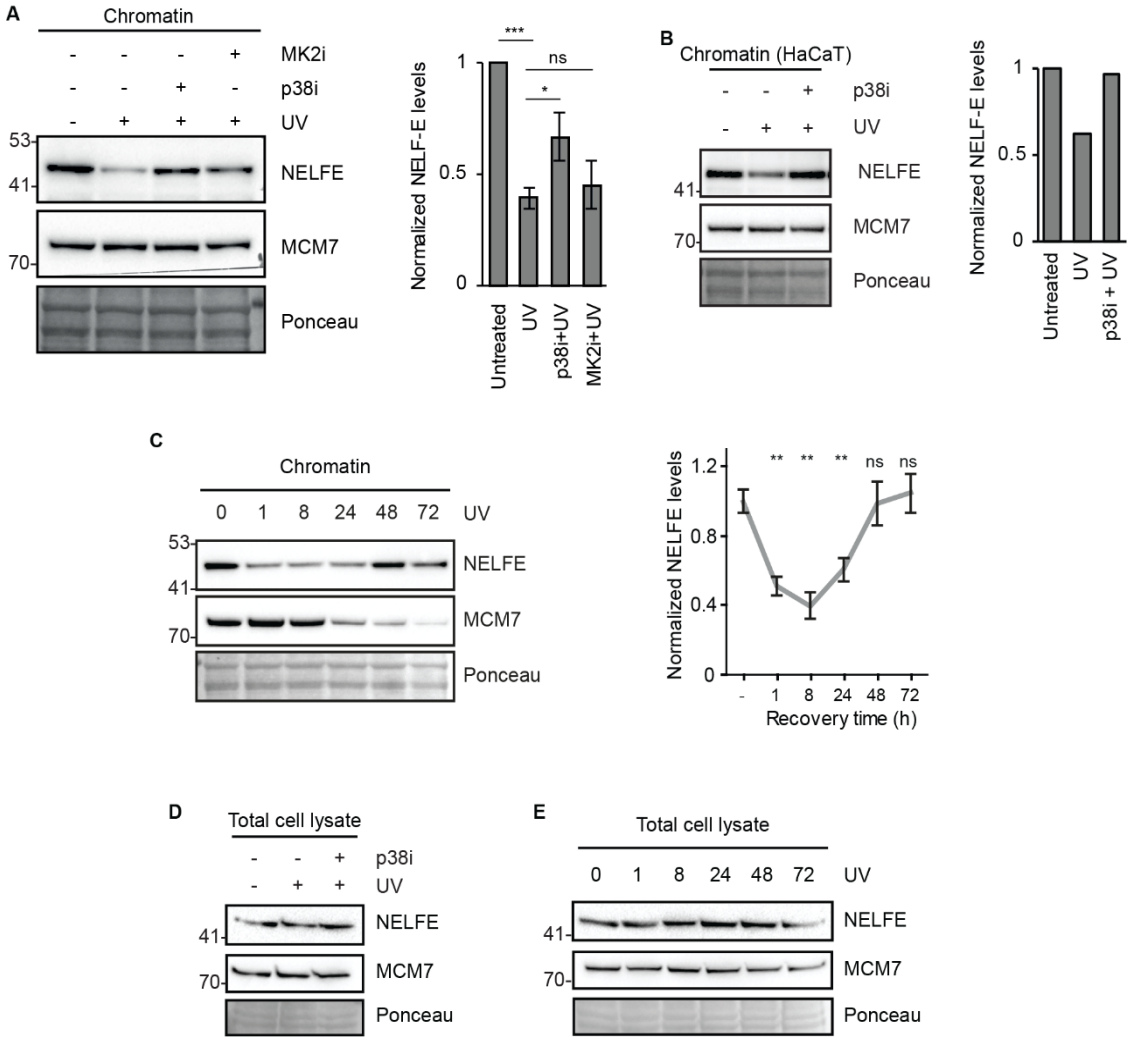

Figure 22. p38-dependent phosphorylation of NELFE promotes its dissociation from chromatin. A *NELFE dissociates from chromatin after UV-light exposure. Chromatin protein fractions from differentially treated U2OS cells were resolved by SDS-PAGE and subjected to western blotting with the indicated antibodies (left). The levels of NELFE on chromatin were quantified from three replicate experiments and normalized to MCM7 levels (right). The error bars show the mean and SD of SILAC ratios quantified from three experiments. Two-sided Student's t-test was used to assess the significance (***p-value < 0.001, **p-value < 0.01).* ***B*** *NELFE dissociates from chromatin in a p38-dependent manner after UV-light exposure in HaCaT cells. Chromatin protein fractions from differentially treated cells were resolved by SDS-PAGE and subjected to western blotting with the indicated antibodies.* ***C*** *Dynamics of NELFE removal from chromatin. Chromatin protein fractions from differentially treated U2OS cells were resolved by SDS-PAGE and subjected to western blotting with the indicated antibodies. The error bars show the mean and SD of SILAC ratios quantified from three experiments. Two-sided Student's t-test was used to assess the significance (**p-value < 0.01).* ***D*** *Amount of NELFE does not show any variation after UV-light irradiation or UV-light with p38 MAPK inhibition on total cell level.* ***E*** *U2OS cells were exposed to UV-light and left to recover for different time points. For* ***D*** *and* ***E*** *total cell lysates of U2OS cells were resolved by SDS-PAGE and proteins were detected with the indicated antibodies.*

2.4.2 p38 MAPK promotes dissociation of the NELF complex from chromatin

We analyzed the composition of the chromatin proteome upon UV-light treatment and in combination with p38 MAPK inhibition. The inhibition of p38 MAPK abolished the UV-light-induced dissociation of all NELF complex subunits from chromatin, according to our chromatin proteome MS analysis, which was confirmed with western blot for NELFE and NELFB (Figure 15E, Figure 22A). UV-light exposure

resulted in NELFE dissociation from chromatin that was also dependent on p38 MAPK activity in the human keratinocyte cell line (HaCaT) (Figure 22B). Monitoring the levels of NELFE on chromatin at various times post-UV-light irradiation revealed that NELFE levels on chromatin returned to normal, as cells recovered from DNA damage, 48 hours after irradiation (Figure 22C). We could detect differences in NELFE amount on total cell lysate level neither after one nor after 72 hours of recovery from UV-light exposure (Figure 22D,E).

2.4.3 NELFE release is accompanied by transcriptional elongation

The established role of NELFE is in the negative regulation of transcriptional elongation. Productive RNA pol 2 elongation into the gene body is achieved by the phosphorylation of the C-terminal domain of RNA pol 2 on S2, as well as NELFE phosphorylation by the P-TEFb complex containing cyclin T and CDK9 (Sawarkar, Sievers, & Paro, 2012; Schaukowitch et al., 2014). To investigate whether P-TEFb, which phosphorylates the NELF complex in unperturbed cells, has a role in regulating the interaction between NELFE and 14-3-3 after cellular stress, we inhibited its activity using 5,6-dichloro-1-β-D-ribofuranosylbenzimidazole (DRB). Inhibition of P-TEFb did not inhibit, but rather augmented, the interaction of NELFE with 14-3-3 (Figure 23A).

The NELF complex interacts with RNA pol 2 at promoter-proximal sites to inhibit transcriptional elongation (Jonkers & Lis, 2015). To further study whether NELF complex dissociation from chromatin after UV-light exposure correlates with changes in RNA pol 2 chromatin binding genome-wide, we performed a chromatin immunoprecipitation sequencing (ChIP-seq) of RNA pol 2 in untreated cells, and after UV-light exposure (40 J/m^2, one-hour recovery). As expected, in untreated cells, we could detect a clear enrichment of RNA pol 2 around transcription start sites (TSSs) (Figure 23B). Exposure of cells to UV-light resulted in a slight decrease of RNA pol 2 enrichment at TSSs, which can occur as a consequence of RNA pol 2 degradation, inhibition of transcriptional initiation, or enhanced RNA pol 2 release into downstream regions caused by NELF complex dissociation from chromatin (Figure 23B). We first tested whether NELF complex dissociation from chromatin leads to the degradation of RNA pol 2 by quantifying the levels of the RNA pol 2 subunits on chromatin by SILAC-based quantitative MS. UV-light exposure did not result in a decreased level of RNA pol 2 on chromatin one-hour post-irradiation (Figure 23C). On the contrary, the levels of RNA pol 2 on chromatin slightly increased at this point (Figure 23B). To test whether UV-light leads to RNA pol 2 release into the downstream regions of genes, we calculated the RNA pol 2 release ratio (polymerase release ratio, or PRR), which is defined as the ratio of the RNA pol 2 signal intensity in downstream regions of genes to the signal intensity at promoters (Figure 27). From RNA pol 2 ChIP-seq, we calculated PRRs for 6,898 RNA pol 2 target genes in U2OS cells. These analyses revealed a significant increase in the PRR of 2,123 genes after UV-light at one-hour

post-irradiation, compared with mock-treated cells (Figure 23D). In contrast, only 25 genes demonstrated a decrease in PRR when applying the same significance threshold. In support of these results, reanalysis of the nascent RNA sequencing (RNA-seq) from Williamson et al. also revealed a general increase in PRRs after UV-light irradiation (Figure 23D) (Williamson et al., 2017). Gene-set enrichment analysis revealed that genes with PRRs upregulated after UV-light are involved in telomere maintenance, RNA metabolism, cell cycle, DNA repair, and RAS/ERK signaling (Figure 24A,B). Notably, a comparison of these genes with NELFE targets determined by

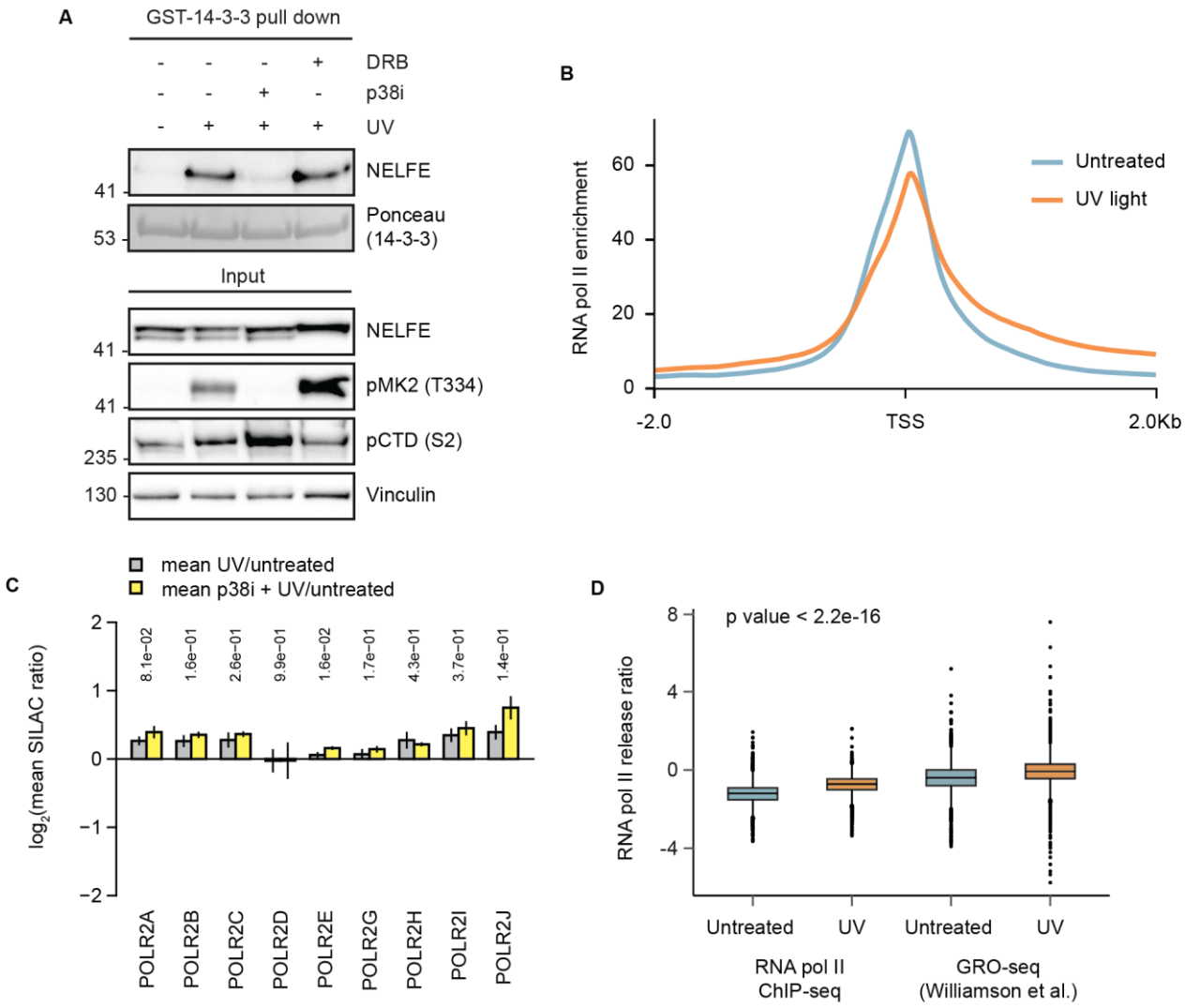

Figure 23. UV-light leads to an increase in transcriptional elongation. A *NELFE interacts with 14-3-3 after the inhibition of P-TEFb. U2OS cells were treated with the p38 inhibitor or P-TEFb inhibitor 5,6-dichloro-1-β-D-ribofuranosylbenzimidazole (DRB) and then irradiated with UV-light. After cell lysis, protein extracts were incubated with the recombinant GST-14-3-3.* ***B*** *Metagene analysis showing total RNA pol 2 occupancy measured by ChIP-seq in mock-treated U2OS cells and cells irradiated with UV-light (40 J/m^2, 1 h recovery). All TSSs bound by RNA pol 2 in untreated cells and after UV-light exposure were used for the analysis. Metagene analysis shows an average of two independent replicate ChIP-seq experiments.* ***C*** *The bar plot shows the levels of RNA pol 2 subunits on chromatin quantified in untreated U2OS cells and after UV-light by SILAC-based quantitative MS. The error bars show the mean and standard deviation of SILAC ratios quantified from three replicate experiments. A two-tailed Student's t test was used to assess the significance.* ***D*** *Comparison of PRRs calculated in untreated and UV-light-treated U2OS cells from two RNA pol 2 ChIP-seq replicate experiments with PRRs calculated from GRO-seq data from the study by Williamson et al.* (Williamson et al., 2017)*. The lower and upper hinges represent the first and third quartiles (25th and 75th percentiles, respectively). The line in the center of the box corresponds to the median of the data range.*

Results

ChIP-seq in HeLa cells identified that 70% of the genes that displayed an increase in the PRR after UV-light are also bound by NELFE (Figure 24C) (Stadelmayer et al., 2014). Taken together, our results demonstrate that the UV-light exposure of human cells results in increased RNA pol 2 elongation in a subset of genes, which temporally correlates with the p38-MK2-dependent NELF complex release from chromatin.

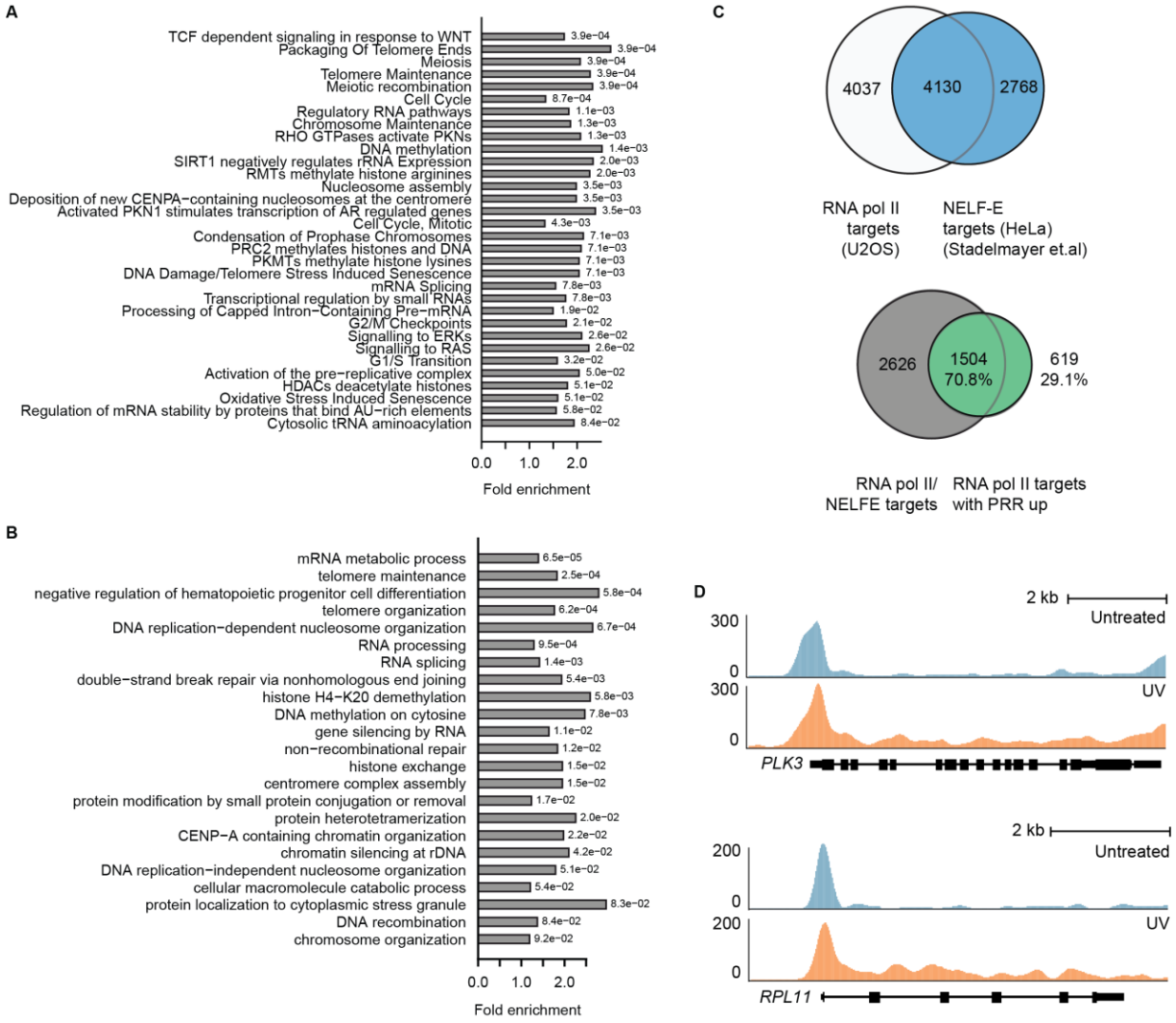

Figure 24. A number of genes show higher PRR after UV-light. ***A*** *REACTOME terms significantly enriched among genes with UV-light upregulated PRRs. The bar plot shows significantly overrepresented REACTOME terms associated with genes containing an upregulated PRR compared with all RNA pol 2 bound genes.* ***B*** *GO terms significantly enriched among genes with UV-light-upregulated PRR. The bar plot shows significantly overrepresented GO terms associated with genes containing upregulated PRR compared to all RNA pol 2 bound genes. For* ***A*** *and* ***B*** *the significance of the enrichment of a specific term was determined using a hypergeometric test. P values were corrected for multiple hypotheses testing using the Benjamini and Hochberg FDR.* ***C*** *NELFE target genes were extracted from the study by Stadelmayer et al. and overlapped with genes displaying significantly increased PRRs after UV-light exposure determined by RNA pol 2 ChIP-seq. 70.8% of genes with an increased PRR were found to be targets of NELFE in HeLa cells.* ***D*** *UCSC Genome Browser tracks displaying the density of RNA pol 2 around PLK3 and RPL11 genes in untreated cells and after exposure of cells to UV-light.*

Discussion

3.1 The p38-MK2/3 pathway is activated independently of canonical DNA damage signaling

In this study, we demonstrated the phosphorylation events induced by the irradiation of human cells with UV-light. We established the dependencies of this phosphorylation on the canonical DNA damage signaling dependent on the ATR kinase or p38-MK2/3 signaling. Furthermore, we demonstrated the role of the p38-MK2/3 pathway in the phosphorylation of RBPs during the UV-light response. We provide an inventory of UV-light-induced, p38-dependent 14-3-3 interactions, which will form a basis for further studies focusing on the function of the p38-MK2/3 pathway in the regulation of RNA metabolism after UV-light exposure. Finally, we demonstrate that the p38-MK2-dependent phosphorylation of NELFE promotes the release of NELF complex from chromatin and hence RNA pol 2 elongation after UV-light exposure.

3.1.1 ATR-CHEK1 pathway in DDR

Exposure of human cells to UV-light induces the formation of bulky UV photoproducts that interfere with DNA replication and transcription (Marteijn et al., 2014). To maintain genome stability, cells must coordinate DNA repair with cell cycle progression, DNA replication, and RNA metabolism. The ATR-CHEK1 pathway is considered the major coordinator of the cellular response to UV-light (Maréchal & Zou, 2013). CHEK1 promotes the activation of cell cycle checkpoints. An analysis of the phosphorylation sequences demonstrated that ATR prefers the S/TQ motif (Kim et al., 1999; O'Neill et al., 2000). Both PI-3Ks, ATM, and ATR were shown to phosphorylate more than 700 proteins with serine or threonine residing within the S/TQ motif in response to IR (Matsuoka et al., 2007). Interestingly, in the phosphoproteome analysis with an ATR inhibitor, we found that only 6% of UV-light-upregulated phosphorylation sites were dependent on ATR (data not shown). Moreover, in this study, we demonstrated that only 20% of all UV-light-upregulated sites possess the canonical S/TQ motif. This suggests that UV-light-induced DDR involves kinases beyond ATR (Figure 25). In accordance with this observation, we found that a number of kinases belonging to the MAPK family were phosphorylated in their activation loops after UV-

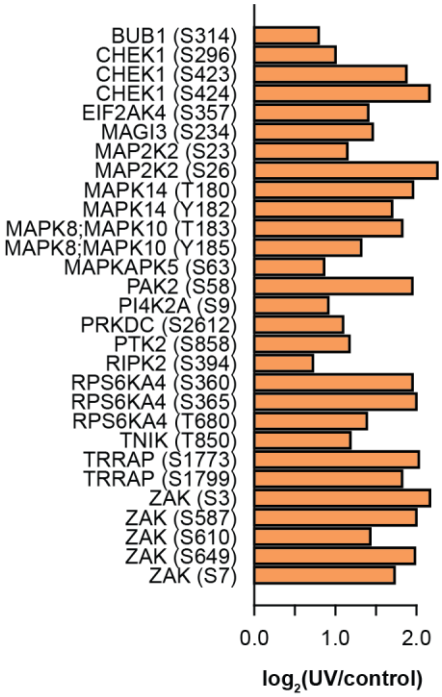

Figure 25. UV-light induces the phosphorylation of protein kinases. *The phosphorylation of kinases was monitored by SILAC-based quantitative phosphoproteomics after exposure of U2OS cells to UV-light (40 J/m^2, one-hour recovery). Protein kinases and the corresponding phosphorylation site(s) induced by UV-light are indicated. Many phosphorylation sites are found in the activation loop.*

light exposure. These include MK5 (MAPKAPK5), p38 MAPK (MAPK14), JNK (MAPK8/10), MAPK2K2, ZAK, MAGI3, and TNIK. Besides the ATR-CHEK1 pathway, the function of other kinase-dependent signaling pathways in cellular UV-light response had previously been poorly understood.

3.1.2 The role of p38 MAPK in DDR

The p38 MAPK is a general stress response regulator. In addition, p38 is crucial for the normal inflammatory response. Activated due to a number of stimuli, such as chemoattractants and bacterial, p38 MAPK modulates the production of proinflammatory cytokines through transcription factor activation (NF-κB) and mRNAs stability (Cargnello & Roux, 2011). Furthermore, the p38 MAPK pathway is activated upon IR-, UV-, ROS- and etoposide-induced DNA damage. Reinhardt et al. reported that after treatment with cisplatin or camptothecin, ATR is required for the activation of p38 MAPK, while in response to DSBs, both ATM and ATR are required for downstream p38 MAPK phosphorylation (Reinhardt et al., 2007). In contrast to these observations, UV-light-induced damage causes p38-MK2 activation that is independent of the PI3K pathways, such as ATR-CHEK1 or ATM-CHEK2 (Bulavin et al., 2001; Reinhardt et al., 2007). In our study, we confirmed that UV-light activates p38 MAPK independently of PI3Ks ATM, ATR, and DNA-PKcs. In line with the aforementioned studies, we observed a rapid activation of p38 MAPK after UV-light-induced DNA damage formation.

p38 MAPK has also been demonstrated to inhibit cell cycle progression at the G2/M and the G1/S checkpoints in response to UV-light. p38 MAPK phosphorylates downstream kinase MK2, which inactivates CDC25B by phosphorylation (Cargnello & Roux, 2011). This leads to cell cycle arrest at the G2/M phase. In contrast to previous studies, we identified the CDC25B as well as CDC25C phosphorylation sites; however, neither are significantly upregulated in our phosphoproteome screens after one-hour of recovery post-UV-irradiation. This may be due to our examining phosphorylation events occurring much earlier than those investigated in previous studies. Moreover, CDC25 phosphorylation is specific for cells in the G2 phase, and we have performed our analysis using an asynchronized cell population.

Another described function of p38 MAPK is apoptosis induction via the phosphorylation of BCL proteins. Indeed, we identified a significantly upregulated phosphorylation site on BCL9L, one of the caspase cascade activators (data not shown). p38 MAPK can also disrupt the CDC2-cyclin B complex, causing G1/S arrest (Jinlian et al., 2007). Moreover, the kinase regulates this checkpoint indirectly via the transcriptional regulation of genes coding cell cycle-involved proteins, for instance, p21 or Gadd45 (Reinhardt & Yaffe, 2009). In agreement with this, we observed increased RNA pol 2 enrichment in the gene body of Gadd45a after UV-light in our ChIP analyses (data not shown).

UV-light also activates JNK1/2 (MAPK8, MAPK10) (Figure 25). JNK phosphorylation and activation were also detected in response to most stimuli that activate p38 MAPK (Cargnello & Roux, 2011). Functionally, JNK regulates the activity

of transcription factors and subsequently the transcription of genes involved in many cellular functions. JNK and p38 MAPK pathways seem to play antagonistic roles in cell proliferation and survival. In mouse embryonic fibroblasts, the inactivation of the JNK leads to defective proliferation and senescence (Wada et al., 2008). Conversely, p38 inhibition initiates cell proliferation. Wada et al. have demonstrated that these two kinase families differentially regulate Cyclin B1-associated CDC2 kinase, which leads to the observed antagonistic effects. Interestingly, p38 MAPK activation was demonstrated to be able to direct cell fate towards both cell proliferation and death (Thornton & Rincon, 2009). In particular, the chemical inactivation of p38 MAPK increases the cell death of cancer cells after UV-light exposure (Thornton & Rincon, 2009). We demonstrated that the inactivation of p38 MAPK radiation leads to a higher sensitivity of U2OS cells to UV-light.

3.1.3 MK2/3 act redundantly downstream of p38 MAPK after UV-light exposure

We identified 138 sites present on 122 proteins that are phosphorylated in a p38-dependent manner after UV-light exposure. We also observed phosphorylation on the p38 MAPK downstream kinase MK5, which was slightly upregulated after UV-light exposure. To distinguish the effects between the downstream kinases, we used the compound PF-3644022, which is reported to inhibit MK2 (Fiore, Forli, and Manetti 2016). However, *in vivo,* it inhibits MK2, MK3, and MK5 because these three are structurally similar (Gaestel et al. 2007). The first two, MK2 and MK3, are very close homologs and were demonstrated to recognize a similar set of targets (Cargnello & Roux, 2011). Nevertheless, MK2 displays higher activity in cells, whereas MK3 knockdown was reported to have little effect (Ronkina et al. 2010). MK5 shares 38% homology with MK2 and MK3. In contrast to MK2 and MK3, MK5 can be also activated by ERKs, another large family of MAP kinases (Cargnello & Roux, 2011).

In our study, we demonstrated that 60% of the p38-dependent phosphorylation sites are downregulated by PF-3644022. We used siRNA knockdown for a more detailed analysis because no specific inhibitors are available for the MK2/3 and MK5. The analysis revealed that 60% of the p38-dependent sites are MK2/3 targets, and 18% belong to MK5. The double knockdown of MK2 and MK3 decreased the phosphorylation of the majority of the p38 MAPK substrates, establishing that MK2 and MK3 are the primary transducers of p38 MAPK signaling after UV-light exposure.

3.2 14-3-3 proteins are general p38-MK2/3 phosphorylation readers

14-3-3 protein family interacts with a wide variety of cellular proteins. It was determined that 14-3-3 prefers the binding motifs RSxp[ST]xP or Rxxxp[ST]xP (Powell et al., 2003). The same motifs are targets for MK2/3/5 phosphorylation, as we also demonstrate in this study. An analysis of the UV-light-induced interaction partners of 14-3-3 revealed CHEK1 and many proteins involved in RNA metabolism (Blasius et al., 2014). This interaction is crucial for CHEK1 activation and its nuclear retention, where CHEK1-14-3-3 inactivates transcriptional repression through atypical E2Fs for the G1/S cell cycle transition (Yuan et al., 2018). The CHEK1 phosphorylation is

regulated by ATR but not affected by p38-MK2 pathway inhibition. 14-3-3 RNA-related targets include the NEXT complex, the mRNA cleavage and polyadenylation complex (CPSF), EIF4E and ZNF598 involved in translational repression, and the NELF complex (this study and (Blasius et al., 2014)). UV-light also induces 14-3-3 binding with PCNA, and it was suggested that this interaction stabilizes non- and mono-ubiquitylated PCNA on the chromatin (Gao et al., 2015). Moreover, we have demonstrated that many of these RBPs are phosphorylated in a p38-MK2/3-dependent manner, and this serves as a platform for the recruitment of 14-3-3 proteins. We have now established that the p38-MK2-dependent recruitment of 14-3-3 to RBPs provides a broad regulatory mechanism that functions rapidly upon the exposure of cells to UV-light.

3.3 Regulation of transcription after UV-light exposure

UV-light-induced DDR includes the complex regulation of transcription. We have demonstrated that p38-MK2/3 phosphorylation, on the one side, and 14-3-3 binding-dependent function, on the other side, form a regulatory pathway for proteins involved in transcriptional regulation after UV-light exposure.

3.3.1 The role of the p38-MK2/3 pathway in transcriptional elongation

The p38-MK2/3 pathway regulates various aspects of cellular function after various stress stimuli. We have demonstrated that UV-light triggers the widespread and rapid phosphorylation of RBPs that is specifically dependent upon the p38-MK2/3 pathway. It was previously shown that UV-light globally affects distinct stages of RNA metabolism, including transcription, splicing, and translation (Wickramasinghe & Venkitaraman, 2016). However, the signaling pathways and mechanisms that regulate RNA metabolism after UV-light exposure remained poorly understood. Recent studies that employed nascent RNA-seq to monitor transcription after UV-light exposure reported changes in transcriptional elongation (Andrade-Lima et al., 2015; Lavigne, Konstantopoulos, Ntakou-Zamplara, Liakos, & Fousteri, 2017; Williamson et al., 2017). It was recently demonstrated that transcriptional elongation is slowed by the significant release of RNA pol 2 from PPP (Williamson et al., 2017). In agreement with this, we observed less RNA pol 2 in TSS regions and an increase in the PRR for a number of genes after one-hour of recovery from UV-light exposure. In our phosphoproteome analysis, we demonstrated that many of the identified p38-MK2 protein substrates are transcriptional regulators. More specifically, we demonstrated that the NELF complex is a substrate of p38-MK2-dependent phosphorylation after the exposure of cells to UV-light. The complex is removed from chromatin after the exposure, most probably in a 14-3-3-dependent manner. In agreement with our results, a recent study reported that UV-light triggers RNA pol 2 elongation and the transcription of highly expressed genes, which leads to enhanced DNA damage sensing by RNA pol 2 and DNA repair through the TC-NER pathway (Lavigne et al., 2017). We also demonstrated that cells lacking either CSB or XPC have a reduced p38-MK2/3 response, which was also previously demonstrated in studies with cisplatin and reactive diol epoxides that cause

the initiation of NER (Schreck et al., 2016). Accordingly, we suggest that the release of RNA pol 2 to check DNA for damage is mediated through the p38-MK2-NELF-14-3-3 mechanism.

In addition to the NELF complex, we found other proteins involved in transcriptional activation and transcriptional elongation (i.e., TRIM28 and LARP7 are phosphorylated by p38 (Bunch et al., 2014; He et al., 2008); LARP7 inhibits P-TEFβ leading to NELF and RNA pol 2 release into elongation (He et al., 2008)). TRIM28 regulates gene expression through an as of yet unclear mechanism that probably involves histone methylation and deacetylation (Bunch et al., 2014). Moreover, the transcription activators MED1, TRRAP, and SUPT6H and the chromatin remodelers ARID1A and CHD6 were also found in the phosphoproteome screen as p38 MAPK targets. These findings suggest that multiple p38-MK2-mediated phosphorylation-dependent events might cooperate to promote RNA pol 2 elongation after UV-light exposure.

3.3.2 The role of the NELF complex in the regulation of transcriptional elongation after UV-light exposure

In human cells, the NELF complex (comprising the four subunits NELFA, NELFB, NELFCD, and NELFE) inhibits RNA pol 2 elongation shortly after initiation to induce PPP (Jonkers & Lis, 2015), which was suggested to occur in many, if not all, genes. It seems to be particularly crucial in the regulation of developmental and stimuli-induced genes (Gaertner et al., 2012; Lagha et al., 2013; Min et al., 2011; Schaukowitch et al., 2014; L. H. Williams et al., 2015). Interestingly, the NELF complex was recently associated with the DSB repair pathway. Awwad *et al.* have demonstrated that only the NELFE and NELFA subunits are recruited to DSBs to repress transcription and promote DNA repair (Awwad, Abu-Zhayia, Guttmann-Raviv, & Ayoub, 2017). On the contrary, we observed that all NELF subunits are equally removed from the chromatin after UV-light irradiation. This suggests that the NELF complex and transcriptional elongation are differentially regulated, depending on the type of DNA damage. Here, we demonstrated the phosphorylation of the RNA-binding subunit NELFE on S49/51, S115, and S251 by MK2. Phosphorylation on serine 115 (S115) significantly promotes NELFE binding to 14-3-3 and the dissociation of the NELF complex from chromatin. This leads to RNA pol 2 elongation in genes functioning in telomere maintenance, RNA metabolism, cell cycle, and DNA repair. Interestingly, we also found that the NELFA subunit of the NELF complex contains a UV-light-induced, p38-dependent phosphorylation site that is predicted to bind to 14-3-3 and could thus provide an alternative secondary binding surface for the 14-3-3 dimer. On the other hand, we observed a decrease in binding between NELFE and 14-3-3 upon the mutation of S49/51 and S251 to alanine, which suggests that one of these phosphorylation sites could also serve as a secondary binding surface for the 14-3-3 homo- or heterodimer *in vivo*.

The knockdown of the NELFE subunit of the NELF complex was shown to result in global RNA pol 2 elongation in unstressed primary cells and in cancer cells (Gibson

et al., 2016; X. Liu et al., 2017). Likewise, the NELFE ADP-ribosylation has been shown to promote RNA pol 2 elongation in unstressed cells (Gibson et al., 2016). It is possible that distinct PTMs of NELFE, including phosphorylation and ADP-ribosylation, cooperate to promote RNA pol 2 elongation in response to UV-light exposure.

After UV-light exposure, p38 MAPK activation leads to NELFE removal from chromatin. We identified that the proteasome inhibitor, MG132, stabilizes NELFE in both untreated and UV-light-radiated cells. Proteins for proteasomal degradation are usually tagged with ubiquitin (Dikic, 2017). Therefore, one possible path to NELFE degradation is ubiquitylation. However, no reported ubiquitylation sites exist on NELFE, and our PTM analysis on NELFE demonstrated changes only in phosphorylation sites (data not shown). For sequence composition and technical reasons, NELFE ubiquitylation sites may have escaped our MS analysis. Western blot and MS analysis of all NELF subunits for potential PTMs, in particular ubiquitylation, could help in understanding the fate of NELF after dissociation. On the other hand, the regulated dissociation of the NELF complex from chromatin by a various mechanism, mediated by enhancer RNAs (eRNAs), was shown to promote the induction of immediate-early genes in response to an increase in neuronal activity (Schaukowitch et al., 2014). It would be interesting to check whether UV-light-induced NELF release is regulated by eRNAs in addition to 14-3-3. To answer this question, nascent RNA from differentially treated samples could be analyzed by precision nuclear run-on sequencing (PRO-Seq) (Mahat et al., 2016; Schaukowitch et al., 2014). PRO-seq includes a run-on reaction with biotin-dNTPs after cell lysis and the enrichment of RNA incorporated the modified nucleotides from the 3’ end. The technique allows the identification of all types of RNA with high resolution.

Taken together, our study suggests a mechanistic model beginning with the activation of p38 MAPK by UV-light, subsequently transferring the phosphorylation onto MK2 and the NELF complex subunit NELFE, and possibly NELFA. The phosphorylation serves as a platform for 14-3-3 protein binding that facilitates the removal of NELF from chromatin and RNA pol 2 elongation (Figure 26). We could also speculate about the upstream and downstream events of this model. XPC was shown to be necessary for p38 MAPK activation during bulky lesions’ repair (Schreck et al., 2016). Accordingly, we validated, with CSB and XPC knockdown, that these proteins are crucial for p38 MAPK activation and for NELFE-14-3-3 binding. Our results suggest that a positive feedback loop may exist. The first recognized UV-light-induced lesions activate NER. CSB or/and XPC trigger the p38-MK2/3 signaling axis and the release of RNA pol 2 through NELF dissociation. The polymerase transcribes until the unrepaired lesions are found. This begins the next round of repair and transcription release.

3.3.3 NELF role in tumorigenesis

The regulation of gene expression through NELF complex was demonstrated, in the first place, to be crucial for stress-induced and developmental genes, such as hsp70, junB, human immunodeficiency virus genes, estrogen-responsive genes in breast cancer cells, and inflammatory response genes in macrophages (Yung, Narita, Komori, Yamaguchi, & Handa, 2009). Any modification in NELF sequence or composition affects cell function. For instance, mutations in NELF subunits were found to be involved in the pathogenesis of breast cancer and Wolf-Hirschhorn syndrome (WHS), as well as leading to problems in early embryogenesis and immune response. Furthermore, the depletion of NELF causes the formation of either multi-nuclei cells or cells with an enlarged nucleus (Yung et al., 2009). Interestingly, the knockdown of the subunits of NELF demonstrates distinct effects on metastasis. The knockdown of NELFE was reported to inhibit the invasion of hepatocellular carcinoma cells (IIDA et al., 2012). In addition, an analysis of NELFE mRNA demonstrated an increase in patients with melanoma, ovarian cancer, and glioma (Uhlen et al., 2017). Conversely, the expression of NELFB, also called the co-factor for BRCA1 (COBRA1), and NELFC/D are decreased in severe breast cancer, and the knockdown of any of these NELF subunits increases the motility of the cancer cells (IIDA et al., 2012). We demonstrated that NELFE knockdown leads to decreased cell viability after UV-light exposure. Altogether, our findings highlight the importance of NELF regulation with the p38-MK2 pathway during the response to UV-light radiation; this may be relevant in the tumorigenesis of melanoma.

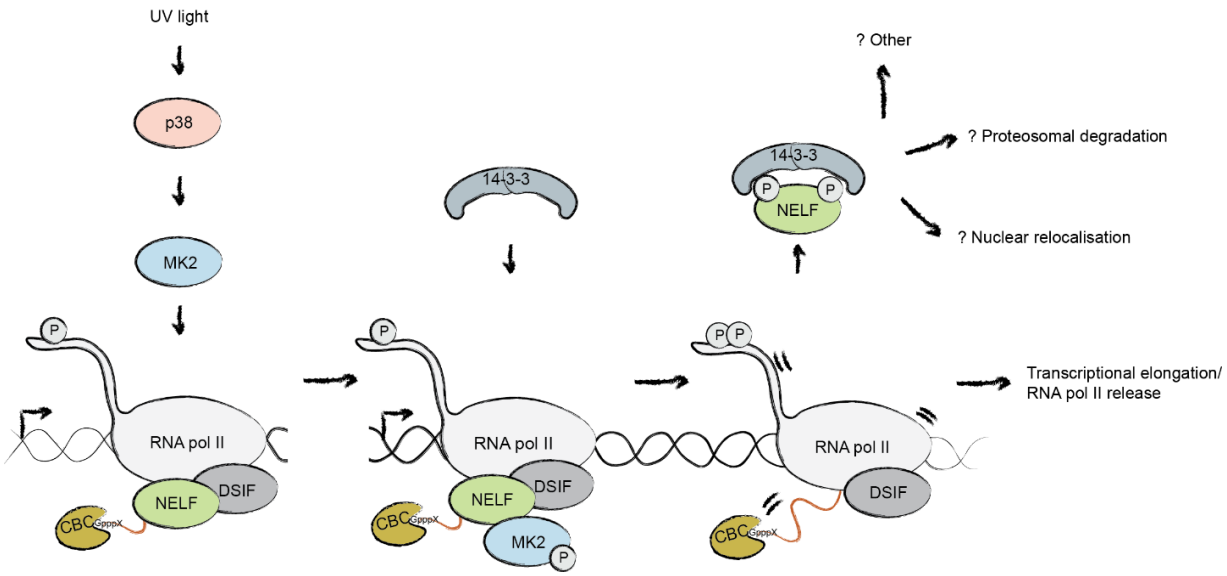

Figure 26. Model for NELF complex regulation by p38-MK2. *Exposure of human cells to UV-light leads to the rapid activation of p38 and its downstream effector kinase MK2. MK2 triggers the widespread phosphorylation of RNA-binding proteins, including the NELF complex subunit NELFE. Site-specific NELFE phosphorylation on S115 induces its transient interaction with 14-3-3. NELFE phosphorylation leads to dissociation of NELF from chromatin that is followed by RNA pol II elongation. Further, NELF is probably degraded by the proteasome.*

3.4 The role of the p38-MK2/3 pathway in RNA splicing, stability, and translation

Globally, UV-light induces a transcription switch to the slower mode and subsequently affects downstream processes such as splicing, termination, mRNA stability and transport, and translation (Gregersen & Svejstrup, 2018). For efficient repair, the cell should produce proteins that help in recovery processes. Several proteins with the GO term “RNA binding,” such as the RNA-binding protein RBM14 and Matrin-3 (MATR3), are potential p38 MAPK targets. Moreover, the p38-MK2/3 pathway is required for the phosphorylation of the U6 snRNA-associated Sm-like protein LSM1, RNA helicases DDX20, and Gem-associated protein GEMIN5. The latter are part of the SMN complex and mediate the biogenesis of spliceosomal small nuclear ribonucleoproteins (snRNPs) (Battle et al., 2006).

The p38 pathway regulates mRNA stability. Activation of the p38 MAPK pathway with UV-light was previously shown to stabilize transcripts containing AU-rich elements (Bollig et al., 2002). These elements are found in the 3’-UTR of many oncogenes and cytokine genes. Accordingly, we found proteins involved in the degradation of ARE-containing mRNA (i.e., PARN, KHSRP, and ZFP36) among p38-MK2 targets. In addition, the phosphorylation of mRNA polyadenylation proteins (WDR33 and SYMPK) also decreased after p38 MAPK inhibition. We also found exosome proteins from the NEXT complex, RBM7, and ZCCHC8 as substrates of p38-MK2. They were previously shown to be substrates of the UV-light-induced p38-MK2 pathway, and their phosphorylation leads to non-coding RNA accumulation (Blasius et al., 2014).

Translation was reported to be partially stopped upon UV-light exposure; however, the transcripts of stress response factors should still be translated (Powley et al., 2009). We identified EIF5, EIF4G1, SRP54, and DHX29 as novel substrates of the p38-MK2/3 pathway. The phosphorylation of these proteins potentially presents the means of translational regulation mediated by the p38-MK2/3 pathway upon UV-light exposure.

These findings extend the understanding of the role of RBPs in DDR and highlight the importance of the p38-MK2/3 pathway in the UV-light response.

Conclusions

Taken together, in this study, we chart a map of the phosphorylation events induced in human cells after irradiation with UV-light and establish the dependencies of this phosphorylation on canonical DNA damage signaling and the p38-MK2/3 signaling axes. We investigated how the p38-MK2 pathway induces transcription through the phosphorylation of a NELF subunit after UV-light exposure in more detail. The provided datasets of UV-light-induced phosphorylation sites and p38-dependent 14-3-3 interactions will enable further studies focusing on the functions of the p38-MK2 pathway in the regulation of various RNA metabolic processes after UV-light exposure.

Materials and methods

4.1 List of solutions and buffers

A complete list of siRNAs, chemicals, inhibitors, plasmid constructs, primers, and antibodies used in this work can be found in the appendix.

4.1.1. Buffers and solutions

Buffer/Solution	Composition
	0.1% Triton-X in PBS
PBS-T	1 × PBS, 0.1% Tween-20
Blocking solution	10% skimmed milk solution in PBS-T
Modified RIPA buffer	50 mM Tris pH 7.5, 150 mM NaCl, 1 mM EDTA, 1% Igepal CA-630, 0.1% sodium deoxycholate
Fractionation buffer A	10 mM HEPFES pH 7.5, 10 mM KCl, 1.5 mM MgCl2, 0.34 M glucose, 10% glycerol, 1 mM DTT, 0.1% Triton-X100
Fractionation buffer B	3 mM EDTA, 0.2 mM EGTA, 1 mM DTT
Lysis buffer	50 mM Tris pH 7.5, 150 mM NaCl
GST Elution buffer	50 mM Tris pH 7.5, 150 mM NaCl, 1 mM DTT, 15 mM reduced glutathione
Peptide dilution buffer	PBS, 0.1% Triton X-100, 2 mM DTT
Peptide wash buffer	PBS, 300 mM NaCl, 0.1% Triton X-100, 2 mM DTT
Denaturation buffer	6 M urea, 2 M thiourea in 10 mM HEPES-NaOH pH 8.0
Binding buffer	50% ACN, 6% TFA
Wash buffer	50% ACN, 0.1% TFA
Elution buffer 1	5% ammonia (NH_4OH)
Elution buffer 2	10% NH_4OH, 25% CAN
SCX wash buffer	40% ACN, 0.1% TFA
SCX elution buffers	40 mM acetic acid, 40 mM boric acid, 40 mM phosphoric acid. (Adjust pH to 3.0, 3.5, 4.5, 6.0, and 8.5 with sodium hydroxide. Add 40% ACN before use)
2× Digestion buffer	50 mM ammonium bicarbonate in water, pH 8.0
Destaining solution	50% Ethanol, 50% 2× digestion buffer
Digestion buffer	25 mM ammonium bicarbonate in water pH 8.0
Trypsin solution	25µl trypsin, 1ml digestion buffer
Peptide extraction buffer	30% ACN, 3% TFA
In-gel Buffer B	80% ACN, 0.5% acetic acid
Buffer A	0.1% formic acid
Buffer B	80% ACN, 0.1% formic acid
C_{18} elution buffer	50% ACN, 0.1% formic acid
Buffer A*	5% ACN, 0.1% TFA
Kinase buffer	25 mM HEPES pH 7.2, 25 mM MgCl, 2 mM DTT
Urea-SDS buffer	8 M Urea, 2% SDS in PBS
Farnham buffer	5 mM PIPES pH 8.0, 85 mM KCl, 0.5% IGEPAL CA-630

Shearing buffer	10 mM Tris-HCl pH 8.0, 0.1% SDS, 1 mM EDTA
Wash buffer 1	10 mM Tris-HCl pH 8.0, 100 mM NaCl, 1 mM EDTA, 0.5 mM EGTA, 0.1% sodium deoxycholate, 0.5% N-Lauroylsarcosine
Wash buffer 2	0.25 M LiCl, 1% IGEPAL CA-630, 1% sodium deoxycholate, 1 mM EDTA
ChIP Elution buffer	1% SDS, 0.1 M $NaHCO_3$

4.1.2. Enzymes, reagents, and commercially available kits

Ezyme	Supplier
Nuclease	Sigma Aldrich
Antarctic Phosphatase	NEB
RNase A (0.2 mg/ml)	Sigma Aldrich
Proteinase K (50 µg/ml)	Sigma Aldrich
Reagent	**Supplier**
Common reagents	
RNase free water	Sigma Aldrich
Methanol	Sigma Aldrich
Ethanol	Sigma Aldrich
Trifluoroacetic acid (TFA)	Sigma Aldrich
Sodium chloride (NaCl)	Sigma Aldrich
Acetic acid	Sigma Aldrich
Acetonitrile (ACN)	Sigma Aldrich
Formic acid	Sigma Aldrich
Acetone	Sigma Aldrich
Cell culture and SILAC labeling	
Dulbecco's Modified Eagle Medium (D-MEM)	Gibco
D-MEM for SILAC without lysine and arginine	Life Technologies
10% fetal bovine serum (FBS)	Gibco
2 mM L-glutamine	Gibco
100 U/ml Penicillin/Streptomycin	Gibco
Puromycin	Invivogen
L-arginine (Arg0)	Cambridge Isotope Laboratories
L-lysine (Lys0)	
L-arginine-U-^{13}C6 99% (Arg6)	
L-lysine-4,4,5,5,-D4 96–98% (Lys4)	
L-arginine-U-13C6-^{15}N4 99% (Arg10)	
L-lysine-U-^{13}C6-^{15}N2 99% (Lys8)	
Dialyzed FBS (10,000 molecular weight cut-off)	Sigma Aldrich
Dulbecco's Phosphate-Buffered Saline (D-PBS)	Gibco
0.05% Trypsin-EDTA	Gibco
Transfection of cells	
Lipofectamine RNAiMAX	Life Technologies
Opti-MEM with GlutaMAX	Gibco
Linear polyethylenimine transfection (PEI, HCl Max, 40000)	Polysciences, Inc.
Colony formation and cell proliferation assays	
0.4% Crystal violet solution	Sigma Aldrich
CellTiter-Blue Cell Viability Assay	Promega

Immunofluorescence and confocal microscopy	
4% paraformaldehyde (PFA) in PBS	Affymetrix
Vectashield mounting medium containing DAPI	Vector Laboratories
Molecular biology	
Gateway LR Clonase II	Invitrogen
Q5 MasterMix	NEB
Dimethyl sulfoxide (DMSO)	Sigma Aldrich
Blunt/TA-ligase master mix	Invitrogen
High efficiency DH5α *E.coli*	NEB
Cell lysis	
Complete protease inhibitor cocktail tablets	Roche Diagnostics
Phosphatase inhibitors: 1 mM sodium orthovanadate 5 mM β-glycerophosphate 5 mM sodium fluoride	Sigma Aldrich
N-ethylmaleimide (NEM)	Sigma Aldrich
QuickStart Bradford 1 × Dye Protein Reagent	BioRad
SDS-PAGE and western blotting	
SuperSignal West Pico Chemiluminescent Substrate	Thermo Scientific
NuPAGE LDS Sample Buffer (4×) (LDS SB)	Thermo Fisher Scientific
Bovine serum albumin (BSA)	Sigma Aldrich
Purification of recombinant proteins	
Isopropyl β-D-1-thiogalactopyranoside (IPTG)	Sigma Aldrich
Lysozyme	Sigma Aldrich
Glutathione Sepharose 4B	GE Healthcare
NeutrAvidin agarose beads	Life Technologies
Co-immunoprecipitation and pull-downs	
StrepTactin sepharose beads	IBA
Dynabeads Protein G	Invitrogen
GFP Trap agarose	Chromotek
λ phosphatase	NEB
Phosphatase reaction buffer	NEB
Mass spectrometry-based proteomic	
All solutions should be prepared with Milli-Q water of 18.2 MΩ·cm resistivity at 25 °C.	
Lysyl endopeptidase (Lys-C)	Wako Chemicals
Sequencing grade Trypsin (0.5 µg/µl in 50 mM acetic acid)	Sigma Aldrich
Chloroacetamide (CAA)	Sigma Aldrich
Dithiothreitol (DTT)	Sigma Aldrich
Titansphere TiO bulk material (TiO_2) 10 µm	GL Sciences Inc
Colloidal Blue Staining Kit	Life Technologies
ATP	Sigma Aldrich
Genomics	
Dynabeads Protein G	Invitrogen
SYBR Green	ABI
Kit	**Supplier**
Qubit dsDNA HS Assay Kit	Life Technologies
NucleoBond Xtra Midi	Macherey-Nagel

4.2 Cell culture

Human osteosarcoma (U2OS), human embryonic kidney 293 (HEK293T), and human retinal pigment epithelium 1 (RPE-1) cells were cultured in D-MEM supplemented with 10% FBS, 2 mM L-glutamine and 100 U/ml Penicillin/Streptomycin. U2OS cells stably expressing Flag-Strep tagged wild-type NELFE or mutants NELFE S115A or NELFE S49/51/115A were cultured in D-MEM additionally supplemented with 1 µg/ml puromycin. For SILAC labeling, cells were cultured in media containing either Arg0 and Lys0, Arg6 and Lys4, or Arg10 and Lys8 (Ong & Mann, 2006). Amino acids were added to a final concentration of 28 mg/L and 48.7 mg/L of arginine and lysine, respectively. For the SILAC D-MEM, dialyzed FBS was used. All cells were cultured at 37°C in a humidified incubator containing 5% CO_2. For maintenance, cells were washed twice with DPBS followed by addition of 0.05% Trypsin-EDTA. After dissociation from the cell culture plates, cells were collected in complete D-MEM, spun down (5 minutes, 250 × *g*), re-suspended in fresh medium and plated at the desired density.

4.2.1 Transfection of cells

Transfection of small interfering RNA (siRNA) was performed using 6 µL Lipofectamine RNAiMAX and 4 µL siRNA. Each was mixed with 100 µL Opti-MEM with GlutaMAX separately and then combined. The mix was incubated for five minutes and added dropwise to cells in a well in 6-well plate. All siRNAs used in this study are ordered from Sigma Aldrich (purification “Deprotected and Desalted”) and listed in Table 5. The stock concentration is 10 µM. Plasmid transfection was performed using 7.5 µL PEI and 2.5 µg plasmid (Longo, Kavran, Kim, & Leahy, 2013). The components were mixed in 100 µL Opti-MEM with GlutaMAX. The mix was incubated for 15 minutes and added to a well of cells in 6-well plate. The constructs and the source of the vectors are shown in Table 8.

4.2.2 Genotoxic treatment of cells

Inhibitors were added to the cells as indicated in Table 6. UV-light irradiation was performed using the in-house built UV chamber with a detector inside. Chemical treatment was performed as indicated in Table 7.

4.2.3 Colony formation assay

Cells were transfected with respective siRNAs in 6-well plates. 24 hours after transfection cells were re-plated on 6 cm tissue culture plates at a density of 1,000-3,000 cells per plate. 72 hours post-transfection, growth medium was aspirated, cells were washed with DPBS and irradiated with the indicated UV-C light dose. Colonies were stained with 0.4% Crystal violet solution in 20% ethanol and counted 12-14 days after irradiation. Each experiment was performed in triplicates. The “Colony survival” ratio was calculated and plotted on logarithmic scales.

$$\text{Colony survival} = \frac{\text{Average } (c_t)}{\text{Average } (c_0)} \frac{(n_t)}{(n_0)},$$

where c_t is the number of colonies in treated plates, c_0 – the number of colonies in untreated plates, n_0 – the number of plated cells for untreated plates, and n_t – the number of plated cells for treated plates.

4.2.4 Cell viability

Cells were plated on 6-well tissue culture plates at a density of 300,000 cells per well. In case of siRNA transfection cell viability was measured 72 hours post-transfection. Cells were treated with the corresponding inhibitor and irradiated with UV-light. 24 h post-treatment, the CellTiter-Blue Cell Viability solution was added to the cells for three hours. 100 µL media from each 6-well was placed into a well of a 96-well plate and measured on the Plate Reader (Tecan) with the parameters: excitation wavelength 560 nm, emission wavelength 590 nm, number of flashes 25, and integration time 20 µs.

4.2.5 Immunofluorescence and confocal microscopy

Cells were fixed with 4% PFA and permeabilized with 0.1% Triton-X in D-PBS. Cells were blocked with 1% bovine serum albumin in PBS and incubated with the primary antibodies and with the corresponding secondary antibody coupled to Alexa Fluor 488 or 568. Mounting was performed with Vectashield mounting medium containing DAPI. Images were taken by the TCS SP5 (Leica) confocal inverted microscope at 63× oil objective. The images were obtained in and exported from Leica Application Suite (LAS). The parameters for the acquisition of pictures were set to default except Scan “bidirectional”, line average 4 with acquisition 2, Speed 1000 Hz, Format 1024x1024, Sequential Scan “between frames”.

4.3 Molecular biology

4.3.1 Gateway cloning

The tagged genes of interest were generated using Gateway LR Clonase II and corresponding destination (DEST) and entry vectors (ENTR, DONR) according to the manufacturer’s instructions. The construct and the source of the vectors are shown in Table 8.

4.3.2 Site-directed mutagenesis

Primers for the point mutations were generated with QuikChange Primer Design II tool (Table 9). The site-directed mutagenesis PCR was performed using Q5 MasterMix according to the manufacturer’s instructions. The mutations were introduced into the pENTR221 NELFE plasmid and the tagged constructs were generated with corresponding Gateway-compatible destination vectors.

PCR mix		PCR Program	
12.5 µL	2x Q5 Master Mix	30 sec at 98 °C	
80 ng	Template	10 sec at 98 °C	30 cycles
1.25 µL	Primer mix forward and reverse (10 mM)	1 min at 50 °C	
0-2 µL	DMSO	4 min 30 sec at 72°C	
Up to 25 µL	RNase free water	2 min at 72 °C	
		Pause at 4°C	

The samples were treated with 0.5 µL DpnI for 30 minutes at 37ºC. For the ligation of 100 ng newly synthesized plasmid, 5 µL Blunt/TA-ligase master mix was incubated for 15 minutes at room temperature and followed by High-efficiency DH5α *E.coli* transformation.

4.4 Biochemistry

4.4.1 SDS-PAGE and western blotting

Lysates were mixed with 4×LDS sample buffer supplemented with 1 mM DTT, heated at 70ºC for 10 min, and loaded onto NuPAGE Bis-Tris gels with 4-12% gradient (Life Technologies). Subsequently, proteins were transferred onto 0.45 µm nitrocellulose membranes. Membranes were blocked using Blocking solution. The list of antibodies used in this study and conditions can be found in Table 10. Secondary antibodies in 5% BSA with PBS-T were used for immunodetection. The membrane was washed in PBS-T four times for five minutes between incubations with primary or secondary antibodies. The detection was performed with SuperSignal West Pico Chemiluminescent Substrate.

4.4.2 Total cell lysis

Cells were lysed in modified RIPA buffer supplemented with protease inhibitors and phosphatase inhibitors, and NEM. To release chromatin-bound proteins, 450 mM NaCl was added to the cell pellet. Lysates were treated with the nuclease or sonicated until the solution became clear and the debris was removed by centrifugation at 16,000×g for 10 minutes. Protein concentrations were estimated using Bradford.

4.4.3 Cellular fractionation

Separation of cellular fractions was performed as described with minor modifications (Méndez & Stillman, 2000). Cells were washed on plates with ice-cold PBS and collected by scraping. Pelleted cells were lysed in Fractionation buffer A supplemented with protease and phosphatase inhibitors, and NEM. Nuclei were pelleted by 1,300 × *g* for five minutes and resuspended in Fractionation buffer B supplemented with protease and phosphatase inhibitors. After incubation, cells were centrifuged 1,700 × *g* for five minutes and chromatin was dissolved in the modified RIPA buffer with a salt concentration adjusted to 450 mM NaCl. To release chromatin-

bound proteins the nuclease was added. The lysates were cleared by centrifugation at 16,000 × *g* for 10 minutes and protein concentrations were estimated using Bradford.

4.4.4 Pull-downs using GFP-Trap agarose or StrepTactin sepharose

Cell lysates were prepared as described in Total cell lysis or Cellular fractionation sections and 4% of input protein was saved. 25 µL of pre-equilibrated StrepTactin sepharose beads or 20 µL of GFP Trap agarose were added to 1 mg of lysate and incubated for one-hour in the cold room on a rotation wheel. The beads were washed four times with modified RIPA buffer supplemented with protease and phosphatase inhibitors. Bound proteins were eluted in 2×LDS sample buffer supplemented with 1 mM DTT, heated at 70ºC for ten minutes, and loaded onto 4-12% gradient SDS-PAGE gels (Life Technologies).

4.4.5 Co-immunoprecipitation

Cell lysates were prepared as described in Total cell lysis or Cellular fractionation sections and 4% of protein input was saved. To preclear the lysate, 20 µl slurry solution of Dynabeads Protein G was washed in modified RIPA buffer and combined with 1 mg lysates and incubated for one-hour in the cold room on a rotation wheel. The precleared lysate was collected and combined with freshly washed 20 µl slurry solution of Dynabeads Protein G with 5 µg of an antibody and incubated for four hours at 4°C. After incubation, beads were washed with modified RIPA buffer 4 times. Elution was done by adding 2×LDS SB supplemented with 1 mM DTT to the beads in a 1:1 volume, and heating at 70ºC for ten minutes. The samples were then loaded onto NuPAGE Bis-Tris gels with 4-12% gradient (Life Technologies).

4.4.6 Purification of GST-14-3-3 and GST-pull downs

High-efficiency DH5α *E.coli* were transformed with a plasmid encoding GST-14-3-3. The protein expression was induced, after the bacteria reached an OD of 0.5-1 nm, by the addition of 1 mM IPTG followed by an incubation of four hours at 25 ºC. Cells were collected after overnight incubation at room temperature by centrifugation and lysed in Lysis buffer supplemented with protease inhibitors, 200 µg/ml lysozyme and 1 µg/ml nuclease. The lysates were incubated with Glutathione Sepharose 4B for three hours at 4ºC. Beads were washed six times with PBS and re-suspended in PBS supplemented with 5% glycerol. For GST-pull-downs, 5 µg of GST-14-3-3 protein was incubated with 1 mg of protein extract for 2 hours at 4ºC with rotation. Pull-downs were washed for four times with modified RIPA buffer and eluted with 2×LDS sample buffer and 10 minutes incubation at 70ºC.

4.4.7 Peptide pull downs

Biotinylated NELFE peptide (QPFQRSIpSADDLQE) was custom synthesized (GenScript) and bound to NeutrAvidin agarose beads. Peptide-bound agarose was mock-treated or subjected to de-phosphorylation with 5 µl λ phosphatase in phosphatase reaction buffer with $MnCl_2$ for two-hours at 30°C. Subsequently, 10 µg of

bound peptide was incubated with 5 µg of the recombinant 14-3-3 ε (provided by Dr. M. Akutsu) in Peptide dilution buffer for three hours at 4ºC with rotation. Pull downs were washed three times with Peptide wash buffer supplemented with protease and phosphatase inhibitors.

4.4.8 Structure determination

In the collaboration with Dr. M. Akutsu, we have generated the crystal structure of the 14-3-3 interaction with the NELFE peptide corresponding to the S115 region. The 14-3-3 ε and synthesized NELFE phosphopeptide were mixed to a molar ratio of 1:5 for crystallization. The crystals of 14-3-3 ε in complex with NELFE phos- phorylated peptide were obtained using 40% pentaerythritol propoxylate, 0.2 M sodium thiocyanate, 0.1 M HEPES pH 7.0, as a reservoir solution by the sitting- drop vapor diffusion method at 293 K. Diffraction data were collected at the Swiss Lightsource SLS, beam line PXIII, and processed with XDS64. The crystal structure was determined by molecular replacement using the 14-3-3 ε structure (PDB: 2BR9) as search model. Manual model building and refinement were done with Coot, CCP4 software suite, and Phenix65–67. The crystal structure of 14- 3-3 ε in a complex with NELFE phosphopeptide reported in this study is deposited in PDB with the accession code 6EIH.

4.5 Mass spectrometry-based proteomics

Phosphoproteome analysis was performed as described in Borisova *et al*. (Borisova, Wagner, & Beli, 2017; Wagner et al., 2015).

4.5.1 Cell lysis for phosphoproteomics

Cells were treated according to the experimental design and washed twice with D-PBS. The following steps were performed on ice. Cells lysed in the modified RIPA buffer supplemented with all inhibitors were collected using a cell scraper in a 15 ml tube and the DNA was released by adding 1:10 volume of 5 M NaCl and sonicating until the lysate loses viscosity. Finally, cell debris was pelleted by high-speed centrifugation (16,000 × g) at 4°C for 15 min. Protein concentration was measured and equal amounts of protein were combined from each SILAC condition in a 50 ml tube.

4.5.2 In-solution digestion

Four volumes of ice-cold acetone were added into the combined sample to precipitate the proteins and the solution was incubated at −20°C for four hours to overnight. The acetone-precipitated proteins were pelleted by centrifugation at 1000 × g for five minutes and dissolved in Denaturation buffer. DTT was added to a final concentration of 1 mM and the samples were incubated at room temperature for one-hour with gentle shaking. Subsequently, CAA was added to a final concentration of 4.5 mM and the samples were incubated at room temperature for 1 hour in the dark with gentle shaking. For pre-digestion, 1 µg of LysC per 150 µg of protein was incubated with the proteins for three hours at room temperature and the samples were diluted with four volumes of water. For the digestion, the protein solution was supplemented

with 1 µg of Trypsin per 150 µg of protein and digested overnight at room temperature. To stop the enzymatic digestion, TFA was used with a final concentration of 0.5% and the samples were incubated at 4°C for a minimum of 1 hour. Acidified peptides were centrifuged for 10 minutes at 4000 × g and the supernatant was transferred to a fresh tube. To purify peptides, C18 cartridge was attached to a 10 ml syringe and washed once with 5 ml of 100% ACN. Consequently, the C18 cartridge was washed three times with 5 ml 0.1% TFA in water and loaded with the clarified peptide solution. To remove salts the C18 cartridge was washed three times with 10 ml 0.1% TFA in water. Later, for the next step, the peptides were eluted with 4.5 ml 50% ACN, 0.1% TFA in water and the concentration was measured by NanoDrop spectrophotometer (A280).

4.5.3 Phosphopeptide enrichment

6 mg of TiO_2 spheres were washed with Binding buffer for five minutes on a rotation wheel. The peptide solution with 0.5 ml of 60% TFA was incubated twice with TiO_2 spheres for one-hour on a rotation wheel. Peptide-loaded spheres from two incubations were washed twice with 1 ml Binding buffer (centrifuged at 1000 × g in between washes) and twice with 1 ml Wash buffer. Using a 17-gauge Hamilton syringe, one disk from a C_8 47 mm extraction disk was cut out and placed into a 200 µl pipette tip. Peptide-loaded spheres were transferred to the C_8 filter tip placed in a StageTip adapter (Rappsilber, Mann, & Ishihama, 2007) and dried by centrifugation at 400–800 × g. Phosphorylated peptides were eluted with 100 µl Elution buffer 1 and additionally with 100 µl Elution buffer 2 by centrifugation at 400 × g into the same tube. The eluted peptides were concentrated with vacuum at 45°C for 15 minutes to remove NH_4OH and adjusted to pH 2 using TFA.

4.5.4 Micro tip-based strong cation exchange chromatography (Micro-SCX)

The micro tip-based strong cation exchange chromatography protocol is based on the following publications (Rappsilber et al., 2007; Weinert et al., 2013; Wiśniewski, Zougman, & Mann, 2009). A 17-gauge Hamilton syringe was used to cut out six disks from a cation exchange 47 mm extraction disk that was placed into a 200 µl pipette tip (SCX tip). It was washed once with 50 µl methanol by centrifugation at 400–800 × g, once with 50 µl SCX elution buffer with pH 8.5, and once with 50 µl SCX wash buffer. The sample was loaded by centrifugation at 400–600 × *g*. Subsequently, the peptides were eluted with 100 µl SCX elution buffer in five pH steps (3.0, 3.5, 4.5, 6.0, 8.5) by centrifugation at 500–800 × g and collected in separate tubes. The eluates were concentrated with vacuum at 45°C for 15 minutes to remove ACN and adjusted to pH 2 using TFA.

4.5.5 In-gel digestion

Following by boiling samples with the LDS sample buffer, 4.5 mM CAA was added and incubated for 30 minutes in the dark. Proteins were resolved in NuPAGE Bis-Tris gels with a 4-12% gradient (Life Technologies) and stained using the Colloidal Blue Staining Kit. Each lane with a sample was cut into 6-10 pieces. The gel pieces

were washed four times with Destaining buffer and twice with absolute ethanol and digested in-gel with 0.625 µg trypsin in Digestion buffer. After overnight incubation at 37°C, the reaction was stopped by adding 50 µl Peptide extraction buffer and incubated for 20 minutes in a thermomixer shaking (400 rpm) at room temperature and collected to fresh tubes. Peptides were extracted from the gel pieces by 20 minutes incubations one by one with Peptide extraction buffer, In-gel Buffer B, and ACN respectively with a volume covering gel pieces (about 100 µl). After each step, the supernatant was collected in the same tube corresponding to each gel piece. Extracted peptides were concentrated with vacuum at 45°C for one-hour to reduce the sample volume to 100 µl. The samples were acidified, if required, to pH 2 with TFA.

4.4.6 Desalting and concentration of peptides

Using a 17-gauge Hamilton syringe, two disks from a C_{18} 47 mm extraction disk were cut out and placed into a 200 µl pipette tip (Rappsilber et al., 2007). C_{18} tips were washed once with 25 µl methanol, once with 25 µl Buffer B, and twice with 25 µl Buffer A by centrifugation at 400–800 × g. The acidified samples were loaded onto the C_{18} tips and again washed once with 50 µl Buffer A. The peptides were directly eluted into a 96-well plate by passing 50 µl C_{18} elution buffer through the C_{18} tips using a syringe and concentrated with vacuum at 45°C for 25 minutes to reduce the sample volume to 4.5–5 µl. Finally, 0.5–1 µl Buffer A* was added to the sample.

4.5.7 MS analysis

A nanospray column (15 cm length, 75 µl inner diameter) with C_{18} reversed phase chromatography material was packed (1.9 µm bead size) using a pressure injection cell (Ishihama, Rappsilber, Andersen, & Mann, 2002). To load the peptide sample onto the C_{18} column, a nano-flow UHPLC system was used. The peptides were eluted from the column with a linear gradient from 5 to 50% ACN in 2 h. The mass spectrometer was operated in data-dependent mode automatically switching between MS and MS_2 acquisitions (Kelstrup, Young, Lavallee, Nielsen, & Olsen, 2012; Michalski et al., 2011). MS spectra (*m*/*z* 300–1650) were acquired in the Orbitrap mass analyzer with a resolution of 70,000 at *m*/*z* = 200, after accumulation of ions to a target value of 3e6 estimated based on predictive automatic gain control from the previous full scan. The ten most intense ions were isolated using the quadrupole mass filter (maximum injection time 120 ms, isolation window 2.6 *m*/*z*, AGC target 1e5) and subsequently fragmented in the higher-energy C-trap dissociation (HCD) cell (Olsen et al., 2007). MS^2 spectra were acquired in the Orbitrap mass analyzer with a resolution of 35,000 at *m*/*z* = 200.

4.5.8 MS peptide identification

Raw data files were analyzed using MaxQuant (version 1.4.2.8) (Cox & Mann, 2008). Parent ion and MS^2 spectra were searched against a database containing 88,473 human protein sequences obtained from UniProtKB released in April 2014 using the Andromeda search engine (Cox et al., 2011). Spectra were searched with a

mass tolerance of 6 ppm in MS mode, 20 ppm in HCD MS^2 mode, strict trypsin specificity and allowing up to three miscleavages. Cysteine carbamidomethylation was searched as a fixed modification, whereas protein N-terminal acetylation, methionine oxidation, and, for the phosphoproteome, phosphorylation of serine, threonine, and tyrosine were searched as variable modifications. Site localization probabilities were determined by MaxQuant using the PTM scoring algorithm as described previously (Cox & Mann, 2008; Olsen et al., 2006). The dataset was filtered for potential contaminants and reverse identifications based on a posterior error probability (PEP) ratio to arrive at a false discovery rate of below 1% estimated using a target-decoy approach (Elias & Gygi, 2007). Only phosphorylated peptides with a localization probability bigger than 0.75, minimum score of 40, and score differences of five were reported and used for the analyses. The MS proteomics data were deposited to the Proteo-meXchange Consortium via the PRIDE partner repository72 with the dataset identifier PXD004255.

4.5.9 Phosphorylation site occupancy analysis

Light-labeled SILAC U2OS cells ectopically expressing GFP-NELFE were mock treated and medium and heavy-labeled cells were irradiated with UV-light (medium and heavy). GFP-NELFE was enriched using GFP Trap agarose as described above except that the fourth wash was done with Urea-SDS buffer followed by two washes with PBS. GFP-NELFE enriched from heavy labeled SILAC condition was dephosphorylated with 5 U of Antarctic Phosphatase for two-hours at room temperature, whereas GFP-NELFE enriched from light and medium labeled cells were mock treated. GFP-NELFE-bound agarose beads from the SILAC conditions were washed three times with PBS supplemented with protease and phosphatase inhibitors and combined after the last wash. Samples were further processed for MS analysis according to In-gel digestion protocol. The raw data were analyzed with MaxQuant as described in MS peptide identification section and the site occupancies were calculated as described (R. Wu et al., 2011). In brief, all unphosphorylated peptides corresponding to the site of interest were extracted after the MaxQuant quantification.

$$\text{Occupancy (Untreated)} = \left(1 - \frac{1}{\text{Average (Ratio H/L normalized)}}\right) * 100\%,$$

$$\text{Occupancy (UV)} = \left(1 - \frac{1}{\text{Average (Ratio H/M normalized)}}\right) * 100\%.$$

4.5.10 *In vitro* kinase assay

Ectopically expressed GFP-tagged NELFE was enriched from total cell lysates using GFP Trap agarose beads. Beads were washed four times with modified RIPA lysis buffer with 1 M NaCl and once with Kinase buffer. Reactions were initiated by adding 400 ng recombinant MK2 (Abcam) and 25 mM ATP to each sample and then incubated for 30 minutes at 30°C with gentle shaking. Samples were further processed for MS analysis according to In-gel digestion protocol.

4.5.11 Computational analysis

Statistical analysis was performed using the R software environment. The correlation coefficient (rho) and significance were determined using Spearman's rank method. Differences in SILAC ratio variance were assessed using the Siegel-Tukey test. Statistical significance was calculated using Wilcoxon rank sum test. Functional protein interaction network analysis was performed using interaction data from the STRING database (Franceschini et al., 2013). Only interactions with a score higher 0.7 are represented in the networks. Cytoscape version 3.1.1 was used for visualization of protein interaction networks (Saito et al., 2012).

4.6 Genomics

4.6.1 Chromatin immunoprecipitation (ChIP)

The samples for ChIP analysis were prepared as described (Arrigoni et al., 2016). Cells (20×10^6/IP) were cross-linked in growth medium containing 1% formaldehyde for 5 minutes at room temperature, quenched with 0.125 M glycine and washed twice with PBS. The cell pellet was resuspended in Farnham buffer (FB) and incubated for 15 minutes at 4°C with rotation. Cells were sonicated in 1 ml AFA tubes (Covaris, 520080) using the Covaris S220 focused ultrasonicator (duty factor: 2%, cycles/burst: 200, intensity: 2, water temperature 4°C). The sonication was stopped when more than 70% of nuclei were isolated (300 sec). NEXSON-isolated nuclei were washed twice with FB and resuspended in 1 ml shearing buffer supplemented with protease and phosphatase inhibitors and sheared for seven minutes to a fragment size distribution of 100–800 base pairs using the Covaris S220 focused ultrasonicator for 600 seconds (duty factor: 5%; cycles/burst: 200, intensity: 4, water temperature 4 °C). 150 µg of precleared chromatin was incubated overnight at 4°C with 5 µg of an antibody followed by three hours of incubation with 20 µl Dynabeads Protein G. Beads were washed twice with Wash buffer 1, twice with Wash buffer 2 and the bound chromatin was eluted with ChIP Elution buffer. Crosslinks were reversed by incubation at 65°C overnight with gentle shaking. Subsequently, chromatin was incubated with RNase A (0.2 mg/ml) for 30 minutes at 37°C and then with proteinase K (50 µg/ml) for three hours at 55°C. DNA was purified by phenol-chloroform extraction followed by ethanol precipitation and recovered in 30 µl (IP samples) or 50 µl (inputs) RNase free water.

4.6.2 Library preparation for the next generation sequencing

Library preparation as well as sequencing were performed by the Genomics Core Facility at the IMB. ChIP-seq library preparation was performed using Ovation® Ultralow System V2 1-96 (NuGEN). Libraries were prepared with a starting amount of 2.44 ng, 3.00 ng and 3.54 ng (normalization within replicates) of ChIP-DNA and were amplified in 11 PCR cycles. Libraries were profiled in a High Sensitivity DNA chip on a 2100 Bioanalyzer (Agilent Technologies) and quantified using the Qubit dsDNA HS Assay Kit, in a Qubit 2.0 Fluorometer (Life technologies). All 18 samples were pooled

in equimolar ratio and sequenced on 1 NextSeq500 flowcell, PE for 2×42 cycles plus eight cycles for the index read.

4.6.3 Computational analysis of ChIP-seq

The reads were mapped against GCRh37 with Bowtie (v.1.1.2, -l 28 -n 2 -e 70 –best –strata –trim5 10). Post-processing was done using SAM tools (v.1.2). Peaks were called using MACS2 (v. 2.1.1-20160309) with default parameters for Human. Afterward, the Diffbind (v.2.0.6 with DESeq2 1.12.4) analysis was performed to detect differentially bound regions for the control condition versus the UV condition. The peaks used for the analysis were the union of intersected peaks per condition combined from replicates. RNA Polymerase II release ratios (PRRs) were calculated as follows: for each gene the TSS region was defined as -300 bp upstream to 1000 bp downstream and the downstream region defined as 1000 bp downstream to 3 kb downstream (2 kb length). The PRR ratio was calculated as the $\log_2$ ratio between the enrichment in the downstream region over the enrichment in the TSS (Figure 27). Only genes with more than 3 kb in length were considered for the analysis. PRRs were filtered based on the highest signal on the TSS in the untreated condition. The genomics data have been deposited in NCBI's Gene Expression Omnibus (Edgar, Domrachev, & Lash, 2002) and are accessible through GEO Series accession number GSE100580.

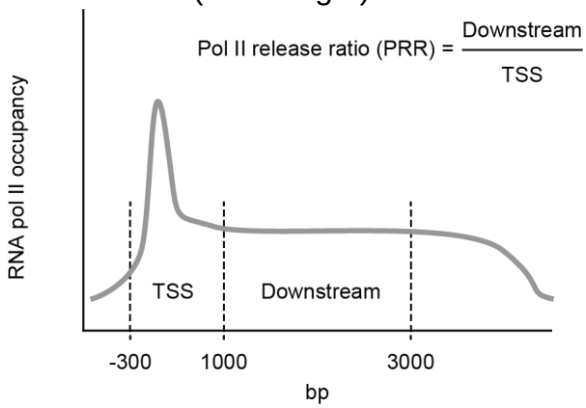

Figure 27. Schematic representation of the approach for the RNA pol 2 release ratio (PRR) calculation.

Appendix

Table 4. Crystallization data collection and refinement statistics. Values in parentheses are for the highest resolution shell.

	14-3-3/NELFE
Data collection statistics	
Beamline	SLS PX III
Wavelength (Å)	1.000
Space Group	C 2 2 2_1
Unit Cell (Å)	*a* = 79.29, *b* = 81.19, *c* = 81.05
	α =90.00, *β* = 90.00, *γ* = 90.00
Resolution (Å)	46.47 - 2.70
	(2.85 - 2.70)
Observed reflections	97555 (14510)
Unique reflections	7463 (1059)
Redundancy	13.1 (13.7)
Completeness (%)	100.0 (100.0)
*R*merge	0.126 (0.821)
<I/σI>	18.4 (3.5)
Refinement statistics	
Reflections in test set	757
*R*cryst	17.2
*R*free	24.1
Number of groups	
Protein residues	234
Ions and ligand atoms	0
Water	4
Wilson B-factor	50.55
RMSD from ideal geometry	
Bond length (Å)	0.012
Bond angles (°)	1.493
Ramachandran Plot Statistics	
In Favoured Regions (%)	224 (97.39)
In Allowed Regions (%)	6 (2.61)
Outliers (%)	0 (0.00)

Table 5. siRNA sequences used in this study

Gene	**Sequence 5'-3'**
p38	gaagcucuccagaccauuu
MK2	ccgaaaucaugaagagcau
MK3	ccaaagauguugugaggaa
MK5	ggagaaagacgcagugcuu
NELFE UTR	acacugagguggaagcuuac
NELFE-1	cagccaaggugugucaaa
XPC	gcaaauggcuucuaucgaa
CSB	ccacugauuacgagauaca

Table 6. List of inhibitors used in this study.

Chemical	Stock concentration/ solvent	Working concentration	Pre-incubation time	Target(s)	Producer
p38 MAPK (SB203580)	10 mM/DMSO	10 µM	1 h	p38 MAPK active site	InvivoGen
MK2 (PF-3644022)	10 mM/DMSO	10 µM	1 h	MK2 active site	Sigma Aldrich
ATM (KU-55933)	10 mM/DMSO	10 µM	1 h	ATM active site	Absource Diagnostics
ATR (VE-821)	1 mM/DMSO	1 µM	1 h	Competition with ATP at ATR active site	Selleckchem .com
DNA-PKcs (KU-57788)	10 mM/DMSO	10 µM	1 h	Competition with ATP at DNA-PKcs active site	Selleckchem .com
Cycloheximide (CHX)	20 µM/DMSO		vary	Translocation activity of ribosome (translation elongation)	Sigma Aldrich
Z-LEU-LEU-LEU-AL (MG132)	10 mM	10 µM	1 h	Proteolytic activity of 26S proteasome complex	Sigma Aldrich
5,6-Dichlorobenzimidazole 1-β-D-ribofuranosid (DRB)	100 mM	10 µM	1 h	RNA polymerase II elongation	Sigma Aldrich
Actinomycin D	1 mg/ml	2 µg/ml	1 h	Binding DNA at the transcription initiation complex	Sigma Aldrich

Table 7. List of chemicals used for inducing DNA damage in this study

Chemical	Stock concentration/ solvent	Working concentration	Incubation time	Type of DNA damage	Producer
Etoposide	10 mM/DMSO	10 µM	1 h	Stalled replication forks, SSB, DSB	Sigma Aldrich
Camptothecin (CPT)	10 mM/miliQ water	10 µM	1 h	Stalled replication forks, SSB, DSB	Sigma Aldrich
Hydroxyurea (HU)	3 M/miliQ water	2 mM	1 h	Stalled replication forks, SSB	Sigma Aldrich
4-nitroquinoline (4-NQO)	10 mM/miliQ water	20 µM	1 h	UV-mimetic, ROS production, SSB	Sigma Aldrich
Neocarzinostatin (NCS)	0.5 mg/ml	400 ng/ml	1 h	DSB	Sigma Aldrich
H_2O_2	500 mM/miliQ water	500 µM	1 h	ROS production, DSB and SSB	Sigma Aldrich

Appendix

Table 8. Plasmids used in this study

Plasmid name	Source
pcDNA-DEST53-GFP	Life Technologies
pcDNA-DEST47-GFP	Life Technologies
pMX-Dest53-IP-FS	Custom made, Beli Lab
pMX-Dest47-IP-FS	Custom made, Beli Lab
pDEST15	Life Technologies
pDEST24	Life Technologies
pENTR221 NELFE	Ultimate ORF Clones, Life Technologies
pENTR221 NELFA	Ultimate ORF Clones, Life Technologies
pENTR201 NELFB	Ultimate ORF Clones, Life Technologies
pDONR223 NELFC/D	Ultimate ORF Clones, Life Technologies
pENTR221 14-3-3β	Ultimate ORF Clones, Life Technologies
pENTR221 14-3-3ε	Ultimate ORF Clones, Life Technologies

Table 9. Primers used for site-directed mutagenesis

Mutant	Sequence 5'-3'
NELFE S49/51A	gacaggctgctctgctagtgcgcgtttgacaccac
NELFE S115A	gtcatcatcagcagctatgctcctctggaacgg
NELFE S251A	ccgttcagggaatgcatccgacctgcgga
NELFE S185A	ggctgcgggctcggggaggggaggc
NELFE S185/187A	tgcggtcccgggcgcgggctcggg
NELFE wt silent	ggtgtaaaacgctcactatcagagc
NELFE S49/51A silent	gacaggctgctctgctagtgcgcgttttacacccc

Table 10. Antibodies used in this study for western blotting, immunoprecipitation (IP), or ChIP.

Protein name	Product number	Manufacturer	Dilution	Origin
GFP	sc-9996	Santa Cruz	1:2000	mouse
FLAG M2	F1804	Sigma Aldrich	1:2000	mouse
pp38 (T180/Y182)	9216	CST	1:1000	rabbit
p38	8690	CST	1:1000	rabbit
pMK2 (T334)	3007	CST	1:1000	rabbit
MK2	3042	CST	1:1000	rabbit
pCHEK2 (T68)	2661	CST	1:1000	rabbit
pCHEK1 (S345)	2344	CST	1:1000	rabbit
Vinculin	V9264	Sigma Aldrich	1:10000	mouse
MCM7	3735	CST	1:1000	mouse
NELFE	ABE48	Millipore	1:1000	rabbit
NELFE (F-9)	377052	Santa Cruz	1:1000, IP	mouse
NELFB	14894	CST	1:1000	rabbit
CDK9 (D6K9A)	2316	CST	1:1000	mouse
14-3-3 (pan)	8312	CST	1:1000	rabbit
14-3-3 (pan)	1657	Santa Cruz	1:1000	mouse
POLR2A (N-20)	sc-899	Santa Cruz	ChIP	rabbit
POLR2A	sc-47701	Santa Cruz	1:1000	mouse
pCTD (S2)	13499	CST	1:1000	rabbit
pCTD (S5)	13523	CST	1:1000	rabbit
XPC	14768	CST	1:1000	rabbit
CSB	sc-398022	Santa Cruz	1:1000	mouse
PCNA (PC10)	sc-56	Santa Cruz	1:1000	mouse

GST (B14)	sc-138	Santa Cruz	1:2000	mouse
pJNK1	9255	CST	1:1000	rabbit
Mouse IgG Alexa Fluor® 488, 568	A11001, A11004	Life Technology	IF 1:1000	
Rabbit IgG Alexa Fluor® 488, 568	A11008, A11011	Life Technology	IF 1:1000	
Secondary antibodies coupled to horseradish peroxidase		Jackson ImmunoResearch Laboratories	1:5000	

Table 11. Software used for processing and analysis of the results

Software	**Application**
FijI/ImageJ	image processing, qualitative and quantitative analysis
ImageLab 4.2.1	gel electrophoresis imaging and analysis, WB imaging and analysis, colony formation assay image processing and assessment
Leica imaging software	SP5 operation, initial image processing and assessment
MS Excel 2010	MS and ChIP–seq QC, numerical troubleshooting and analysis, graphical processing, text processing, mathematical data analysis, WB quantification analysis
MS Word 2010	text processing, sequence analysis
NCBI Primer-BLAST	PCR primer design for cloning
UCSC browser	visual track analysis and graphical processing
Adobe Illustator CC2017	graphical processing
Adobe Photoshop CC2017	graphical processing
Primer3web 4.1.0	qPCR primer design for cloning
Cytoscape version 3.1.1	visualization of protein interaction networks
R studio 1.1.442	Statistical analysis of the proteome and genomic data
MaxQuant 1.5.2.8	analysis of raw MS data
Perseus 1.6.1.3	Viewer for MS data
Thermo Xcalibur 3.0.63	MS raw data visualization and assessment
ViiA 7 Real-Time PCR system	RT-qPCR data visualization and assessment

Abbreviations

4-NQO	4-nitroquinoline-1-oxide
DRB	5,6-dichloro-1-β-D-ribofuranosylbenzimidazole
6-4PPs	6'-4' photoproducts
AP-site	abasic site
alt-NHEJ	alternative NHEJ
bp	base pairs
BER	base-excision repair
CTKD	C-terminus kinase domain
CTD	carboxy-terminal domain
ChIP	chromatin immunoprecipitation
CPDs	cyclopyrimidine dimers
dNTP	deoxynucleotide
DDR	DNA damage response
dHJ	double HJ
DSB	double-strand break
DUSPs	dual-specificity phosphatases
FLAG	DYKDDDDK-peptide
GG-NER	Global-Genome NER
hnRNPs	heterogeneous nuclear ribonucleoproteins
HJ	Holliday junction
HR	Homologous recombination
NHEJ	non-homologous end joining
HRP	horse radish peroxidase
IP	Immunoprecipitation
IR	ionizing radiation
kbp	1,000 base pairs
kDa	1,000 Dalton
LC-MS/MS	liquid chromatography-tandem MS
MAP2K	MAPK kinase
MAP3K	MAPK kinase kinase
MKPs	MAPK phosphatases
MAPKAPK	MAPK-activated protein kinase
MS	mass spectrometry
Mbp	1,000,000 base pairs
MMR	mismatch repair
MAPK	Mitogen-activated protein kinase
mRNA	messenger RNA
n.s.	not significant
NGS	next generation sequencing
NTKD	N-terminus kinase domain
NES	nuclear export signal
NLS	nuclear localization signal
NER	nucleotide-excision repair
PI-3Ks	phosphatidylinositol 3-kinases
PAAG	polyacrylamide gel electrophoresis
PAR	Poly-ADP-ribose chains
PCR	polymerase chain reaction
PEP	posterior error probability
PTM	posttranslational modifications
PPP	promoter-proximal pausing
ROS	reactive oxygen species
RF	replication fork
PRR	RNA pol 2 release ratio
RNA pol 2	RNA polymerase
RBPs	RNA-binding proteins
RRM	RNA-recognizing motif
RNA-seq	RNA-sequencing
RT	room temperature (~22-23°C)
rpm	rotations per minute
S/TQ motif	serine or threonine residues followed by glutamine
SR factors	serine-arginine factors
ssDNA	single-strand DNA
SSB	single-strand DNA break
snRNPs	small nuclear ribonucleoproteins
SILAC	stable isotope labeling with amino acids in cell culture
TSS	transcription start site
TC-NER	Transcription-Coupled NER
TLS	translesion synthesis
UV	ultraviolet
WB	western blot

Aghazadeh, Y., & Papadopoulos, V. (2016). The role of the 14-3-3 protein family in health, disease, and drug development. *Drug Discovery Today*, *21*(2). https://doi.org/10.1016/j.drudis.2015.09.012

Andrade-Lima, L. C., Veloso, A., Paulsen, M. T., Menck, C. F. M., & Ljungman, M. (2015). DNA repair and recovery of RNA synthesis following exposure to ultraviolet light are delayed in long genes. *Nucleic Acids Research*, *43*(5), 2744–56. https://doi.org/10.1093/nar/gkv148

Ardehali, M. B., & Lis, J. T. (2009). Tracking rates of transcription and splicing in vivo. *Nature Structural & Molecular Biology*, *16*(11), 1123–1124. https://doi.org/10.1038/nsmb1109-1123

Arrigoni, L., Richter, A. S., Betancourt, E., Bruder, K., Diehl, S., Manke, T., & Bönisch, U. (2016). Standardizing chromatin research: a simple and universal method for ChIP-seq. *Nucleic Acids Research*, *44*(7), e67–e67. https://doi.org/10.1093/nar/gkv1495

Awwad, S. W., Abu-Zhayia, E. R., Guttmann-Raviv, N., & Ayoub, N. (2017). NELF-E is recruited to DNA double-strand break sites to promote transcriptional repression and repair. *EMBO Reports*, e201643191. https://doi.org/10.15252/embr.201643191

Babula, J. J., & Liu, J.-Y. (2015). Integrate Omics Data and Molecular Dynamicsd Simulations toward Better Understanding of Human 14-3-3 Interactomes and Better Drugs for Cancer Therapy. *Journal of Genetics and Genomics*, *42*(10), 531–547. https://doi.org/10.1016/J.JGG.2015.09.002

Ball, H. L., Myers, J. S., & Cortez, D. (2005). ATRIP Binding to Replication Protein A-Single-stranded DNA Promotes ATR-ATRIP Localization but Is Dispensable for Chk1 Phosphorylation. *Molecular Biology of the Cell*, *16*(5), 2372–2381. https://doi.org/10.1091/mbc.E04-11-1006

Bass, T. E., Luzwick, J. W., Kavanaugh, G., Carroll, C., Dungrawala, H., Glick, G. G., … Cortez, D. (2016). ETAA1 acts at stalled replication forks to maintain genome integrity. *Nature Cell Biology*, *18*(11), 1185–1195. https://doi.org/10.1038/ncb3415

Battle, D. J., Kasim, M., Yong, J., Lotti, F., Lau, C.-K., Mouaikel, J., … Dreyfuss, G. (2006). The SMN complex: an assembly machine for RNPs. *Cold Spring Harbor Symposia on Quantitative Biology*, *71*, 313–20. https://doi.org/10.1101/sqb.2006.71.001

Bekker-Jensen, S., Danielsen, J. R., Fugger, K., Gromova, I., Nerstedt, A., Bartek, J., … Mailand, N. (2010). HERC2 coordinates ubiquitin-dependent assembly of DNA repair factors on damaged chromosomes. *Nature Cell Biology*, *12*(1), 80–86. https://doi.org/10.1038/ncb2008

Beli, P., Lukashchuk, N., Wagner, S. A., Weinert, B. T., Olsen, J. V, Baskcomb, L., … Choudhary, C. (2012). Proteomic investigations reveal a role for RNA processing factor THRAP3 in the DNA damage response. *Molecular Cell*, *46*(2), 212–25. https://doi.org/10.1016/j.molcel.2012.01.026

Bensimon, A., Aebersold, R., & Shiloh, Y. (2011). Beyond ATM: the protein kinase landscape of the DNA damage response. *FEBS Letters*, *585*(11), 1625–39. https://doi.org/10.1016/j.febslet.2011.05.013

Besaratinia, A., Yoon, J.-I., Schroeder, C., Bradforth, S. E., Cockburn, M., & Pfeifer, G. P. (2011). Wavelength dependence of ultraviolet radiation-induced DNA damage as determined by laser irradiation suggests that cyclobutane pyrimidine dimers are the principal DNA lesions produced by terrestrial sunlight. *FASEB Journal : Official Publication of the Federation of American Societies for Experimental Biology*, *25*(9), 3079–91. https://doi.org/10.1096/fj.11-187336

Bito, T., Sumita, N., Masaki, T., Shirakawa, T., Ueda, M., Yoshiki, R., … Nishigori, C. (2010). Ultraviolet light induces Stat3 activation in human keratinocytes and fibroblasts through reactive oxygen species and DNA damage. *Experimental Dermatology*, *19*(7), 654–660. https://doi.org/10.1111/j.1600-0625.2010.01084.x

Blasius, M., Wagner, S. A., Choudhary, C., Bartek, J., & Jackson, S. P. (2014). A quantitative 14-3-3 interaction screen connects the nuclear exosome targeting complex to the DNA damage response. *Genes & Development*, *28*(18), 1977–1982. https://doi.org/10.1101/gad.246272.114

Blazek, D., Kohoutek, J., Bartholomeeusen, K., Johansen, E., Hulinkova, P., Luo, Z., … Peterlin, B. M. (2011). The Cyclin K/Cdk12 complex maintains genomic stability via regulation of expression of DNA damage response genes. *Genes & Development*, *25*(20), 2158–2172. https://doi.org/10.1101/gad.16962311

Boeing, S., Williamson, L., Encheva, V., Gori, I., Saunders, R. E., Instrell, R., … Svejstrup, J. Q. (2016). Multiomic Analysis of the UV-Induced DNA Damage Response. *Cell Reports*, *15*(7), 1597. https://doi.org/10.1016/j.celrep.2016.04.047

Bohgaki, M., Bohgaki, T., El Ghamrasni, S., Srikumar, T., Maire, G., Panier, S., … Hakem, R. (2013). RNF168 ubiquitylates 53BP1 and controls its response to DNA double-strand breaks. *Proceedings of the National Academy of Sciences of the United States of America*, *110*(52), 20982–7. https://doi.org/10.1073/pnas.1320302111

Bolderson, E., Tomimatsu, N., Richard, D. J., Boucher, D., Kumar, R., Pandita, T. K., … Khanna, K. K. (2010). Phosphorylation of Exo1 modulates homologous recombination repair of DNA double-strand breaks. *Nucleic Acids Research*, *38*(6), 1821–1831. https://doi.org/10.1093/nar/gkp1164

Bollig, F., Winzen, R., Kracht, M., Ghebremedhin, B., Ritter, B., Wilhelm, A., … Holtmann, H. (2002). Evidence for general stabilization of mRNAs in response to UV light. *European Journal of Biochemistry*, *269*(23), 5830–5839. https://doi.org/10.1046/j.1432-1033.2002.03300.x

Borisova, M. E., Wagner, S. A., & Beli, P. (2017). Mass Spectrometry-Based Proteomics for Quantifying DNA Damage-Induced Phosphorylation. In *Methods in molecular biology (Clifton, N.J.)* (Vol. 1599, pp. 215–227). https://doi.org/10.1007/978-1-4939-6955-5_16

Bothmer, A., Robbiani, D. F., Feldhahn, N., Gazumyan, A., Nussenzweig, A., & Nussenzweig, M. C. (2010). 53BP1 regulates DNA resection and the choice between classical and alternative end joining during class switch recombination. *The Journal of Experimental Medicine*, *207*(4), 855–65. https://doi.org/10.1084/jem.20100244

Bulavin, D. V., Higashimoto, Y., Popoff, I. J., Gaarde, W. A., Basrur, V., Potapova, O., … Fornace, A. J. (2001). Initiation of a G2/M checkpoint after ultraviolet radiation requires p38 kinase. *Nature*, *411*(6833), 102–107. https://doi.org/10.1038/35075107

Bunch, H., Zheng, X., Burkholder, A., Dillon, S. T., Motola, S., Birrane, G., … Calderwood, S. K. (2014). TRIM28 regulates RNA polymerase II promoter-proximal pausing and pause release. *Nature Structural & Molecular Biology*, *21*(10), 876–83. https://doi.org/10.1038/nsmb.2878

Bussen, W., Raynard, S., Busygina, V., Singh, A. K., & Sung, P. (2007). Holliday Junction Processing Activity of the BLM-Topo III␣-BLAP75 Complex * □ S. https://doi.org/10.1074/jbc.M706116200

Calses, P. C., Dhillon, K. K., Tucker, N., Sugasawa, K., Saijo, M., Taniguchi, T., … Taniguchi, T. (2017). DGCR8 Mediates Repair of UV-Induced DNA Damage Independently of RNA Processing. *Cell Reports*, *19*(4), 162–174. https://doi.org/10.1016/j.celrep.2017.03.021

Cargnello, M., & Roux, P. P. (2011). Activation and Function of the MAPKs and Their Substrates, the MAPK-Activated Protein Kinases. *Microbiology and Molecular Biology Reviews*, *75*(1), 50–83. https://doi.org/10.1128/MMBR.00031-10

Caunt, C. J., & Keyse, S. M. (2013). Dual-specificity MAP kinase phosphatases (MKPs): shaping the outcome of MAP kinase signalling. *The FEBS Journal*, *280*(2), 489–504. https://doi.org/10.1111/j.1742-4658.2012.08716.x

Chapman, J. R., & Jackson, S. P. (2008). Phospho-dependent interactions between NBS1 and MDC1 mediate chromatin retention of the MRN complex at sites of DNA damage.

EMBO Reports, *9*(8), 795–801. https://doi.org/10.1038/embor.2008.103

Chiou, Y.-Y., Hu, J., Sancar, A., & Selby, C. P. (2018). RNA polymerase II is released from the DNA template during transcription-coupled repair in mammalian cells. *The Journal of Biological Chemistry*, *293*(7), 2476–2486. https://doi.org/10.1074/jbc.RA117.000971

Chowdhury, D., Choi, Y. E., & Brault, M. E. (2013). Charity begins at home: non-coding RNA functions in DNA repair. *Nature Reviews Molecular Cell Biology*, *14*(3), 181–189. https://doi.org/10.1038/nrm3523

Christian Reinhardt, H., & Yaffe, M. B. (2013). Phospho-Ser/Thr-binding domains: navigating the cell cycle and DNA damage response. *Nature Publishing Group*, *14*. https://doi.org/10.1038/nrm3640

Chu, W. K., & Hickson, I. D. (2009). RecQ helicases: multifunctional genome caretakers. *Nature Reviews Cancer*, *9*(9), 644–654. https://doi.org/10.1038/nrc2682

Ciccia, A., & Elledge, S. J. (2010). The DNA damage response: making it safe to play with knives. *Molecular Cell*, *40*(2), 179–204. https://doi.org/10.1016/j.molcel.2010.09.019

Ciccia, A., McDonald, N., & West, S. C. (2008). Structural and Functional Relationships of the XPF/MUS81 Family of Proteins. *Annual Review of Biochemistry*, *77*(1), 259–287. https://doi.org/10.1146/annurev.biochem.77.070306.102408

Cimprich, K. A., & Cortez, D. (2008). ATR: an essential regulator of genome integrity. *Nature Reviews. Molecular Cell Biology*, *9*(8), 616–27. https://doi.org/10.1038/nrm2450

Cook, P. J., Ju, B. G., Telese, F., Wang, X., Glass, C. K., & Rosenfeld, M. G. (2009). Tyrosine dephosphorylation of H2AX modulates apoptosis and survival decisions. *Nature*, *458*(7238), 591–596. https://doi.org/10.1038/nature07849

Cooper, S. J., & Bowden, G. T. (2007). Ultraviolet B regulation of transcription factor families: roles of nuclear factor-kappa B (NF-kappaB) and activator protein-1 (AP-1) in UVB-induced skin carcinogenesis. *Current Cancer Drug Targets*, *7*(4), 325–34. Retrieved from http://www.ncbi.nlm.nih.gov/pubmed/17979627

Cortez, D., Guntuku, S., Qin, J., & Elledge, S. J. (2001). ATR and ATRIP: partners in checkpoint signaling. *Science (New York, N.Y.)*, *294*(5547), 1713–6. https://doi.org/10.1126/science.1065521

Cox, J., & Mann, M. (2008). MaxQuant enables high peptide identification rates, individualized p.p.b.-range mass accuracies and proteome-wide protein quantification. *Nature Biotechnology*, *26*(12), 1367–1372. https://doi.org/10.1038/nbt.1511

Cox, J., Neuhauser, N., Michalski, A., Scheltema, R. A., Olsen, J. V, & Mann, M. (2011). Andromeda: A peptide search engine integrated into the MaxQuant environment. *Journal of Proteome Research*, *10*(4), 1794–1805. Journal Article. https://doi.org/10.1021/pr101065j

Cruz-García, A., López-Saavedra, A., & Huertas, P. (2014). BRCA1 Accelerates CtIP-Mediated DNA-End Resection. *Cell Reports*, *9*(2), 451–459. https://doi.org/10.1016/j.celrep.2014.08.076

Cuadrado, A., & Nebreda, A. R. (2010). Mechanisms and functions of p38 MAPK signalling. *Biochemical Journal*, *429*(3), 403–417. https://doi.org/10.1042/BJ20100323

Dantuma, N. P., & van Attikum, H. (2016). Spatiotemporal regulation of posttranslational modifications in the DNA damage response. *The EMBO Journal*, *35*(1), 6–23. https://doi.org/10.15252/embj.201592595

Davis, A. J., & Chen, D. J. (2013). DNA double strand break repair via non-homologous end-joining. *Translational Cancer Research*, *2*(3), 130–143. https://doi.org/10.3978/j.issn.2218-676X.2013.04.02

Deng, J., Harding, H. P., Raught, B., Gingras, A.-C., Berlanga, J. J., Scheuner, D., … Sonenberg, N. (2002). Activation of GCN2 in UV-Irradiated Cells Inhibits Translation. *Current Biology*, *12*(15), 1279–1286. https://doi.org/10.1016/S0960-9822(02)01037-0

Di Giammartino, D. C., Nishida, K., & Manley, J. L. (2011). Mechanisms and consequences of alternative polyadenylation. *Molecular Cell*, *43*(6), 853–866.

https://doi.org/10.1016/j.molcel.2011.08.017
Diepgen, T. L., & Mahler, V. (2002). The epidemiology of skin cancer. *The British Journal of Dermatology*, *146 Suppl 61*, 1–6. Retrieved from http://www.ncbi.nlm.nih.gov/pubmed/11966724
Diffey, B. L. (2002). Sources and measurement of ultraviolet radiation. *Methods*, *28*(1), 4–13. https://doi.org/10.1016/S1046-2023(02)00204-9
Dikic, I. (2017). Proteasomal and Autophagic Degradation Systems. *Annual Review of Biochemistry*, *86*(1), 193–224. https://doi.org/10.1146/annurev-biochem-061516-044908
Dougherty, M. K., & Morrison, D. K. (2004). Unlocking the code of 14-3-3. *Journal of Cell Science*, *117*(Pt 10), 1875–84. https://doi.org/10.1242/jcs.01171
Edgar, R., Domrachev, M., & Lash, A. E. (2002). Gene Expression Omnibus: NCBI gene expression and hybridization array data repository. *Nucleic Acids Research*, *30*(1), 207–10.
Elias, J. E., & Gygi, S. P. (2007). Target-decoy search strategy for increased confidence in large-scale protein identifications by mass spectrometry. *Nat Methods*, *4*(3), 207–214. Journal Article. https://doi.org/10.1038/nmeth1019
Escós, A., Risco, A., Alsina-Beauchamp, D., & Cuenda, A. (2016). p38γ and p38δ Mitogen Activated Protein Kinases (MAPKs), New Stars in the MAPK Galaxy. *Frontiers in Cell and Developmental Biology*, *4*, 31. https://doi.org/10.3389/fcell.2016.00031
Fiore, M., Forli, S., & Manetti, F. (2016). Targeting Mitogen-Activated Protein Kinase-Activated Protein Kinase 2 (MAPKAPK2, MK2): Medicinal Chemistry Efforts To Lead Small Molecule Inhibitors to Clinical Trials. *Journal of Medicinal Chemistry*, *59*, 3609–3634. https://doi.org/10.1021/acs.jmedchem.5b01457
Fong, Y. W., Cattoglio, C., & Tjian, R. (2013). The Intertwined Roles of Transcription and Repair Proteins. *Molecular Cell*, *52*(3), 291–302. https://doi.org/10.1016/j.molcel.2013.10.018
Franceschini, A., Szklarczyk, D., Frankild, S., Kuhn, M., Simonovic, M., Roth, A., … Jensen, L. J. (2013). STRING v9.1: Protein-protein interaction networks, with increased coverage and integration. *Nucleic Acids Research*, *41*(Database issue), D808-15. Journal Article. https://doi.org/10.1093/nar/gks1094
Franklin, W. A., & Haseltine, W. A. (1986). The role of the (6-4) photoproduct in ultraviolet light-induced transition mutations in E. coli. *Mutation Research*, *165*(1), 1–7. Retrieved from http://www.ncbi.nlm.nih.gov/pubmed/3001515
Frit, P., Barboule, N., Yuan, Y., Gomez, D., & Calsou, P. (2014). Alternative end-joining pathway(s): Bricolage at DNA breaks. *DNA Repair*, *17*, 81–97. https://doi.org/10.1016/J.DNAREP.2014.02.007
Gaertner, B., Johnston, J., Chen, K., Wallaschek, N., Paulson, A., Garruss, A. S., … Zeitlinger, J. (2012). Poised RNA Polymerase II Changes over Developmental Time and Prepares Genes for Future Expression. *Cell Reports*, *2*(6), 1670–1683. https://doi.org/10.1016/J.CELREP.2012.11.024
Gaestel, M., Mengel, A., Bothe, U., & Asadullah, K. (2007). Protein kinases as small molecule inhibitor targets in inflammation. *Current Medicinal Chemistry*, *14*(21), 2214–34. Retrieved from http://www.ncbi.nlm.nih.gov/pubmed/17896971
Gaillard, H., García-Muse, T., & Aguilera, A. (2015). Replication stress and cancer. *Nature Reviews Cancer*, *15*(5), 276–289. https://doi.org/10.1038/nrc3916
Galanos, P., Vougas, K., Walter, D., Polyzos, A., Maya-Mendoza, A., Haagensen, E. J., … Gorgoulis, V. G. (2016). Chronic p53-independent p21 expression causes genomic instability by deregulating replication licensing. *Nature Cell Biology*, *18*(7), 777–789. https://doi.org/10.1038/ncb3378
Gao, X., Dan, S., Xie, Y., Qin, H., Tang, D., Liu, X., … Liu, L. (2015). 14-3-3ζ Reduces DNA Damage by Interacting With and Stabilizing Proliferating Cell Nuclear Antigen. *Journal*

of Cellular Biochemistry, *116*(1), 158–169. https://doi.org/10.1002/jcb.24955

García-Rodríguez, N., Wong, R. P., & Ulrich, H. D. (2016). Functions of Ubiquitin and SUMO in DNA Replication and Replication Stress. *Frontiers in Genetics*, *7*, 87. https://doi.org/10.3389/fgene.2016.00087

Gardino, A. K., Smerdon, S. J., & Yaffe, M. B. (2006). Structural determinants of 14-3-3 binding specificities and regulation of subcellular localization of 14-3-3-ligand complexes: A comparison of the X-ray crystal structures of all human 14-3-3 isoforms. *Seminars in Cancer Biology*, *16*(3), 173–182. https://doi.org/10.1016/j.semcancer.2006.03.007

Giannattasio, M., Follonier, C., Tourrière, H., Puddu, F., Lazzaro, F., Pasero, P., … Muzi-Falconi, M. (2010). Exo1 Competes with Repair Synthesis, Converts NER Intermediates to Long ssDNA Gaps, and Promotes Checkpoint Activation. *Molecular Cell*, *40*(1), 50–62. https://doi.org/10.1016/j.molcel.2010.09.004

Gibson, B. A., Zhang, Y., Jiang, H., Hussey, K. M., Shrimp, J. H., Lin, H., … Kraus, W. L. (2016). Chemical genetic discovery of PARP targets reveals a role for PARP-1 in transcription elongation. *Science*. https://doi.org/10.1126/science.aaf7865 (2016)

Gong, F., Kwon, Y., & Smerdon, M. J. (2005). Nucleotide excision repair in chromatin and the right of entry. *DNA Repair*, *4*(8), 884–896. https://doi.org/10.1016/j.dnarep.2005.04.007

Gregersen, L. H., & Svejstrup, J. Q. (2018). The Cellular Response to Transcription-Blocking DNA Damage. *Trends in Biochemical Sciences*, *43*(5), 327–341. https://doi.org/10.1016/j.tibs.2018.02.010

Gu, L., Hong, Y., McCulloch, S., Watanabe, H., & Li, G. M. (1998). ATP-dependent interaction of human mismatch repair proteins and dual role of PCNA in mismatch repair. *Nucleic Acids Research*, *26*(5), 1173. Retrieved from http://pubmedcentralcanada.ca/pmcc/articles/PMC147380/

Halim, V. A., García-Santisteban, I., Warmerdam, D. O., van den Broek, B., Heck, A. J. R., Mohammed, S., & Medema, R. H. (2018). Doxorubicin-induced DNA damage causes extensive ubiquitination of ribosomal proteins associated with a decrease in protein translation. *Molecular & Cellular Proteomics : MCP*, mcp.RA118.000652. https://doi.org/10.1074/mcp.RA118.000652

Han, X., Han, Y., Jiao, H., & Jie, Y. (2015). 14-3-3ζ regulates immune response through Stat3 signaling in oral squamous cell carcinoma. *Molecules and Cells*, *38*(2), 112–21. https://doi.org/10.14348/molcells.2015.2101

Hanasoge, S., & Ljungman, M. (2007). H2AX phosphorylation after UV irradiation is triggered by DNA repair intermediates and is mediated by the ATR kinase. *Carcinogenesis*, *28*(11), 2298–2304. https://doi.org/10.1093/carcin/bgm157

Harris, S. L., & Levine, A. J. (2005). The p53 pathway: positive and negative feedback loops. *Oncogene*, *24*(17), 2899–2908. https://doi.org/10.1038/sj.onc.1208615

He, N., Jahchan, N. S., Hong, E., Li, Q., Bayfield, M. A., Maraia, R. J., … Zhou, Q. (2008). A La-Related Protein Modulates 7SK snRNP Integrity to Suppress P-TEFb-Dependent Transcriptional Elongation and Tumorigenesis. *Molecular Cell*, *29*(5), 588–599. https://doi.org/10.1016/j.molcel.2008.01.003

Healy, S., Khan, D., & Davie, J. R. (2011). Gene Expression Regulation Through 14-3-3 Interactions with Histones and HDACs. *Discovery Medicine*, *11*(59), 349–358. Retrieved from http://www.discoverymedicine.com/Shannon-Healy/2011/04/20/gene-expression-regulation-through-14-3-3-interactions-with-histones-and-hdacs/

Heyer, W.-D. (2004). Recombination: Holliday Junction Resolution and Crossover Formation. *Current Biology*, *14*(2), R56–R58. https://doi.org/10.1016/J.CUB.2003.12.043

Hoeijmakers, J. H. J. (2009). DNA Damage, Aging, and Cancer. *New England Journal of Medicine*, *361*(15), 1475–1485. https://doi.org/10.1056/NEJMra0804615

IIDA, M., IIZUKA, N., TSUNEDOMI, R., TSUTSUI, M., YOSHIDA, S., MAEDA, Y., … OKA, M. (2012). Overexpression of the RD RNA binding protein in hepatitis C virus-related hepatocellular carcinoma. *Oncology Reports*, *28*(2), 728–734. https://doi.org/10.3892/or.2012.1821

Ip, S. C. Y., Rass, U., Blanco, M. G., Flynn, H. R., Skehel, J. M., & West, S. C. (2008). Identification of Holliday junction resolvases from humans and yeast. *Nature*, *456*(7220), 357–361. https://doi.org/10.1038/nature07470

Ishihama, Y., Rappsilber, J., Andersen, J. S., & Mann, M. (2002). Microcolumns with self-assembled particle frits for proteomics. *Journal of Chromatography. A*, *979*(1–2), 233–9. Retrieved from http://www.ncbi.nlm.nih.gov/pubmed/12498253

Iyer, D. R., & Rhind, N. (2017). The Intra-S Checkpoint Responses to DNA Damage. *Genes*, *8*(2). https://doi.org/10.3390/genes8020074

Jackson, S. P. P., & Durocher, D. (2013). Regulation of DNA damage responses by ubiquitin and SUMO. *Molecular Cell*, *49*(5), 795–807. https://doi.org/10.1016/j.molcel.2013.01.017

Jean-Philippe, J., Paz, S., & Caputi, M. (2013). hnRNP A1: the Swiss army knife of gene expression. *International Journal of Molecular Sciences*, *14*(9), 18999–9024. https://doi.org/10.3390/ijms140918999

Jinlian, L., Yingbin, Z., & Chunbo, W. (2007). p38 MAPK in regulating cellular responses to ultraviolet radiation. *Journal of Biomedical Science*, *14*(3), 303–312. https://doi.org/10.1007/s11373-007-9148-4

Jiricny, J. (2006). The multifaceted mismatch-repair system. *Nature Reviews Molecular Cell Biology*, *7*(5), 335–346. https://doi.org/10.1038/nrm1907

Jones, D. H., Ley, S., & Aitken, A. (1995). Isoforms of 14-3-3 protein can form homo- and heterodimers in vivo and in vitro: implications for function as adapter proteins. *FEBS Letters*, *368*(1), 55–8. Retrieved from http://www.ncbi.nlm.nih.gov/pubmed/7615088

Jones, R. M., & Petermann, E. (2012). Replication fork dynamics and the DNA damage response. *Biochem. J*, *443*, 13–26. https://doi.org/10.1042/BJ20112100

Jonkers, I., & Lis, J. T. (2015). Getting up to speed with transcription elongation by RNA polymerase II. *Nature Reviews Molecular Cell Biology*, *16*(3), 167–177. https://doi.org/10.1038/nrm3953

Kelstrup, C. D., Young, C., Lavallee, R., Nielsen, M. L., & Olsen, J. V. (2012). Optimized fast and sensitive acquisition methods for shotgun proteomics on a quadrupole orbitrap mass spectrometer. *J Proteome Res*, *11*(6), 3487–3497. Journal Article. https://doi.org/10.1021/pr3000249

Kim, S. T., Lim, D. S., Canman, C. E., & Kastan, M. B. (1999). Substrate specificities and identification of putative substrates of ATM kinase family members. *The Journal of Biological Chemistry*, *274*(53), 37538–43. https://doi.org/10.1074/JBC.274.53.37538

Klusmann, I., Rodewald, S., Müller, L., Friedrich, M., Wienken, M., Li, Y., … Levine, A. J. (2016). p53 Activity Results in DNA Replication Fork Processivity. *Cell Reports*, *17*(7), 1845–1857. https://doi.org/10.1016/j.celrep.2016.10.036

Krokan, H. E., & Bjoras, M. (2013). Base Excision Repair. *Cold Spring Harbor Perspectives in Biology*, *5*(4), a012583–a012583. https://doi.org/10.1101/cshperspect.a012583

Kwak, H., & Lis, J. T. (2013). Control of Transcriptional Elongation. *Annual Review of Genetics*, *47*(1), 483–508. https://doi.org/10.1146/annurev-genet-110711-155440

Lagha, M., Bothma, J. P., Esposito, E., Ng, S., Stefanik, L., Tsui, C., … Levine, M. S. (2013). Paused Pol II Coordinates Tissue Morphogenesis in the Drosophila Embryo. *Cell*, *153*(5), 976–987. https://doi.org/10.1016/j.cell.2013.04.045

Lans, H., Marteijn, J. A., Schumacher, B., Hoeijmakers, J. H. J., Jansen, G., & Vermeulen, W. (2010). Involvement of global genome repair, transcription coupled repair, and chromatin remodeling in UV DNA damage response changes during development. *PLoS Genetics*, *6*(5), e1000941. https://doi.org/10.1371/journal.pgen.1000941

Lans, H., Marteijn, J. A., & Vermeulen, W. (2012). ATP-dependent chromatin remodeling in the DNA-damage response. *Epigenetics & Chromatin*, *5*, 4. https://doi.org/10.1186/1756-8935-5-4

Larrea, A. A., Lujan, S. A., & Kunkel, T. A. (2010). SnapShot: DNA Mismatch Repair. *National Institutes of Environmental Health Sciences Cell Cell*, *141*(141). https://doi.org/10.1016/j.cell.2010.05.002

Lavigne, M. D., Konstantopoulos, D., Ntakou-Zamplara, K. Z., Liakos, A., & Fousteri, M. (2017). Global unleashing of transcription elongation waves in response to genotoxic stress restricts somatic mutation rate. *Nature Communications*, *8*(1), 2076. https://doi.org/10.1038/s41467-017-02145-4

Lee, J.-H., & Paull, T. T. (2005). ATM Activation by DNA Double-Strand Breaks Through the Mre11-Rad50-Nbs1 Complex. *Science*, *308*(5721), 551–554. https://doi.org/10.1126/science.1108297

Lee, J., Kumagai, A., & Dunphy, W. G. (2007). The Rad9-Hus1-Rad1 Checkpoint Clamp Regulates Interaction of TopBP1 with ATR. *Journal of Biological Chemistry*, *282*(38), 28036–28044. https://doi.org/10.1074/jbc.M704635200

Li, G.-M. (2008). Mechanisms and functions of DNA mismatch repair. *Cell Research*, *18*(1), 85–98. https://doi.org/10.1038/cr.2007.115

Lin, R., Heylbroeck, C., Pitha, P. M., & Hiscott, J. (1998). Virus-dependent phosphorylation of the IRF-3 transcription factor regulates nuclear translocation, transactivation potential, and proteasome-mediated degradation. *Molecular and Cellular Biology*, *18*(5), 2986–96. Retrieved from http://www.ncbi.nlm.nih.gov/pubmed/9566918

Liu, S., Bekker-Jensen, S., Mailand, N., Lukas, C., Bartek, J., & Lukas, J. (2006). Claspin operates downstream of TopBP1 to direct ATR signaling towards Chk1 activation. *Molecular and Cellular Biology*, *26*(16), 6056–64. https://doi.org/10.1128/MCB.00492-06

Liu, S., Shiotani, B., Lahiri, M., Maréchal, A., Tse, A., Leung, C. C. Y., … Zou, L. (2011). ATR Autophosphorylation as a Molecular Switch for Checkpoint Activation. *Molecular Cell*, *43*(2), 192–202. https://doi.org/10.1016/j.molcel.2011.06.019

Liu, X., Gogate, A. A., Tastemel, M., Malladi, V. S., Yao, H., Nguyen, K., … Bai, X. (2017). Dynamic Change of Transcription Pausing through Modulating NELF Protein Stability Regulates Granulocytic Differentiation. *Blood Advances*, *1*(18), 1358–1367. https://doi.org/10.1182/bloodadvances.2017008383

Loman, N., & Watson, M. (2013). So you want to be a computational biologist? *Nature Biotechnology*, *31*(11), 996–998. https://doi.org/10.1038/nbt.2740

Longo, P. A., Kavran, J. M., Kim, M.-S., & Leahy, D. J. (2013). Chapter Eighteen – Transient Mammalian Cell Transfection with Polyethylenimine (PEI). In *Methods in Enzymology* (Vol. 529, pp. 227–240). https://doi.org/10.1016/B978-0-12-418687-3.00018-5

Lukas, J., Lukas, C., & Bartek, J. (2011). More than just a focus: The chromatin response to DNA damage and its role in genome integrity maintenance. *Nature Cell Biology*, *13*(10), 1161–1169. https://doi.org/10.1038/ncb2344

Madeira, F., Tinti, M., Murugesan, G., Berrett, E., Stafford, M., Toth, R., … Barton, G. J. (2015). 14-3-3-Pred: improved methods to predict 14-3-3-binding phosphopeptides. *Bioinformatics (Oxford, England)*, btv133-. https://doi.org/10.1093/bioinformatics/btv133

Mahat, D. B., Kwak, H., Booth, G. T., Jonkers, I. H., Danko, C. G., Patel, R. K., … Lis, J. T. (2016). Base-pair-resolution genome-wide mapping of active RNA polymerases using precision nuclear run-on (PRO-seq). *Nature Protocols*, *11*(8), 1455–1476. https://doi.org/10.1038/nprot.2016.086

Mandemaker, I. K., van Cuijk, L., Janssens, R. C., Lans, H., Bezstarosti, K., Hoeijmakers, J. H., … Marteijn, J. A. (2017). DNA damage-induced histone H1 ubiquitylation is mediated by HUWE1 and stimulates the RNF8-RNF168 pathway. *Scientific Reports*,

7(1), 15353. https://doi.org/10.1038/s41598-017-15194-y
Manke, I. A., Nguyen, A., Lim, D., Stewart, M. Q., Elia, A. E. H., & Yaffe, M. B. (2005). MAPKAP Kinase-2 Is a Cell Cycle Checkpoint Kinase that Regulates the G2/M Transition and S Phase Progression in Response to UV Irradiation. *Molecular Cell*, *17*(1), 37–48. https://doi.org/10.1016/j.molcel.2004.11.021
Mansilla, S. F., Soria, G., Vallerga, M. B., Habif, M., Martinez-Lopez, W., Prives, C., & Gottifredi, V. (2013). UV-triggered p21 degradation facilitates damaged-DNA replication and preserves genomic stability. *Nucleic Acids Research*, *41*(14), 6942–6951. https://doi.org/10.1093/nar/gkt475
Maréchal, A., & Zou, L. (2013). DNA damage sensing by the ATM and ATR kinases. *Cold Spring Harbor Perspectives in Biology*, *5*(9). https://doi.org/10.1101/cshperspect.a012716
Marini, F., Nardo, T., Giannattasio, M., Minuzzo, M., Stefanini, M., Plevani, P., & Falconi, M. M. (2006). DNA nucleotide excision repair-dependent signaling to checkpoint activation. *Proceedings of the National Academy of Sciences*, *103*(46), 17325–17330. https://doi.org/10.1073/pnas.0605446103
Marteijn, J. A., Lans, H., Vermeulen, W., & Hoeijmakers, J. H. J. (2014). Understanding nucleotide excision repair and its roles in cancer and ageing. *Nature Reviews Molecular Cell Biology*, *15*(7), 465–481. https://doi.org/10.1038/nrm3822
Matsuoka, S., Ballif, B. A., Smogorzewska, A., McDonald, E. R., Hurov, K. E., Luo, J., … Elledge, S. J. (2007). ATM and ATR substrate analysis reveals extensive protein networks responsive to DNA damage. *Science (New York, N.Y.)*, *316*(5828), 1160–6. https://doi.org/10.1126/science.1140321
Maynard, S., Schurman, S. H., Harboe, C., de Souza-Pinto, N. C., & Bohr, V. A. (2008). Base excision repair of oxidative DNA damage and association with cancer and aging. *Carcinogenesis*, *30*(1), 2–10. https://doi.org/10.1093/carcin/bgn250
Meek, K., Dang, V., & Lees-Miller, S. P. (2008). DNA-PK: the means to justify the ends? In *Advances in immunology* (Vol. 99, pp. 33–58). Elsevier. https://doi.org/10.1016/S0065-2776(08)00602-0
Meier, A., Fiegler, H., Muñoz, P., Ellis, P., Rigler, D., Langford, C., … Jackson, S. P. (2007). Spreading of mammalian DNA-damage response factors studied by ChIP-chip at damaged telomeres. *The EMBO Journal*, *26*(11), 2707–2718. https://doi.org/10.1038/sj.emboj.7601719
Melander, F., Bekker-Jensen, S., Falck, J., Bartek, J., Mailand, N., & Lukas, J. (2008). Phosphorylation of SDT repeats in the MDC1 N terminus triggers retention of NBS1 at the DNA damage–modified chromatin. *The Journal of Cell Biology*, *181*(2), 213–226. https://doi.org/10.1083/jcb.200708210
Méndez, J., & Stillman, B. (2000). Chromatin association of human origin recognition complex, cdc6, and minichromosome maintenance proteins during the cell cycle: assembly of prereplication complexes in late mitosis. *Molecular and Cellular Biology*, *20*(22), 8602–12. Retrieved from http://www.ncbi.nlm.nih.gov/pubmed/11046155
Michalski, A., Damoc, E., Hauschild, J.-P., Lange, O., Wieghaus, A., Makarov, A., … Horning, S. (2011). Mass spectrometry-based proteomics using Q Exactive, a high-performance benchtop quadrupole Orbitrap mass spectrometer. *Molecular & Cellular Proteomics : MCP*, *10*(9), M111.011015. https://doi.org/10.1074/mcp.M111.011015
Min, I. M., Waterfall, J. J., Core, L. J., Munroe, R. J., Schimenti, J., & Lis, J. T. (2011). Regulating RNA polymerase pausing and transcription elongation in embryonic stem cells. *Genes & Development*, *25*(7), 742–754. https://doi.org/10.1101/gad.2005511
Mohammad, D. H., & Yaffe, M. B. (2009). 14-3-3 proteins, FHA domains and BRCT domains in the DNA damage response. *DNA Repair*, *8*(9), 1009–1017. https://doi.org/10.1016/J.DNAREP.2009.04.004
Montecucco, A., & Biamonti, G. (2013). Pre-mRNA processing factors meet the DNA

damage response. *Frontiers in Genetics*, *4*, 102. https://doi.org/10.3389/fgene.2013.00102

Mordes, D. A., Glick, G. G., Zhao, R., & Cortez, D. (2008). TopBP1 activates ATR through ATRIP and a PIKK regulatory domain. *Genes & Development*, *22*(11), 1478–89. https://doi.org/10.1101/gad.1666208

Müller-McNicoll, M., Botti, V., de Jesus Domingues, A. M., Brandl, H., Schwich, O. D., Steiner, M. C., … Neugebauer, K. M. (2016). SR proteins are NXF1 adaptors that link alternative RNA processing to mRNA export. *Genes & Development*, *30*(5), 553–66. https://doi.org/10.1101/gad.276477.115

Muñoz, I. M., Hain, K., Déclais, A.-C., Gardiner, M., Toh, G. W., Sanchez-Pulido, L., … Rouse, J. (2009). Coordination of structure-specific nucleases by human SLX4/BTBD12 is required for DNA repair. *Molecular Cell*, *35*(1), 116–27. https://doi.org/10.1016/j.molcel.2009.06.020

Muñoz, M. J., Pérez Santangelo, M. S., Paronetto, M. P., de la Mata, M., Pelisch, F., Boireau, S., … Kornblihtt, A. R. (2009). DNA damage regulates alternative splicing through inhibition of RNA polymerase II elongation. *Cell*, *137*(4), 708–20. https://doi.org/10.1016/j.cell.2009.03.010

Nam, E. A., & Cortez, D. (2011). ATR signalling: more than meeting at the fork. *The Biochemical Journal*, *436*(3), 527–36. https://doi.org/10.1042/BJ20102162

Narita, T., Yamaguchi, Y., Yano, K., Sugimoto, S., Chanarat, S., Wada, T., … Handa, H. (2003). Human transcription elongation factor NELF: identification of novel subunits and reconstitution of the functionally active complex. *Molecular and Cellular Biology*, *23*(6), 1863–73. Retrieved from http://www.pubmedcentral.nih.gov/articlerender.fcgi?artid=149481&tool=pmcentrez&rendertype=abstract

Narita, T., Yung, T. M. C., Yamamoto, J., Tsuboi, Y., Tanabe, H., Tanaka, K., … Handa, H. (2007). NELF interacts with CBC and participates in 3' end processing of replication-dependent histone mRNAs. *Molecular Cell*, *26*(3), 349–65. https://doi.org/10.1016/j.molcel.2007.04.011

Nouspikel, T. (2009). DNA Repair in Mammalian Cells. *Cellular and Molecular Life Sciences*, *66*(6), 994–1009. https://doi.org/10.1007/s00018-009-8737-y

O'Connell, B. C., & Harper, J. W. (2007). Ubiquitin proteasome system (UPS): what can chromatin do for you? *Current Opinion in Cell Biology*, *19*(2), 206–14. https://doi.org/10.1016/j.ceb.2007.02.014

O'Neill, T., Dwyer, A. J., Ziv, Y., Chan, D. W., Lees-Miller, S. P., Abraham, R. H., … Rathbun, G. A. (2000). Utilization of oriented peptide libraries to identify substrate motifs selected by ATM. *The Journal of Biological Chemistry*, *275*(30), 22719–27. https://doi.org/10.1074/jbc.M001002200

Ohle, C., Tesorero, R., Schermann, G., Dobrev, N., Sinning, I., Fischer, T., … Ira, G. (2016). Transient RNA-DNA Hybrids Are Required for Efficient Double-Strand Break Repair. *Cell*, *167*(4), 1001–1013.e7. https://doi.org/10.1016/j.cell.2016.10.001

Olsen, J. V, Blagoev, B., Gnad, F., Macek, B., Kumar, C., Mortensen, P., & Mann, M. (2006). Global, in vivo, and site-specific phosphorylation dynamics in signaling networks. *Cell*, *127*(3), 635–648. Journal Article. https://doi.org/10.1016/j.cell.2006.09.026

Olsen, J. V, Macek, B., Lange, O., Makarov, A., Horning, S., & Mann, M. (2007). Higher-energy C-trap dissociation for peptide modification analysis. *Nat Methods*, *4*(9), 709–712. Journal Article. https://doi.org/10.1038/nmeth1060

Ong, S.-E., & Mann, M. (2006). A practical recipe for stable isotope labeling by amino acids in cell culture (SILAC). *Nature Protocols*, *1*(6), 2650–60. https://doi.org/10.1038/nprot.2006.427

Orphanides, G., & Reinberg, D. (2002). A Unified Theory of Gene Expression. *Cell*, *108*(4), 439–451. https://doi.org/10.1016/S0092-8674(02)00655-4

Paronetto, M. P., Miñana, B., & Valcárcel, J. (2011). The Ewing Sarcoma Protein Regulates DNA Damage-Induced Alternative Splicing. *Molecular Cell*, *43*(3), 353–368. https://doi.org/10.1016/j.molcel.2011.05.035

Paull, T. T. (2015). Mechanisms of ATM Activation. *Annual Review of Biochemistry*, *84*(1), 711–738. https://doi.org/10.1146/annurev-biochem-060614-034335

Paulsen, R. D., Soni, D. V., Wollman, R., Hahn, A. T., Yee, M.-C., Guan, A., … Cimprich, K. A. (2009). A Genome-wide siRNA Screen Reveals Diverse Cellular Processes and Pathways that Mediate Genome Stability. *Molecular Cell*, *35*(2), 228–239. https://doi.org/10.1016/j.molcel.2009.06.021

Polo, S. E., & Jackson, S. P. (2011). Dynamics of DNA damage response proteins at DNA breaks: a focus on protein modifications. *Genes & Development*, *25*(5), 409–33. https://doi.org/10.1101/gad.2021311

Powell, D. W., Rane, M. J., Joughin, B. A., Kalmukova, R., Hong, J.-H., Tidor, B., … McLeish, K. R. (2003). Proteomic identification of 14-3-3zeta as a mitogen-activated protein kinase-activated protein kinase 2 substrate: role in dimer formation and ligand binding. *Molecular and Cellular Biology*, *23*(15), 5376–87. https://doi.org/10.1128/MCB.23.15.5376-5387.2003

Powley, I. R., Kondrashov, A., Young, L. A., Dobbyn, H. C., Hill, K., Cannell, I. G., … Willis, A. E. (2009). Translational reprogramming following UVB irradiation is mediated by DNA-PKcs and allows selective recruitment to the polysomes of mRNAs encoding DNA repair enzymes. *Genes & Development*, *23*(10), 1207–20. https://doi.org/10.1101/gad.516509

Psakhye, I., & Jentsch, S. (2012). Protein Group Modification and Synergy in the SUMO Pathway as Exemplified in DNA Repair. *Cell*, *151*(4), 807–820. https://doi.org/10.1016/j.cell.2012.10.021

Ramadan, K. (2012). p97/VCP- and Lys48-linked polyubiquitination form a new signaling pathway in DNA damage response. *Cell Cycle*, *11*(6), 1062–1069. https://doi.org/10.4161/cc.11.6.19446

Rappsilber, J., Mann, M., & Ishihama, Y. (2007). Protocol for micro-purification, enrichment, pre-fractionation and storage of peptides for proteomics using StageTips. *Nat Protoc*, *2*(8), 1896–1906. Journal Article. https://doi.org/10.1038/nprot.2007.261

Reinhardt, H. C., Aslanian, A. S., Lees, J. A., & Yaffe, M. B. (2007). p53-Deficient Cells Rely on ATM- and ATR-Mediated Checkpoint Signaling through the p38MAPK/MK2 Pathway for Survival after DNA Damage. *Cancer Cell*, *11*(2), 175–189. https://doi.org/10.1016/j.ccr.2006.11.024

Reinhardt, H. C., Cannell, I. G., Morandell, S., & Yaffe, M. B. (2011). Is post-transcriptional stabilization, splicing and translation of selective mRNAs a key to the DNA damage response? *Cell Cycle (Georgetown, Tex.)*, *10*(1), 23–7. https://doi.org/10.4161/cc.10.1.14351

Reinhardt, H. C., & Yaffe, M. B. (2009). Kinases that control the cell cycle in response to DNA damage: Chk1, Chk2, and MK2. *Current Opinion in Cell Biology*, *21*(2), 245–55. https://doi.org/10.1016/j.ceb.2009.01.018

Richard, D. J., Savage, K., Bolderson, E., Cubeddu, L., So, S., Ghita, M., … Khanna, K. K. (2011). hSSB1 rapidly binds at the sites of DNA double-strand breaks and is required for the efficient recruitment of the MRN complex. *Nucleic Acids Research*, *39*(5), 1692–702. https://doi.org/10.1093/nar/gkq1098

Rockx, D. A. P., Mason, R., van Hoffen, A., Barton, M. C., Citterio, E., Bregman, D. B., … Mullenders, L. H. F. (2000). UV-induced inhibition of transcription involves repression of transcription initiation and phosphorylation of RNA polymerase II. *Proceedings of the National Academy of Sciences*, *97*(19), 10503–10508. https://doi.org/10.1073/pnas.180169797

Rogakou, E. P., Pilch, D. R., Orr, A. H., Ivanova, V. S., & Bonner, W. M. (1998). DNA double-

stranded breaks induce histone H2AX phosphorylation on serine 139. *The Journal of Biological Chemistry*, *273*(10), 5858–68. Retrieved from http://www.ncbi.nlm.nih.gov/pubmed/9488723

Ronkina, N., Menon, M. B., Schwermann, J., Tiedje, C., Hitti, E., Kotlyarov, A., & Gaestel, M. (2010). MAPKAP kinases MK2 and MK3 in inflammation: Complex regulation of TNF biosynthesis via expression and phosphorylation of tristetraprolin. *Biochemical Pharmacology*, *80*(12), 1915–1920. https://doi.org/10.1016/j.bcp.2010.06.021

Saini, P., Li, Y., & Dobbelstein, M. (2015). Wee1 is required to sustain ATR/Chk1 signaling upon replicative stress. *Oncotarget*, *6*(15), 13072–87. https://doi.org/10.18632/oncotarget.3865

Saito, R., Smoot, M. E., Ono, K., Ruscheinski, J., Wang, P.-L., Lotia, S., … Ideker, T. (2012). A travel guide to Cytoscape plugins. *Nature Methods*, *9*(11), 1069–76. https://doi.org/10.1038/nmeth.2212

Savage, K. I., Gorski, J. J., Barros, E. M., Irwin, G. W., Manti, L., Powell, A. J., … Harkin, D. P. (2014). Identification of a BRCA1-mRNA Splicing Complex Required for Efficient DNA Repair and Maintenance of Genomic Stability. *Molecular Cell*, *54*(3), 445–459. https://doi.org/10.1016/j.molcel.2014.03.021

Sawarkar, R., Sievers, C., & Paro, R. (2012). Hsp90 Globally Targets Paused RNA Polymerase to Regulate Gene Expression in Response to Environmental Stimuli. *Cell*, *149*(4), 807–818. https://doi.org/10.1016/j.cell.2012.02.061

Schärer, O. D. (2013). Nucleotide Excision Repair in Eukaryotes. *Cold Spring Harbor Perspectives in Biology*, *5*(10), a012609. https://doi.org/10.1101/cshperspect.a012609

Schaukowitch, K., Joo, J.-Y., Liu, X., Watts, J. K., Martinez, C., & Kim, T.-K. (2014). Enhancer RNA facilitates NELF release from immediate early genes. *Molecular Cell*, *56*(1), 29–42. https://doi.org/10.1016/j.molcel.2014.08.023

Schreck, I., Grico, N., Hansjosten, I., Marquardt, C., Bormann, S., Seidel, A., … Weiss, C. (2016). The nucleotide excision repair protein XPC is essential for bulky DNA adducts to promote interleukin-6 expression via the activation of p38-SAPK. *Oncogene*, *35*(7), 908–918. https://doi.org/10.1038/onc.2015.145

Shaw, P. H. (1996). The Role of p53 in Cell Cycle Regulation. *Pathology - Research and Practice*, *192*(7), 669–675. https://doi.org/10.1016/S0344-0338(96)80088-4

Shkreta, L., & Chabot, B. (2015). The RNA Splicing Response to DNA Damage. *Biomolecules*, *5*(4), 2935–2977. https://doi.org/10.3390/biom5042935

Skalska, L., Beltran-Nebot, M., Ule, J., & Jenner, R. G. (2017). Regulatory feedback from nascent RNA to chromatin and transcription. *Nature Reviews Molecular Cell Biology*, *18*(5), 331–337. https://doi.org/10.1038/nrm.2017.12

Sonntag, C. von. (2006). *Free-radical-induced DNA damage and its repair: a chemical perspective*. Berlin; New York: Springer.

Srivastava, M., & Raghavan, S. C. (2015). DNA Double-Strand Break Repair Inhibitors as Cancer Therapeutics. *Chemistry & Biology*, *22*(1), 17–29. https://doi.org/10.1016/j.chembiol.2014.11.013

Stadelmayer, B., Micas, G., Gamot, A., Martin, P., Malirat, N., Koval, S., … Benkirane, M. (2014). Integrator complex regulates NELF-mediated RNA polymerase II pause/release and processivity at coding genes. *Nature Communications*, *5*, 5531. https://doi.org/10.1038/ncomms6531

Stelter, P., & Ulrich, H. D. (2003). Control of spontaneous and damage-induced mutagenesis by SUMO and ubiquitin conjugation. *Nature*, *425*(6954), 188–191. https://doi.org/10.1038/nature01965

Strzalka, W., & Ziemienowicz, A. (2011). Proliferating cell nuclear antigen (PCNA): a key factor in DNA replication and cell cycle regulation. *Annals of Botany*, *107*(7), 1127–40. https://doi.org/10.1093/aob/mcq243

Sugasawa, K., Ng, J. M. ., Masutani, C., Iwai, S., van der Spek, P. J., Eker, A. P. ., …

Hoeijmakers, J. H. . (1998). Xeroderma Pigmentosum Group C Protein Complex Is the Initiator of Global Genome Nucleotide Excision Repair. *Molecular Cell*, *2*(2), 223–232. https://doi.org/10.1016/S1097-2765(00)80132-X

Sugasawa, K., Okuda, Y., Saijo, M., Nishi, R., Matsuda, N., Chu, G., … Hanaoka, F. (2005). UV-induced ubiquitylation of XPC protein mediated by UV-DDB-ubiquitin ligase complex. *Cell*, *121*(3), 387–400. https://doi.org/10.1016/j.cell.2005.02.035

Tan, W.-H., Baris, H., Robson, C. D., & Kimonis, V. E. (2005). Cockayne syndrome: The developing phenotype. *American Journal of Medical Genetics Part A*, *135A*(2), 214–216. https://doi.org/10.1002/ajmg.a.30731

Thomas, M. C., & Chiang, C.-M. (2006). The General Transcription Machinery and General Cofactors. *Critical Reviews in Biochemistry and Molecular Biology*, *41*(3), 105–178. https://doi.org/10.1080/10409230600648736

Thornton, T. M., & Rincon, M. (2009). Non-classical p38 map kinase functions: cell cycle checkpoints and survival. *International Journal of Biological Sciences*, *5*(1), 44–51. Retrieved from http://www.ncbi.nlm.nih.gov/pubmed/19159010

Tiedje, C., Lubas, M., Tehrani, M., Menon, M. B., Ronkina, N., Rousseau, S., … Gaestel, M. (2015). p38 ^{MAPK} /MK2-mediated phosphorylation of RBM7 regulates the human nuclear exosome targeting complex. *RNA*, *21*(2), 262–278. https://doi.org/10.1261/rna.048090.114

Tollenaere, M. A. X., Villumsen, B. H., Blasius, M., Nielsen, J. C., Wagner, S. A., Bartek, J., … Bekker-Jensen, S. (2015). p38- and MK2-dependent signalling promotes stress-induced centriolar satellite remodelling via 14-3-3-dependent sequestration of CEP131/AZI1. *Nature Communications*, *6*, 10075. https://doi.org/10.1038/ncomms10075

Uhlen, M., Zhang, C., Lee, S., Sjöstedt, E., Fagerberg, L., Bidkhori, G., … Ponten, F. (2017). A pathology atlas of the human cancer transcriptome. *Science*, *357*(6352), eaan2507. https://doi.org/10.1126/science.aan2507

Ulrich, H. D. (2012). Ubiquitin and SUMO in DNA repair at a glance. *Journal of Cell Science*, *125*(Pt 2), 249–54. https://doi.org/10.1242/jcs.091801

Ulrich, H., & Jentsch, S. (2000). Two RING finger proteins mediate cooperation between ubiquitin-conjugating enzymes in DNA repair. *The EMBO Journal*, *19*(13), 3388–3397. https://doi.org/10.1093/emboj/19.13.3388

Unsal-Kaçmaz, K., & Sancar, A. (2004). Quaternary structure of ATR and effects of ATRIP and replication protein A on its DNA binding and kinase activities. *Molecular and Cellular Biology*, *24*(3), 1292–300. Retrieved from http://www.ncbi.nlm.nih.gov/pubmed/14729973

Uziel, T., Lerenthal, Y., Moyal, L., Andegeko, Y., Mittelman, L., & Shiloh, Y. (2003). Requirement of the MRN complex for ATM activation by DNA damage. *The EMBO Journal*, *22*(20), 5612–5621. https://doi.org/10.1093/emboj/cdg541

Valensin, D., Cau, Y., Calandro, P., Vignaroli, G., Dello Iacono, L., Chiariello, M., … Botta, M. (2016). Molecular insights to the bioactive form of BV02, a reference inhibitor of 14-3-3σ protein–protein interactions. *Bioorganic & Medicinal Chemistry Letters*, *26*(3), 894–898. https://doi.org/10.1016/J.BMCL.2015.12.066

Vohhodina, J., Barros, E. M., Savage, A. L., Liberante, F. G., Manti, L., Bankhead, P., … Savage, K. I. (2017). The RNA processing factors THRAP3 and BCLAF1 promote the DNA damage response through selective mRNA splicing and nuclear export. *Nucleic Acids Research*, *45*(22), 12816–12833. https://doi.org/10.1093/nar/gkx1046

Volker, M., Moné, M. J., Karmakar, P., van Hoffen, A., Schul, W., Vermeulen, W., … Mullenders, L. H. (2001). Sequential assembly of the nucleotide excision repair factors in vivo. *Molecular Cell*, *8*(1), 213–24. Retrieved from http://www.ncbi.nlm.nih.gov/pubmed/11511374

Vos, S. M., Farnung, L., Urlaub, H., & Cramer, P. (2018). Structure of paused transcription

complex Pol II–DSIF–NELF. *Nature*. https://doi.org/10.1038/s41586-018-0442-2

Vos, S. M., Pöllmann, D., Caizzi, L., Hofmann, K. B., Rombaut, P., Zimniak, T., … Cramer, P. (2016). Architecture and RNA binding of the human negative elongation factor. *ELife*, *5*. https://doi.org/10.7554/eLife.14981

Wada, T., Stepniak, E., Hui, L., Leibbrandt, A., Katada, T., Nishina, H., … Penninger, J. M. (2008). Antagonistic control of cell fates by JNK and p38-MAPK signaling. *Cell Death & Differentiation*, *15*(1), 89–93. https://doi.org/10.1038/sj.cdd.4402222

Wagner, S. A., Oehler, H., Voigt, A., Dalic, D., Freiwald, A., Serve, H., & Beli, P. (2015). ATR inhibition rewires cellular signalling networks induced by replication stress. *Proteomics*. https://doi.org/10.1002/pmic.201500172

Wang, M., Wu, W., Wu, W., Rosidi, B., Zhang, L., Wang, H., & Iliakis, G. (2006). PARP-1 and Ku compete for repair of DNA double strand breaks by distinct NHEJ pathways. *Nucleic Acids Research*, *34*(21), 6170–6182. https://doi.org/10.1093/nar/gkl840

Ward, I. M., Minn, K., & Chen, J. (2004). UV-induced ataxia-telangiectasia-mutated and Rad3-related (ATR) activation requires replication stress. *The Journal of Biological Chemistry*, *279*(11), 9677–80. https://doi.org/10.1074/jbc.C300554200

Waterman, M. J. F., Stavridi, E. S., Waterman, J. L. F., & Halazonetis, T. D. (1998). ATM-dependent activation of p53 involves dephosphorylation and association with 14-3-3 proteins. *Nature Genetics*, *19*(2), 175–178. https://doi.org/10.1038/542

Watson, J., Baker, T., Bell, S., Gann, A., Levine, M., & Losick, R. (2013). *Molecular Biology of the Gene* (7th ed). Pearson. Retrieved from https://archive.org/stream/WatsonMolecularBiologyOfTheGene7thEditionC2014Txtbk/Watson Molecular Biology of the Gene 7th Edition c2014 txtbk#page/n3/mode/2up

Weinert, B. T., Schölz, C., Wagner, S. A., Iesmantavicius, V., Su, D., Daniel, J. A., & Choudhary, C. (2013). Lysine succinylation is a frequently occurring modification in prokaryotes and eukaryotes and extensively overlaps with acetylation. *Cell Reports*, *4*(4), 842–51. https://doi.org/10.1016/j.celrep.2013.07.024

Weston, C. R., & Davis, R. J. (2002). The JNK signal transduction pathway. *Current Opinion in Genetics & Development*, *12*(1), 14–21. https://doi.org/10.1016/S0959-437X(01)00258-1

Wickramasinghe, V. O., & Venkitaraman, A. R. (2016). RNA Processing and Genome Stability: Cause and Consequence. *Molecular Cell*, *61*(4), 496–505. https://doi.org/10.1016/j.molcel.2016.02.001

Williams, L. H., Fromm, G., Gokey, N. G., Henriques, T., Muse, G. W., Burkholder, A., … Adelman, K. (2015). Pausing of RNA polymerase II regulates mammalian developmental potential through control of signaling networks. *Molecular Cell*, *58*(2), 311–322. https://doi.org/10.1016/j.molcel.2015.02.003

Williams, R. S., Williams, J. S., & Tainer, J. A. (2007). Mre11–Rad50–Nbs1 is a keystone complex connecting DNA repair machinery, double-strand break signaling, and the chromatin templateThis paper is one of a selection of papers published in this Special Issue, entitled 28th International West Coast Chromatin and Chromosome Conference, and has undergone the Journal's usual peer review process. *Biochemistry and Cell Biology*, *85*(4), 509–520. https://doi.org/10.1139/O07-069

Williamson, L., Saponaro, M., Boeing, S., East, P., Mitter, R., Kantidakis, T., … Svejstrup, J. Q. (2017). UV Irradiation Induces a Non-coding RNA that Functionally Opposes the Protein Encoded by the Same Gene. *Cell*, *168*(5), 843–855.e13. https://doi.org/10.1016/j.cell.2017.01.019

Wilson, M. D., Harreman, M., & Svejstrup, J. Q. (2013). Ubiquitylation and degradation of elongating RNA polymerase II: The last resort. *Biochimica et Biophysica Acta (BBA) - Gene Regulatory Mechanisms*, *1829*(1), 151–157. https://doi.org/10.1016/j.bbagrm.2012.08.002

Wiśniewski, J. R., Zougman, A., & Mann, M. (2009). Combination of FASP and StageTip-

Based Fractionation Allows In-Depth Analysis of the Hippocampal Membrane Proteome. *Journal of Proteome Research*, *8*(12), 5674–5678. https://doi.org/10.1021/pr900748n

Woodhead, A. D., Setlow, R. B., & Tanaka, M. (1999). Environmental factors in nonmelanoma and melanoma skin cancer. *Journal of Epidemiology*, *9*(6 Suppl), S102-14. Retrieved from http://www.ncbi.nlm.nih.gov/pubmed/10709358

Wu, L., Luo, K., Lou, Z., & Chen, J. (2008). MDC1 regulates intra-S-phase checkpoint by targeting NBS1 to DNA double-strand breaks. *Proceedings of the National Academy of Sciences*, *105*(32), 11200–11205. https://doi.org/10.1073/pnas.0802885105

Wu, R., Haas, W., Dephoure, N., Huttlin, E. L., Zhai, B., Sowa, M. E., & Gygi, S. P. (2011). A large-scale method to measure absolute protein phosphorylation stoichiometries. *Nature Methods*, *8*(8), 677–83. https://doi.org/10.1038/nmeth.1636

Xu, X., Vaithiyalingam, S., Glick, G. G., Mordes, D. A., Chazin, W. J., & Cortez, D. (2008). The Basic Cleft of RPA70N Binds Multiple Checkpoint Proteins, Including RAD9, To Regulate ATR Signaling. *Molecular and Cellular Biology*, *28*(24), 7345–7353. https://doi.org/10.1128/MCB.01079-08

Yaffe, M. B., Rittinger, K., Volinia, S., Caron, P. R., Aitken, A., Leffers, H., … Cantley, L. C. (1997). The structural basis for 14-3-3:phosphopeptide binding specificity. *Cell*, *91*(7), 961–71. Retrieved from http://www.ncbi.nlm.nih.gov/pubmed/9428519

Yamaguchi, Y., Shibata, H., & Handa, H. (2013). Transcription elongation factors DSIF and NELF: Promoter-proximal pausing and beyond. *Biochimica et Biophysica Acta (BBA) - Gene Regulatory Mechanisms*, *1829*(1), 98–104. https://doi.org/10.1016/j.bbagrm.2012.11.007

Yang, X., Lee, W. H., Sobott, F., Papagrigoriou, E., Robinson, C. V., Grossmann, J. G., … Elkins, J. M. (2006). Structural basis for protein-protein interactions in the 14-3-3 protein family. *Proceedings of the National Academy of Sciences*, *103*(46), 17237–17242. https://doi.org/10.1073/pnas.0605779103

Yazdi, P. T., Wang, Y., Zhao, S., Patel, N., Lee, E. Y.-H. P., & Qin, J. (2002). SMC1 is a downstream effector in the ATM/NBS1 branch of the human S-phase checkpoint. *Genes & Development*, *16*(5), 571–582. https://doi.org/10.1101/gad.970702

You, Z., & Bailis, J. M. (2010). DNA damage and decisions: CtIP coordinates DNA repair and cell cycle checkpoints. *Trends in Cell Biology*, *20*(7), 402–409. https://doi.org/10.1016/j.tcb.2010.04.002

Yuan, R., Vos, H. R., van Es, R. M., Chen, J., Burgering, B. M., Westendorp, B., & de Bruin, A. (2018). Chk1 and 14-3-3 proteins inhibit atypical E2Fs to prevent a permanent cell cycle arrest. *The EMBO Journal*, *37*(5), e97877. https://doi.org/10.15252/embj.201797877

Yung, T. M. C., Narita, T., Komori, T., Yamaguchi, Y., & Handa, H. (2009). Cellular dynamics of the negative transcription elongation factor NELF. *Experimental Cell Research*, *315*(10), 1693–705. https://doi.org/10.1016/j.yexcr.2009.02.013

Zeke, A., Misheva, M., Reményi, A., & Bogoyevitch, M. A. (2016). JNK Signaling: Regulation and Functions Based on Complex Protein-Protein Partnerships. *Microbiology and Molecular Biology Reviews : MMBR*, *80*(3), 793–835. https://doi.org/10.1128/MMBR.00043-14

Zeman, M. K., & Cimprich, K. A. (2014). Causes and consequences of replication stress. *Nature Cell Biology*, *16*(1), 2–9. https://doi.org/10.1038/ncb2897

Zhou, Q., Li, T., & Price, D. H. (2012). RNA Polymerase II Elongation Control. *Annual Review of Biochemistry*, *81*(1), 119–143. https://doi.org/10.1146/annurev-biochem-052610-095910

Zou, L., Cortez, D., & Elledge, S. J. (2002). Regulation of ATR substrate selection by Rad17-dependent loading of Rad9 complexes onto chromatin. *Genes & Development*, *16*(2), 198–208. https://doi.org/10.1101/gad.950302

Zou, L., Liu, D., Elledge, S. J., Takemura, H., Kohn, K., Pommier, Y., … Nussenzweig, A. (2003). Replication protein A-mediated recruitment and activation of Rad17 complexes. *Proceedings of the National Academy of Sciences of the United States of America*, *100*(24), 13827–32. https://doi.org/10.1073/pnas.2336100100